Simulating the Characteristics of Tropical Cyclones over the South West Indian Ocean Using an Adaptive Stretched-Grid Global Climate Model

Author:

Molulaqhooa Linda Maoyi

Student Number:

MYXMOL001

Supervisor:

Dr Babatunde J. Abiodun

Co-Supervisor:

Dr Jennifer Veitch

Dissertation presented for the degree of

Master of Science (Atmospheric Science)

Department of Environmental & Geographical Science

Faculty of Science

University of Cape Town

August, 2015

DECLARATION

I know the meaning of plagiarism and declare that all the work in this dissertation, save for that is properly acknowledged, is my own.

Signature: Signed by candidate
signature removed

Molulaqhooa Linda Maoyi

ABSTRACT

Tropical Cyclones are one of the most devastating natural phenomena. Previous attempts to simulate Tropical Cyclones (TCs) over the South West Indian Ocean (SWIO) have used Global Circulation Models (GCMs) with uniform grid. This study examines the capability of a GCM with adaptive grid stretching (CAM-EULAG, hereafter CEU) in simulating the characteristics of TCs over the SWIO. In the study, the CEU model is applied with a fine horizontal grid resolution (0.5°x0.5°) over the SWIO and coarser resolution (1°x1° – 2°x2.25°) over the rest of the globe. The model simulation is performed for 11 years (1999-2010) and validated against the Joint Typhoon Warning Centre (JTWC) best track observation, Global Precipitation Climatology Project (GPCP) satellite data, and ERA-Interim (ERAINT) reanalysis data. The study also considers the impact of El Niño Southern Oscillation (ENSO), Indian Ocean Dipole (IOD) and the South Atlantic Subtropical Dipole (SASD) on TC counts over the SWIO.

The results of this study show that CEU gives a realistic simulation of the SWIO. However, there are notable discrepancies in the climatic features over the Mozambique Channel (MC). These discrepancies include a substantial cyclonic feature over the MC that produces a high TC count bias in the model simulation. Despite this bias, the CEU model shows some skill in simulating the spatial distribution of TC genesis locations and tracks over much of the basin. The dynamical structure and intensities of the simulated CEU TCs compare well with observation, though the model struggles to sustain TCs with a deeper pressure centre. The reanalysis has the same problem. The monthly and interannual variation of TC occurrence is well produced by the model, but the model does not show any notable differences in TC counts during an El Niño, La Niña or the neutral phase of ENSO. However, the model agrees well with observation on relative frequencies of TCs during the positive phases of SASD and IOD. This study has an application in improving and adopting the GCM with adaptive grid for seasonal forecasting over the SWIO.

ACKNOWLEDGEMENTS

Foremost, I would like to thank God for giving me the courage and strength in undertaking this mammoth of a degree. The road was tough, challenging and sometimes unclear but through you Lord, I fought uphill battles, persevered through stormy terrains and finally conquered! All praise and honour is yours almighty Father!

I would also like to express my deepest gratitude to my Supervisor, Dr Babatunde J. Abiodun for converting me from a general Computer Scientist into a specialist Climate Modeller. In addition to that, I would like to thank the great doctor for his awesome teachings on life, for his constant support and motivation throughout the degree as well as the research training he provided in writing captivating and interesting research papers.

My deepest gratitude also goes out to my co-supervisor Dr Jennifer Veitch for her guidance as well as for nominating me for the National Research Foundation (NRF) grant award of which this research was generously supported by through the Thuthuka Fund.

My Gratitude goes out to Dr Penny Driver for her endless hours spent on teaching me on how to configure and run a climate model on a cluster, even on a Sunday Afternoon! Thank you very much Penny, you were literally one of the only three people in this planet who knew how to configure and run CAM-EULAG. Because of you, I am now the fourth.

Thank you so much to Sabina Abba Omar for her invaluable contribution to the Tropical Cyclone Tracking Algorithm. The many months we spent designing, implementing and testing the algorithm did not go in vain.

I would also like to thank Mr Phillip Mukwenha for his selfless assistance and incredible work ethic when I had trouble installing the various software packages I needed to conduct my research. Waita zvako!

I would also like to thank the members of the extreme weather research group (Temitope Egbebiyi, Lawal Kamoru, Arlindo Meque, Johnson Oloruntade, Romaric Odoulami and Gemma Bluff) for their constructive critique during the writing stages of this work as well as for making sure that each paragraph started with a “claim” and was well backed up.

I would also like to give thanks to the Centre for High Performance Computing (CHPC) for allocating me resources so I can run my model experiments. Gratitude also goes out to the support team especially Sticks Mabakane who always took my calls and solved my problems.

To my colleagues at ICTS, thank you for showing interest in my work and for always encouraging me to finish this dissertation especially at times when I was in complete darkness. Thank you to Pierre Neethling for giving me time off work at moment's notice so I could complete writing this dissertation. A big thank you to Morwamadibane Ntwape for letting me hijack his external hard drive that housed all my data for the entire year.

To my former colleagues at eNCA: Lynette Van Schalkwyk, Joel Chabata, Gerrie Keyser and Luis Fernandes; thank you for training me in the art of weather forecasting, it really helped a lot during the data analysis section of this work.

I would like to thank all my friends both here in Cape Town and back home in Johannesburg for all the love and encouragement you have shown me. Your company has helped me keep sane.

To my wonderful family, without whose love and support I could have never achieved such a great accomplishment, ke leboga go menagane! To Mampho and Teboho Maoyi, I have laid down the path, it is up to you to continue the legacy. To my father Israel Maoyi and mother Tsholofelo Maoyi, ka nnete, Morena o entse tse holo!

~God Bless You All~

DEDICATION

To all those who lost their lives due to Tropical Cyclones

May your souls rest in peace.

LIST OF ACRONYMS

ACE	Accumulated Cyclone Energy
ARF	Annual Relative Frequency
ARPEGE	Action de Recherche Petite Echelle Grande Echelle (Research project on small and large scales)
BOB	Bay of Bengal
CAM	Community Atmosphere Model
CAM-SE	CAM-Spectral Element
CAM-EULAG	CAM-Euler-Lagrange
CAPE	Convective Available Potential Energy
CCAM	Conformal Cubic Atmosphere Model
CES	CAM-Eulerian Spectral
CEU	CAM-EULAG
CFV	CAM-Finite Volume
DMI	Dipole Mode Index
ECHAM	European Centre Hamburg Model
ECMWF	European Centre for Medium Range Weather Forecasting
EEIO	Eastern Equatorial Indian Ocean
ENSO	El Niño Southern Oscillation
ERAINT	European Centre for Medium Range Weather Forecast - Interim
ERSST	Extended Reconstructed Sea Surface Temperature
ESCAP/WMO	United Nations Economic and Social Commission for Asia and the Pacific/ World Meteorological Organization
GCM	Global Climate Model

GPCP	Global Precipitation Climatology Project
IOD	Indian Ocean Dipole
ITC	Intense Tropical Cyclone
ITCZ	Inter Tropical Convergence Zone
JTWC	Joint Typhoon Warning Centre
LBC	Lateral Boundary Condition
LULC	Land Use Land Cover
MC	Mozambique Channel
MJO	Madden–Julian Oscillation
MSLP	Mean Sea Level Pressure
MSW	Maximum Sustained Wind
NCAR	National Center for Atmospheric Research
NCEP	National Center for Environmental Prediction
NWP	Numerical Weather Prediction
NWS	National Weather Service
ONI	Oceanic Niño Index
PBL	Planetary Boundary Layer
RCM	Regional Climate Model
SADC	Southern African Development Community
SASD	South Atlantic Subtropical Dipole
SIOD	South Indian Ocean Dipole
SST	Sea Surface Temperature
SWIO	South West Indian Ocean
TC	Tropical Cyclone
WEIO	Western Equatorial Indian Ocean

TABLE OF CONTENTS

LIST OF FIGURES

LIST OF TABLES

1 INTRODUCTION

1.1 Definition of a Tropical Cyclone

A Tropical Cyclone (hereafter TC) is a generic term for a warm-core, non-frontal, low-pressure synoptic scale system that develops over tropical or subtropical waters with persistent, organized deep convection and a closed cyclonic surface circulation about a well-defined centre (Holland 1993) (See Figure 1.1). Further classification of TCs is reliant on the wind speeds near the eye-wall of the system with the maximum mean sustained surface 10-minute wind speed being the most common measure of TC intensity. However, in the United States of America (USA), a 1-minute wind speed average is usually used (Australia Bureau of Meteorology, 2013). The maximum sustained wind speed (hereafter MSW) is defined as the wind speed averaged over a period of 10 minutes and is generally measured at 10 m above the surface. Cyclones with a MSW of less than 63 km/h are known as tropical depressions and become tropical storms once they reach a MSW of at least 63 km/h. If the cyclone MSW reaches 118 km/h then they are classified as TCs. However, the term TC is not universal across all ocean basins and different names are used to classify these systems according to the region they occur.

- The term hurricane is used in the North Atlantic, North-east pacific east of the dateline, or South Pacific Ocean east of 160°E.
- The name Typhoon is used in the Northwest Pacific Ocean west of the dateline.
- The term TC is commonly used in the Indian Ocean.

In the "hurricane" regions, TCs are classified into five categories, distinguished by the intensities of their MSW, using the Saffir-Simpson wind scale, which was developed by wind engineer Herb Saffir and meteorologist Bob Simpson (See Table 1.1). Over the years, the scale has been widely used for alerting the public on the potential impacts of TCs based on their intensities (National Hurricane Center, 2013). The scale is based on a 1-minute average MSW and provides examples on the type of damage associated with the designated intensity. Elsewhere, TCs are categorized differently but do not have an official name for the categorization. Over the South West Indian Ocean (hereafter SWIO), TCs are monitored by the Météo-France meteorological centre in La Réunion Island, which is located between Madagascar and Mauritius. Météo-France uses seven categories, which shall be denoted as the Météo-France TC scale, to classify storms in the SWIO and this classification is based on

a 10-minute average MSW (see Table 1.2).

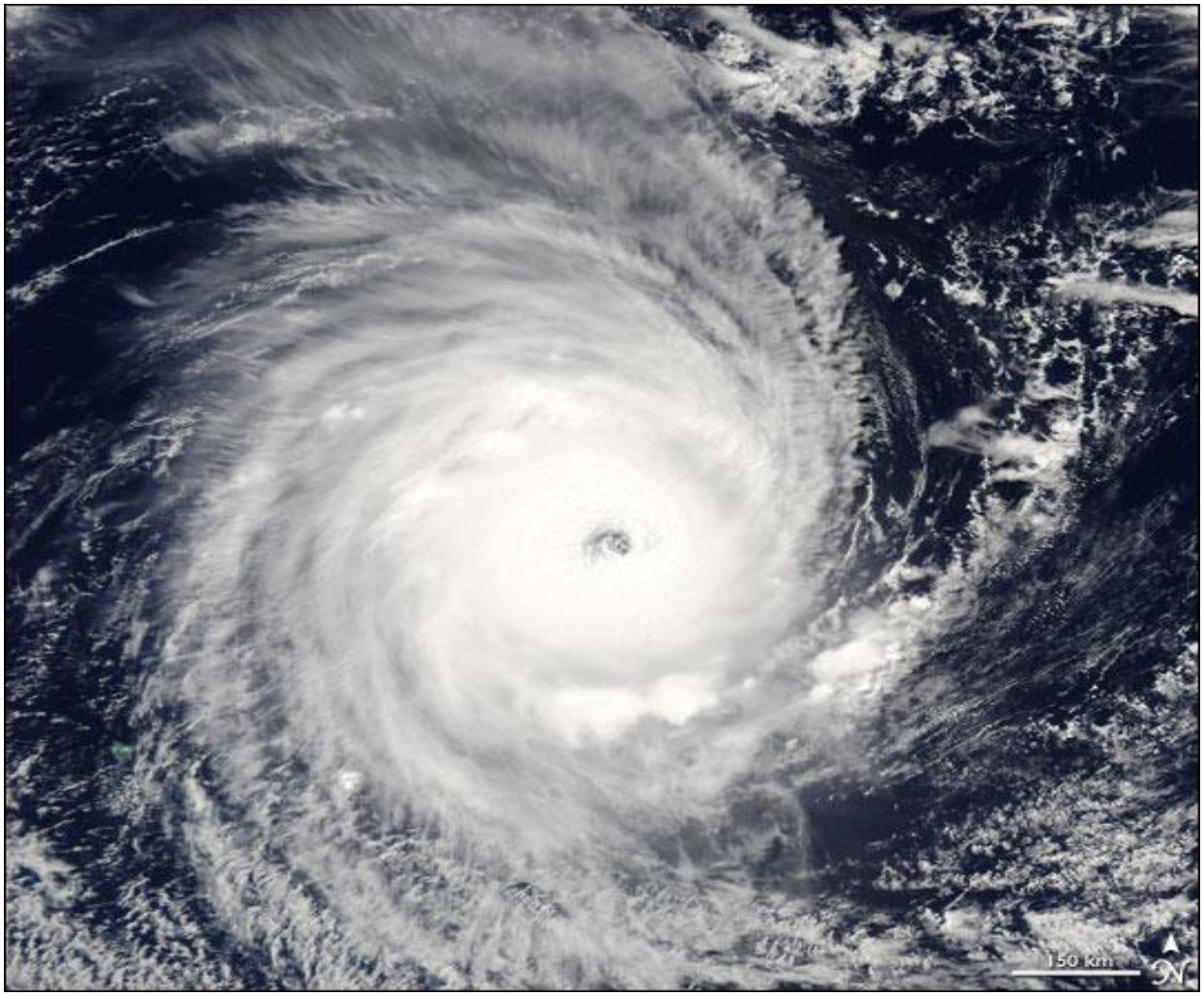

Figure 1.1: Satellite picture of Tropical Cyclone Adeline-Juliet on 9 April 2005. The storm developed over the Indian Ocean and never threatened any landmass. The centre of the storm had a well-defined eye and spiral bands (Source: NASA earth observatory, 2005).

Table 1.1: The Saffir-Simpson wind scale based on a Tropical Cyclones Maximum Sustained winds. The scale has been adopted from the National Hurricane Website (Source: National Hurricane Center, 2013).

Category	Maximum Sustained Winds	Types of Damage Due to Tropical Cyclone Winds
1	119-153 km/h	**Very dangerous winds will produce some damage:** Well-constructed frame homes could have damage to roof, shingles, vinyl siding and gutters. Large branches of trees will snap and shallowly rooted trees may be toppled. Extensive damage to power lines and poles likely will result in power outages that could last a few to several days.
2	154-177 km/h	**Extremely dangerous winds will cause extensive damage:** Well-constructed frame homes could sustain major roof and siding damage. Many shallowly rooted trees will be snapped or uprooted and block numerous roads. Near-total power loss is expected with outages that could last from several days to weeks.
3 (major)	178-208 km/h	**Devastating damage will occur:** Well-built framed homes may incur major damage or removal of roof decking and gable ends. Many trees will be snapped or uprooted, blocking numerous roads. Electricity and water will be unavailable for several days to weeks after the storm passes.
4 (major)	209-251 km/h	**Catastrophic damage will occur:** Well-built framed homes can sustain severe damage with loss of most of the roof structure and/or some exterior walls. Most trees will be snapped or uprooted and power poles downed. Fallen trees and power poles will isolate residential areas. Power outages will last weeks to possibly months. Most of the area will be uninhabitable for weeks or months.
5 (major)	252 km/h or higher	**Catastrophic damage will occur:** A high percentage of framed homes will be destroyed, with total roof failure and wall collapse. Fallen trees and power poles will isolate residential areas. Power outages will last for weeks to possibly months. Most of the area will be uninhabitable for weeks or months.

Table 1.2: Météo-France Tropical Cyclone Wind Scale. The damage potential of winds is based on the Beaufort wind force scale (Source: Rowlett, 2001).

Category	**Maximum Sustained Winds**	**Damage Potential (Beaufort Wind Scale)**
Tropical Disturbance	<50 km/h	Large tree branches moving, umbrellas used with difficulty.
Tropical Depression	51-62 km/h	Whole trees in motion, difficulty walking against the wind.
Moderate Tropical Storm	63-88 km/h	Twigs breaking of trees and slight structural damage.
Severe Tropical Storm	89-117 km/h	Trees uprooted , considerable wide spread structural damage
Tropical Cyclone	118-165 km/h	Considerable and widespread damage to structures
Intense Tropical Cyclone	166-212 km/h	Not generally seen on land but super catastrophic damage.
Very Intense Tropical Cyclone	212 km/h or higher	

1.2 The Structure of a Tropical Cyclone

TCs are characterized by nearly cloud-free regions near their centre, called the eye. In the centre of the storm, air sinks forming the "eye" of the storm which is relatively warm with light winds and clear or broken clouds (Figure 1.2). According to the National Weather Service (2010), the eye is typically 32-64 km wide in diameter and usually develops when the TC becomes more organized when MSWs reach ~118 km/h. Upon reaching TC status (118 km/h), the substantial rotation of air around the TC balances inflow into the centre causing air to rise to about 16-35 km from the centre forming the eyewall (National Weather Service, 2010). Near the eyewall, intense convection and strong updrafts (~5-10 m/s) are often found. As a result, the eyewall is generally the location of maximum winds, thunderstorms and torrential rain.

According to the National Weather Service (2010), the eyewall of a TC can grow or shrink in size and concentric (double) eyewalls can form. As a result, changes in the anatomy of the eye and eyewall can instigate changes in wind speeds which determine the intensity of the storm. Radially outward of the eyewall, a region of predominantly stratiform precipitation can be found. Continuing radially from the moat region, mature TCs often possess secondary eyewalls. The secondary eyewall formation is associated with high values of potential intensity, small values of vertical wind shear, a deep thermocline, weak upper tropospheric zonal winds, and middle to upper relative humidity (Kossin and Sitkowski, 2009). In addition to that, the formation of a secondary eyewall may temporarily interrupt the intensification of a TC by cutting off the radial inflow into the inner eyewall.

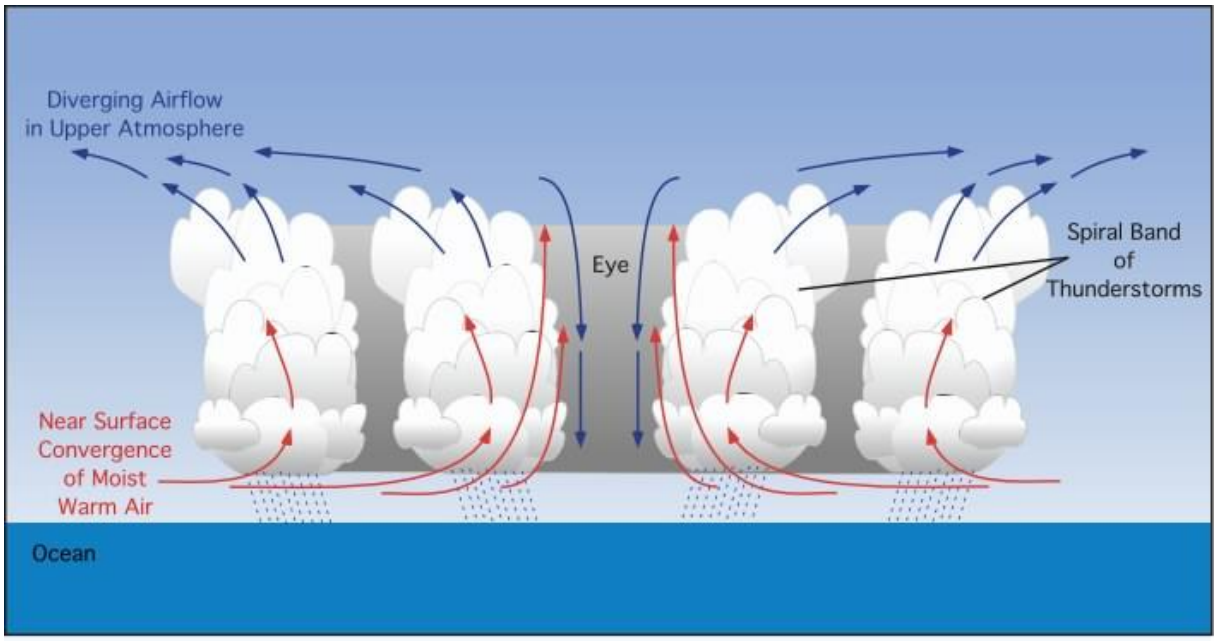

Figure 1.2: The vertical cross-section view of the air circulation, eye, spiral band of thunderstorms and precipitation of a typical Tropical Cyclone (Source: PhysicalGeography.net, 2014).

Beyond the secondary eyewall is an area of heavy rains and squall of winds and tornadoes called rainbands. The raindbands can be further characterized as principal, secondary or distant (Figure 1.3). Principal rainbands are generally found close to centre of the storm (<200 km) and are characterized by convective cells embedded in stratiform precipitation and spiral inward towards the TC centre (Didlake Jr *et al*., 2009). Interestingly, these rainbands remain relatively stationary (i.e. they do not rotate around the TC to a significant extent). Furthermore, these raindbands can continue to impact the overall TC by strengthening the storm through the generation and advection of potential vorticity to the centre or weaken the storm by hindering the inflow of warm, moist air. Radially inward of principal rainbands, secondary rainbands can be found and often, the two intersect each other. Furthermore, secondary rainbands have characteristics of vortex Rossby waves since they propagate cyclonically and outward at the rate of speed much less than the mean tangential flow of the TC (Chen and Yau, 2001). Radially outward of the inner core of a TC, distant rain bands occur where the environmental convective available potential energy (CAPE) is largest and are characterized by significant vertical motion and lightning activity. In addition to that, tornadic activity is also possible along distant rain bands implying a predominantly convective nature in this area.

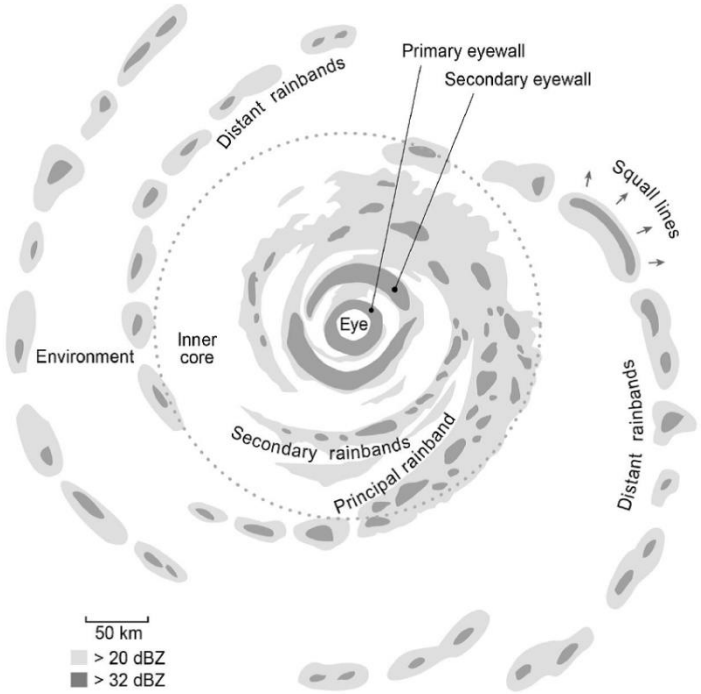

Figure 1.3: Top view radar reflectivity (in dBz) image of a Northern Hemisphere Tropical Cyclone with a concentric eyewall. (Source: Houze, 2010).

1.3 The Nomenclature of Tropical Cyclones

Some TCs have been named for the holiday they occurred on e.g. Labour Day Hurricane of 1935 (Knowles, 2009), the saint's days of which they made landfall e.g. Hurricane Santa Anna of 1825 (Fitzpatrick, 2006) or their intensity e.g. the Big Blow of 1913 also known as the White Hurricane (NOAA, 2013). Before the 1940's, forecasters used latitude and longitude identifications for naming TCs. However, the naming convention was somewhat impractical to use and often confusing when multiple storms were present. In order to solve the issues regarding latitude and longitude identifications, an Australian meteorologist by the name of Clement Wragge pioneered the naming of cyclones. Wragge originally used Greek letters and mythical characters from Greek and Roman mythology to designate various TCs. Later on, Wragge amusingly used the names of politicians he was not fond of and as a result, he was able to aggressively declare in forecasts that the politicians were "causing great distress" or "wandering aimlessly about the Pacific" (Landsea and Dorst, 2014). He is also credited as the first person to give cyclones female names. During World War II, meteorologists in the North West Pacific informally named cyclones after their girlfriends and

wives (Landsea and Dorst, 2014). This queer practice was inspired by the 1941 book "Storm" by George Stewart, where a junior meteorologist named Pacific extratropical storms after former girlfriends (Landsea and Dorst, 2014). This tradition became popular and well established and in the beginning of 1945, North West pacific storms were officially given female names. In 1950, Atlantic storms were named according to military phonetic alphabets (e.g. Able, Baker, Charlie). Three years later, the US Weather Bureau changed this to a female list of names with an addition of male names in 1979. In recent years, the lists of names which are predetermined and rotated every six years have been further diversified to reflect the many regions where cyclones form. However, names of devastating cyclones with major loss of life and economic impact such as Katrina in 2005 and Andrew in 1992 are permanently retired.

Although the origin of naming TCs is rather whimsical, presently, there are strict procedures in determining a list of TC names in an ocean basin by the TC regional body responsible for that basin (World Meteorological Organization, 2015). According to the World Meteorological Organization (2015), there are five TC regional bodies, i.e. ESCAP/WMO Typhoon Committee, WMO/ESCAP Panel on TCs, Regional Association 1 (RA1) TC Committee, RA IV Hurricane Committee, and RA V TC Committee. Over the SWIO, the RA1 TC committee (established in 1974) is responsible for formulating a list of TC names and boasts a membership of 15 countries (i.e. Botswana, Comoros, France, Kenya, Lesotho, Madagascar, Malawi, Mauritius, Mozambique, Namibia, Seychelles, South Africa, Swaziland, Tanzania and Zimbabwe). In addition, the RA1 committee pre-designates a list of TCs names for 6 years separately at its annual session. The importance of this naming is to facilitate TC disaster risk awareness, preparedness, management and reduction (World Meteorological Organization, 2015). However, Unlike Wragge, the RA1 committee does not name TCs after any particular person.

1.4 Seasonal Occurrence of Tropical Cyclones

TCs are a seasonal phenomenon, with 80-90 forming around the globe annually. In addition to that, in most ocean basins, the maximum frequency of TC occurrence happens during late summer to early autumn (Henderson-Sellers *et al*., 1998). According to Frank and Roundy (2006), the six major basins in which TCs generally occur are the (1) North Indian Ocean, (2) South Indian Ocean, (3) North West Pacific Ocean, (4) South Pacific Ocean, (5) North East Pacific Ocean and (6) North Atlantic Ocean (Figure 1.4). The western North Pacific typhoon season runs from May to November with peak TC activity in August (World Meteorological

Organization, 2015). In addition to that, the western North Pacific is the only region where TC genesis has been observed in all the months of the year (Henderson-Sellers *et al*., 1998). In the Americas, hurricane season is typically from June to November and peaks between August and September. Over the Bay of Bengal (BoB) and Arabian Sea, TC season runs from April to June, and September to November respectively. In the South Pacific as well as the Indian Ocean, TCs usually occur from November to April. The late summer to early autumn period in which TC activity is prevalent, is associated with periods of maximum Sea Surface Temperatures (SSTs), which are key to the development of TCs (Henderson-Sellers *et al*., 1998).

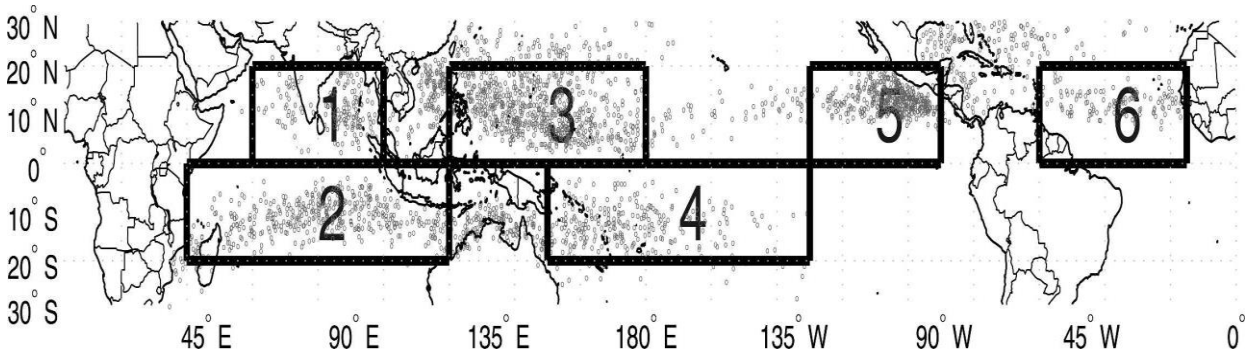

Figure 1.4: The six major cyclone basins outlined by the rectangular boxes, namely (1) North Indian Ocean, (2) South Indian Ocean, (3) North West Pacific Ocean, (4) South Pacific Ocean, (5) North East Pacific Ocean and (6) North Atlantic Ocean. The dots present genesis locations for the individual storms between 1974-2002 (Source: Frank and Roundy, 2006).

SWIO TCs mainly occur from November to April with an average of 10.6 TCs per year (Henderson-Sellers, 1998). The SWIO has a prevalence of TCs in January and February which is simultaneous with the peak austral summer. However, Intense TCs (ITCs), category 3-5, are more common from late summer to early autumn (February-April) than from late spring to summer (November to January) (Mavume *et al*., 2009). In addition to that, ITCs are less common over the Mozambique Channel (hereafter MC) in comparison to the SWIO basin as a whole. SWIO TCs typically form when the mean SST is 29.25°C over the basin, but near the MC, a higher mean SST value, approximately 29.75°C, is required. Moreover, cyclones that occur in the eastern parts (80-100°E) develop at lower SSTs (28.25-29.75°C) than those in the western parts (50-80°E) with SSTs between 29.25°C and 30.25°C.

1.5 Impact of Tropical Cyclones

TCs and associated storm surges are amongst the most devastating natural disasters (Girishkumar and Ravichandran, 2012). They cause unusual flooding (Figure 1.5), damage properties (Figure 1.6) and cause loss of human lives (Badarinath *et al.*, 2012; Girishkumar and Ravichandran, 2012). Over the SWIO (0-40°S; 30-75°E), TCs are a huge threat to people, animals and properties in the central and northern coasts of Mozambique and Madagascar, where strong winds, heavy rainfall and flooding associated with landfalling TCs takes place on an almost annual basis (Mavume, 2008). According to Mavume (2008), Mozambique and Madagascar have coastlines of approximately 2700 and 4800 km respectively and more than 60% of their population reside in coastal areas, feeding on rain-fed farming and fishing. In consideration of the coastal communities, TC associated storm surges of up to 5 m may occur along the coastline, further aggravating the devastation and lead to social and economic concern. Furthermore, Maputo's port, its rail links and oil facilities, which are on an estuary, are also subject to flooding from these storms (IRIN, 2015a).

Figure 1.5: People crossing a flooded road in the Sabotsy Namehana commune, north of Antananarivo Madagascar on the 14 of February 2012 after Intense Tropical Cyclone Giovanna pounded Madagascar (Source: Al-Imdaad Foundation, 2015).

TCs form over open oceans where they hardly cause severe damage; however, the greatest threat is when they make landfall. Between 1952 and 2007, 152 cyclones out of a total of 633 in the SWIO made landfall in Madagascar and Mozambique (Mavume *et al.*, 2009). For example, in late February 2000, floods in the wake of TC Eline caused approximately 2 million people to be displaced and about 600 people died (Mavume, 2008). On February 22 2007, TC Favio made landfall on the southern coast of Mozambique as a category 3 cyclone after developing in the South Indian Ocean a week earlier (Klinman and Reason, 2008). Klinman and Reason (2008) reported that Favio worsened an already occurring flooding situation and led to the deaths of 4 people and injured 70. Businesses, hospitals and schools were destroyed as well as a prison from which 600 inmates escaped. In addition, the flooding displaced over 120000 people in Mozambique. More recently, TC Haruna pounded heavily on Madagascar on February 25 2013. The islands National Disaster Risk Management Office reported that more than 17000 people were affected by the storm with 13 reported deaths and approximately 1500 homes destroyed or flooded (IRIN, 2015b).

Figure 1.6: Boats piled up at Port Hinchinbrook Australia in the aftermath of Severe Tropical Cyclone Yasi (2011) (Source: News.com.au, 2014).

1.6 Impact of Sea Surface Temperature Variability

Although Sea Surface Temperatures (SSTs) are not the dominant factor that determine TC intensity (Evans, 1993; Mavume *et al*, 2009), they play an important role in the formation of TCs (Palmén, 1948). In light of that, SST oscillations such as the El Niño Southern Oscillation (ENSO), Indian Ocean Dipole (IOD) and the South Atlantic Subtropical Dipole (SASD) have been shown to directly or indirectly impact TC activity in various ocean basins (Carmargo and Sobel, 2005; Saha and Wasimi, 2013; Rodrigues *et al*., 2015). On a global scale, ENSO is one of the most important coupled ocean-atmosphere phenomenon affecting interannual climate variability. ENSO consists of three phases: El Niño (the warm or positive phase), the neutral phase and La Niña (the cold or negative phase). During El Niño, anomalous west to east winds form and drive warm equatorial waters from the western Pacific towards the eastern Pacific and the northern parts of South America. However, in the neutral phase, the trade winds blow westward on the ocean surface resulting in a westward current. Additionally this wind flow during the neutral phase is intensified during La Niña.

Although ENSO plays an important role on climate variability on a global scale, the IOD plays an important role in the interannual climate variability in the Indian Ocean (Saji *et al*., 1999). The IOD is characterized by positive SST anomalies in the North West Indian Ocean with anomalously low SSTs in the eastern Indian Ocean. During a positive IOD event, anomalous winds blow south-eastward from Sumatra and from east to west along the equator. This in turn causes heavy rainfall over east Africa and severe droughts over the Indonesian region (JAMSTEC, 2010). Moreover, the IOD plays an important role as a modulator of the Indian monsoon rainfall (Ashok *et al*., 2001). Over the South Atlantic, the SASD is the dominant mode of coupled ocean-atmosphere variability and is characterized by a dipole-like pattern of SST anomalies oriented northeast-southwest and a monopole structure in the sea level pressure (Rodrigues *et al*., 2015). Apart from the South Atlantic, the SASD mode has an important role over the South Indian Ocean in strengthening the South Indian Ocean High Pressure system (also known as the Mascerene high) during its positive phase (Morioka *et al*., 2012). This strengthening of the Mascerene high may possibly inhibit TC formation due to suppression of convection which is intrinsic to cyclogenesis.

1.7 Numerical modelling of Tropical Cyclones

Early modelling experiments have shown the applicability of Global Climate Models in simulating TCs (e.g. Manabe *et al*., 1970; Bengtsson *et al*., 1995; 1996; Vitart *et al*., 2003). However, most of them are based on the simulation of TC-like structures in low-resolution (more than 100 km) Global Climate Models (hereafter GCMs) and coupled ocean-atmospheric models. Some of the characteristics of those low-resolution model cyclones, such as the spatial and temporal distribution, resemble, to a certain degree, observed TCs. However, the main limitation with these model cyclones is that the intensities of the simulated TCs are weaker and the spatial scales are larger than observed TCs due to the low-model resolution (Vitart *et al*., 1997). This limitation on horizontal resolution makes it difficult to describe small-scale features, which are characteristic of the inner parts of TCs and are indicative to their intensification. However, at 100 km horizontal resolution, GCMs exhibit skill in simulating some aspects of the structure of TCs as well as the spatial distribution and seasonal variability. Moreover, in certain areas, particularly in the north-east Pacific, a more realistic number of TCs is only generated by a GCM when the horizontal resolution is finer than 100 km; apparently, this is due to a finer orographic detail and well described coast lines (Bengtsson *et al*., 1995; 1996).

Unlike most early GCMs, Regional Climate Models (RCMs) can be run at resolutions that allow representation of small scale processes within TCs (less than 60 km) but with limitations on model domains. However, it is well known that TCs are governed by large-scale systems that operate on spatial scales of thousands of kilometres (Gray, 1979), which have an impact on RCM domains. As a remedy for the limitations on the domain, RCMs are often coupled with lower resolution GCMs, e.g., Mbedzi (2010), in order to study large scale systems but these often lead to errors in the boundary forcing. This in turn leads to a weak representation of large-scale processes like El Niño Southern Oscillation (ENSO) and Madden–Julian oscillation (MJO) which are known to drive TC activity (Ho *et al*., 2006). Recent attempts have been made to resolve low-resolution issues on GCMs by employing high resolution GCMs (Smith *et al*., 2010; Zhao and Held, 2012; Strachan *et al*., 2013, Bell *et al*., 2014). However, most of them use high uniform resolution throughout the globe which has a lot of impact on computing time and resources, and is not ideal for the nations of the Southern African Development Community (SADC) due to financial and resource constraints. In light of that, not much has been done in utilizing variable resolution GCMs with grid stretching capabilities to study TCs over the SWIO. This will be beneficial for SADC nations in terms of reducing simulation costs involved with high uniform resolution GCMs.

Bengtsson *et al.* (1995) established that T106 (125 km) resolution provided a realistic geographical distribution of TCs. In addition to that, the structure of the simulated storms agreed well with observation. However, the authors noted that finer resolutions (less than 100 km) may improve the realism. Therefore, evaluating the GCMs simulation using a high resolution stretched-grid (less than 60 km) over the area of interest (0-40°S; 30-75°E) (Figure 1.7) whilst keeping the surrounding areas at a lower resolution may help in better representation of SWIO TCs. Such knowledge will improve the understanding of TC activity over the SWIO.

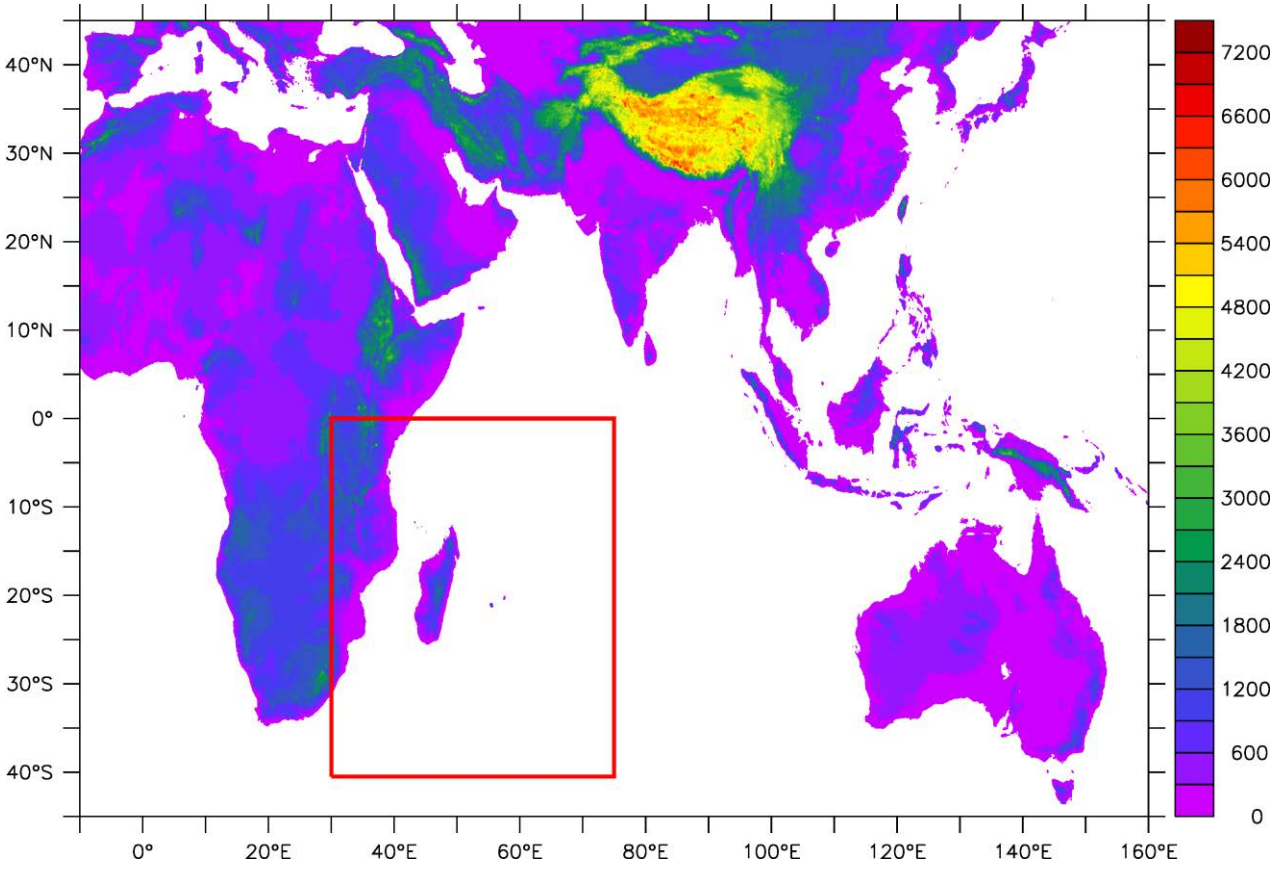

Figure 1.7: Topographical map (in metres) showing the South West Indian basin defined by coordinates 0 – 40°S; 30– 75°E and highlighted by the red box.

1.8 Aim and Objectives

The aim of the present work is to evaluate the performance of a GCM with adaptive grid stretching in simulating the characteristics of TCs over the SWIO basin. In the SWIO, this is important for the vulnerable nations of Mozambique and Madagascar which face high risks of damage and loss of life from these systems (Klinman and Reason, 2008). Both of these countries are amongst the developing countries in the world and their high vulnerability to TCs further compounds the socio-economic issue. This serves to emphasize the need for more thorough understanding of these systems. Therefore, the objectives of the study are to:

- Evaluate the ability of a stretched-grid GCM in simulating the climatology of the SWIO basin during the TC season (November -April).

- Examine how well the stretched-grid GCM simulates TC structure, intensity, interannual and seasonal variability as well as the spatial distribution of genesis locations and tracks.

- Study how TC occurrence varies during El Niño Southern Oscillation (ENSO), Indian Ocean Dipole (IOD) and the South Atlantic Subtropical Dipole Mode (SASD).

The present work is divided into 5 chapters. Chapter 2 reviews literature pertaining to TCs as well as the controversies surrounding the subject. Chapter 3 describes the observations, reanalysis and simulated datasets used in the study as well as the methods. The results of this study are discussed in Chapter 4 followed by the conclusion in Chapter 5.

2 LITERATURE REVIEW

This chapter reviews the relevant literature pertaining to the study of Tropical Cyclones (TCs) for this dissertation. The formation of TCs are discussed in section 2.1 followed by the impact of equatorial waves on TC formation in section 2.2. The impact of Land Use Land Cover on TCs is discussed in section 2.3 while section 2.4 discusses the impact of large-scale Sea Surface Temperature parameters on TC activity. Literature on TC simulation studies using climate models is discussed in section 2.5 followed by section 2.6 which discusses studies relating to TC detection and tracking algorithms in gridded datasets.

2.1 Formation of Tropical Cyclones

An early study by Palmén (1948) showed that TCs are likely to form in oceanic regions where the surface water exceeded 26-27°C, which provides the necessary heat energy for TC development. In addition to that, Palmén (1948) stated that no cyclones can be formed in the immediate vicinity of the equator where the planetary vorticity is zero. That is because TCs represent areas of large cyclonic vorticity produced by the convergence of air. Gray (1968) suggested the following physical parameters necessary for TC formation:

i) Large values of positive (negative) low-level relative vorticity in the northern (southern) hemisphere. TCs spin clockwise in the southern hemisphere and spin anti-clockwise in the northern hemisphere due to the Coriolis force hence the difference in the sign of the vorticity value.

ii) A distance which is several degrees of latitude away from the equator where there is an adequately large planetary vorticity.

iii) Weak vertical wind shear of the horizontal winds in order to promote the formation of an upright vortex that is resilient to the infiltration of cool, dry air from the external environment.

iv) Conditional instability via a deep tropospheric layer in order to advance the development of a deep, moist convection in the area of a tropical disturbance.

v) Large values of relative humidity in the middle and lower troposphere in order to obliterate the effects of convectively-generated downdrafts upon the lower tropospheric circulation of a tropical disturbance.

vi) Sea Surface Temperatures (SSTs) exceeding 26°C and a deep thermocline.

Gray (1968) defined the product of (i), (ii) and (iii) as the dynamic potential for cyclogenesis and the product of (iv), (v) and (vi) as the thermodynamic potential. Moreover Gray (1998) stated that the product of the dynamic and thermodynamic potential specified a seasonal genesis parameter which gives a good estimate of the long-term TC frequency occurrence in almost all ocean basins. Gray (1968) also stated that each physical parameter is multiplicative, meaning that all the parameters must be met in order for a TC to form. However, Henderson-Sellers (1998) argued that the aforementioned physical parameters are all necessary but not sufficient for TC genesis.

2.2 Impact of Equatorial Waves on Tropical Cyclone Formation

Equatorial waves have been shown to influence TC formation by a number of studies, but with some controversy. Frank and Roundy (2006) showed that three classes of equatorial waves were significant in the annual cyclogenesis of TCs within the six major cyclone basins (i.e. North Indian Ocean, South Indian Ocean, North West Pacific Ocean, South Pacific Ocean, North East Pacific Ocean and North Atlantic Ocean). These wave types include the Madden-Julian Oscillation (MJO), equatorial Rossby (ER) waves and high-frequency westward-moving waves and tropical-depression-like disturbances (MRG-TD-type). According to Frank and Roundy (2006), the MJO heightens both the convergence and low-level vorticity at the area of formation and ER waves also strengthen cyclogenesis by enhancing the rotation and convection and also cause significant easterly shear anomalies at genesis locations in approximately half of the ocean basins. However, Frank and Roundy (2006) noted that the South Indian Ocean (SIO) shows no tendency to form TCs when the basin has enhanced MJO or ER but shows a weak inclination for TC genesis when the MRG-TD-type is above normal. Interestingly, using the methodology of Wheeler and Hendon (2004) in categorizing MJO phases, which is based on the empirical orthogonal function (EOF) examination of equatorially averaged (15°S-15°N) daily zonal wind at 850 and 200hPa as well as satellite retrieved outgoing longwave radiation, Ho *et al*. (2006) found that TC activity in the SIO is enhanced in phases 2-4 (approximately 10 TCs in 100 days) while there was less TC frequency in the rest of the phases (about 5 TCs in 100 days). Bessafi and

Wheeler (2006) found a large and compelling modulation of SIO TCs by the MJO and ER waves. It is worth noting that earlier studies by Waliser *et al*. (2003) and Wheeler and Weickmann (2001) asserted that both MJO and ER waves can be predicted several days to a few weeks in advance, thus expanding TC predictability techniques for numerical forecast models. This contradicts the finding of Frank and Roundy (2006) that demonstrates that the South Indian Ocean (SIO) shows no tendency to form TCs when the basin has enhanced MJO or ER

2.3 Impact of Land Use Land Cover on Tropical Cyclones

Land Use Land Cover (LULC), one of the dynamical features that undergoes change due to human impact on the environment (Badarinath *et al.*, 2012) , has been shown to impact land falling TCs by a number of studies. These human induced impacts on the environment include the colonization of coastal lands, deforestation, degradation of dry lands, landscape fragmentation and rapid urbanization (Lambin and Geist, 2007). Betts *et al.* (1996) stated that land surfaces affect the weather via the exchange of heat, moisture and momentum between the atmosphere and the earth's surface. In addition to that, Badarinath *et al.* (2012) asserted that LULC changes influence surface winds, temperature and humidity, which in turn affects the Planetary Boundary Layer (PBL).

When TCs make landfall, most of the damage caused by winds occur within the first few hours. This is when the wind fields change rapidly due to changes in the surface conditions, which are characterized by the rapid decrease in the TCs intensity due to the surface friction (Zhu, 2008). However, Wakimoto and Black (1994) pointed out that an increase in surface friction can heighten cross isobar inflow which in turn will lead to increased convergence and TC intensification. Furthermore, Zhu (2008) stated that TC damaging winds can still possess their strength inland which indicates the complication of the decaying process of land falling TCs. Moreover, there are other processes that play a part in strengthening TC winds or slowing down the decay (Zhu, 2008). Wong and Chan (2006) showed that friction, but not surface-moisture flux over land, was essential for TC movement towards land. However, Wakimoto and Black (1994) showed that the intense damage caused by Hurricane Andrew (1992) after landfall may be attributed to the high surface evaporation due to its path over the Everglade swamps. In accordance with that, Shen *et al*. (2002) demonstrated that interior waters reduce the decay of land falling TCs due to the heightened inland surface evaporation. However, Zhu (2008) reasoned that since surface evaporation is largely driven by surface winds, weak surface winds may reduce the surface evaporation even though there is inland

water present. Furthermore, Zhu (2008) pointed out that not all the processes that impact land falling TCs are well understood and there is presently insufficient knowledge about which of these tend to dominate the others in the intensification of land falling TC winds.

2.4 Impact of Large-scale Sea Surface Temperature parameters

2.4.1 El Niño Southern Oscillation

El Niño Southern Oscillation (ENSO) is the most important source of interannual variability in the tropics (Vitart *et al*., 2003), and its influence on TC activity in the various ocean basins has been studied over the years. Over the Atlantic, Gray *et al.* (1993) and Knaff (1997) showed that TCs are more prominent during La Niña years in comparison to El Niño years. In addition to that, ENSO affects TC intensity, genesis locations as well as the number of land falling TCs in the US (Carmargo *et al.*, 2007). In the western North Pacific, there is a south-westward (north-westward) shift of TC activity during El Niño (La Niña) years (Wang and Chan, 2002). This shift has been attributed to the eastward extension of the monsoon trough and westerlies in the western North Pacific as well as the reduction of vertical wind shear (Carmargo *et al*. 2007). In addition to that, during El Niño, TCs (referred to as Typhoons in the North Pacific) are likely to last longer and become more intense (Carmargo and Sobel, 2005). Over the central Pacific, TCs tend to form during the warm phase of ENSO in comparison to La Niña periods. In addition to that, more TCs occur near Hawaii. Chu (2004) attributed this to large values of low-level relative vorticity as well as small values of vertical wind shear present near Hawaii.

In the southern hemisphere, the climatology of SWIO TCs in relation to ENSO has been investigated in a number of studies, with disputes at times. A study by Kuleshov and de Hoedt (2003) found that TC numbers increased east of 70°E concurrently with the cold phase of ENSO whilst the opposite happens west of 70° during El Niño periods. Ho *et al*. (2006) also demonstrated a similar east-west dipole structure i.e. TC numbers increase in the western half of the SIO and decrease in the eastern half during El Niño in comparison to La Niña. However, they noted a border latitude of 75° to the dipole pattern in comparison to Kuleshov and de Hoedt (2003). Vitart *et al*. (2003) showed that the warm phase of ENSO increased the probability of positive zonal steering flow (averaged for 850-200 hPa) while the cold phase increased the probability of negative zonal steering flow over the SIO. The authors' result showed an increased risk of land falling TCs over Mozambique during La Niña years, simultaneous with a negative zonal steering flow, as compared to El Niño. However, Ash and Matyas (2010) argued that periods of strong westerly or easterly steering flow in the SWIO

should not be attributed exclusively to a La Niña or El Niño phase, but the concurrent Subtropical Indian Ocean Dipole (SIOD) phase should be considered. Interestingly, Vitart *et al.* (2003) noted that the impact of ENSO on the zonal steering flow does suffer notable exceptions. Mavume *et al*. (2009) asserted that more intense TCs (Category 3-5) over the SWIO formed during La Niña periods compared to El Niño. Jury (1993) and Bove *et al.* (1998) have attributed the suppressed activity of intense TCs during El Niño to a stronger vertical westerly shear and smaller upper layer anti-cyclonic vorticity which inhibits TCs from intensifying beyond category 2 status. Despite the aforementioned teleconnections between ENSO and TC activity, ENSO alone does not explain the interannual variation of TC activity (or intensity), although in combination with other atmospheric indices, may be important (Mavume *et al*., 2009, Ash and Matyas, 2010). The present study briefly examines the role of ENSO in combination with other atmospheric indices in modulating TC occurrence over the SWIO.

2.4.2 Indian Ocean Dipole

Since the discovery of the dipole mode in the Indian Ocean by Saji *et al*. (1999), the role of the Indian Ocean Dipole (IOD) with respect to TC activity has gained attention over the years. Singh *et al*. (2008) observed a negative and significant correlation between the IOD mode index from September to October and November with regards to TC frequency and suggested that with a lead time of 1 month, the IOD mode index could be a potential indicator of the intense cyclone of November over the Bay of Bengal (BoB). Similarly, Saha and Wasimi (2013) found a significant correlation between the previous month's dipole and the following month's occurrences of TCs over the Australian basin. Girishkumar and Ravichandran (2012) showed that a negative IOD phase may trigger Intense TCs over the BoB just as La Niña events do. Moreover, Francis *et al*. (2007) observed a TC-IOD feedback and suggested that the occurrence of severe TCs (April - May) over the BoB may activate a positive IOD event. They stated that after an occurrence of a severe TC over the BoB, there is an intensification of the south easterly wind flow off Sumatra and the reduction of the integrated water vapour content, which in turn leads to the suppression of convection over the eastern equatorial Indian Ocean (EEIO). The suppression of convection over the EEIO may lead to an enhancement of convection over the western equatorial Indian Ocean (WEIO), which in turn leads to a positive feedback over the EEIO, which may activate a positive IOD phase.

Despite the importance of the IOD in modulating TC activity over various ocean basins, there is a dearth of academic literature on the role of the IOD on SWIO TCs. A close attempt by

Ash and Matyas (2010) studied the impact of the Subtropical Indian Ocean Dipole (SIOD) on TC trajectories in the SWIO and found that TC activity over the SWIO is more prominent during simultaneous negative SIOD and positive ENSO periods. However, despite the author's findings, the SIOD is characterized by the Subtropical Dipole Index (SDI) which is not the same as the IOD which is characterized by the Dipole Index Mode (DMI). Therefore, much work still needs to be done in filling the gap in literature with regards to the IOD-TC association over the SWIO. The present study succinctly represents the first known investigation of IOD and TC occurrence over the SWIO.

2.4.3 South Atlantic Dipole

Although many studies over the years have been conducted on the South Atlantic Subtropical Dipole (SASD) mode (e.g. Venegas at al., 1997; Sterl and Hazeleger, 2003; Morioka *et al*., 2011, Rodrigues *et al*., 2015), there remains a large gap in the literature on the impact of the SASD on SWIO TCs. Despite the shortage in TC-SASD literature, there are a few studies that have looked at the link between SASD and ENSO, since it is well known that ENSO affects TC activity (Carmargo *et al*., 2007). However, the link between the SASD and ENSO has been controversial over the years. Fauchereau (2003) observed a very weak and insignificant link between ENSO and SASD, but Hermes and Reason (2005) found a significant relationship with a correlation of -0.64 at 99% confidence level. However, Hermes and Reason (2005) chose different areas to create the index, in comparison to Fauchereau (2003). Moreover, Hermes and Reason (2005) applied a 2-7-year filter on the SASD and ENSO time series, which may have partly contributed to the higher correlation. More recently, Rodrigues *et al*. (2015) examined that almost all SASD events happened during ENSO years for the period of 1950-2010, suggesting a relationship between the central Pacific ENSO events and the southern hemisphere through the Pacific-South American wave train (PSA). In addition to that, Rodrigues *et al*.(2015) disputed an earlier study by Ciasto *et al*.(2014) who found a weak link (correlation of 0.26) between the central Pacific ENSO and the atmospheric circulation over the southern hemisphere for the austral summer.

The aforementioned disputes may very well be linked to the inconsistencies found in the literature when calculating the ENSO and SASD indices. For example, as mentioned above, Hermes and Reason (2005) used a different area in comparison to Fauchereau (2003) in calculating the SASD index. Rodrigues *et al*. (2015) defined ENSO using the 3-month running mean SST anomaly for Niño 3.4 region (i.e. 5°N-5°S,120-170°W) whilst Ciasto *et al*.(2014) used SST anomalies averaged over 10°N-10°S,90-150°W which coincides with the

Niño-3 region. However, Rodrigues *et al*. (2015) argued that the central Pacific ENSO events are most capable in triggering SASD events in comparison to eastern Pacific ENSO events which do not affect circulation over the South Atlantic in a way that generates SASD events.

2.5 Tropical Cyclone Simulation in Climate Models

2.5.1 Global Climate Models

Past studies have shown that GCMs can reasonably produce the structure and tracks of observed TCs but with deficiencies. Manabe *et al*. (1970) was one of the first to show that a low-resolution GCM could produce TC-type vortices. However, Camargo *et al*. (2007) argued that these TC-type vortices are much weaker in amplitude and larger in scale in comparison to observed TCs due to low resolution. Vitart *et al*. (1997) found that a T42 GCM was able to simulate the physical structure of a TC that is qualitatively similar to observed storms. Moreover, Vitart *et al*. (1997) suggested that the realism of the structure of a model TC may depend on the model resolution as well as the model parameterization. This dependence on parametrization schemes was shown by Vitart *et al*. (2001) by observing that the T42 GCM simulated tropical-storm frequency, intensity, structure and interannual variability exhibit significant sensitivities to the convection parametrization. Bengtsson *et al*. (2007) demonstrated that the European Centre Hamburg Model 5 (ECHAM5) GCM at T159 resolution can simulate TCs realistically both in space and time. However, the model underestimated the intensities of the most intense TCs (based on their MSW). Despite these deficiencies, TC activity has been studied in GCMs for various purposes. One purpose is in understanding the influence of large-scale climate parameters on TC activity, and this has led to useful results (Carmago *et al*., 2007). For example, Carmago *et al.* (2007) stated that vertical wind shear and midlevel relative humidity are important in many basins especially the western North Pacific, the North Atlantic and the Southern Hemisphere in tropical cyclogenesis. The authors also observed that vorticity anomalies contribute substantially in the central Pacific (both north and south) where TCs tend to form near the equator during El Niño events. Another matter of interest has been the ability of GCMs in simulating the interannual variability of TCs. Although the relatively low-resolution of most GCMs lack in simulating individual TC tracks and intensities, some models exhibit skill in simulating the year-to-year variability (Bengtsson, 2001).

In recent times, high-resolution GCMs have been shown to adequately simulate TCs with some caveats (Chauvin *et al*., 2006; Oouchi *et al*., 2006; Yoshimura *et al*., 2006). Oouchi *et*

al. (2006) employed the Meteorological Research Institute (MRI)/ Japan Meteorological Agency (JMA) unified model at 20 km resolution and found that the model sufficiently produced the inner structures of a TC. However, even at 20 km, the model struggled to simulate ITCs (e.g. MSW of more than 216 km/h). It may be argued that the 20 km/h resolution may still be coarse to simulate the inner mesoscale features of TCs which play an important part to their intensities. On another hand, the use of the cumulus parametrization in the model may have had an effect on simulated TCs since Vitart *et al.* (2001) showed that moist processes play an important role in TC formation and development.

2.5.2 Regional Climate Models

Although GCMs can be run at very high resolution (e.g. 20 km as in Oouchi *et al*., (2006)), Regional Climate Models (RCMs) have been found to be more computationally economical than most high-resolution GCM simulations (Walsh and Watterson 1997; Landman *et al*, 2005). In light of that, RCMs have been found to simulate TCs that are more realistic than GCM simulated but still weaker than the observation (Walsh and Watterson 1997; Nguyen and Walsh, 2001). However both studies used a horizontal resolution of 125 km which is too coarse for TC simulations since the horizontal scale of a TC core as well as the rain-bands in the TC circulation is only tens of kilometre. Liu at al. (1997) conducted an experiment in simulating the inner-core structure of Hurricane Andrew (1992) using the Penn State–NCAR non-hydrostatic, two-way interactive, movable, triply nested grid (54,18 and 6 km) mesoscale model 5 (MM5) and found out that the MM5 showed considerable skill in simulating the structure, intensity and progression of Hurricane Andrew. Despite that, even at 6 km, the model showed some deficiencies in simulating the radius of the eye wall. However, one could also argue that these deficiencies may not necessarily derive from the models horizontal resolution but from the low-resolution (2°x2°) NCEP reanalysis that was used to initialize the model.

Although studies have shown that RCMs are more computationally economical that most GCMs, they suffer from notable deficiencies, mainly due to issues of nesting. In RCMs, the choice of domain size and horizontal resolution is typically a compromise between physical and computational consideration (Giorgi and Mearns, 1999). Giorgi and Mearns (1999) stated that the domain should be big enough to permit full development of internal mesoscale processes and include significant regional forcings and the resolution should sufficiently capture the scale and influence of these forcings. Moreover, the choice of domain size should encompass the areas that include forcings and climatic circulations which directly affect climate over the region of interest. Landman *et al*. (2005) investigated the influence of model

domain size and the positioning of its lateral boundaries on TC-like vortices using a 60 km horizontal RCM over the SWIO. They found out that the intensity of TC-like vortices is well simulated near the eastern boundary of the model domain but the TC-like vortices become weaker as they move westward. Moreover, they observed that the simulated low-level core temperatures exhibit a cold bias which in turn inhibits deep convection. This deficiency in the simulation may be due to the model domains over land since lateral boundaries over land may cause unrealistic surface energy budget calculations near the boundaries (Giorigi and Mearns, 1999). Another issue in RCMs is that the models are driven by time-dependant large-scale fields typically provided by GCM output in the intermediary region close to the lateral boundaries of the model domain. According to Giorgi and Mearns (1999), because of the lateral boundary forcing, the large-scale circulations simulated by a RCM do not differ considerably from the GCM forcings, notably, in the middle and upper troposphere.

2.5.3 Variable resolution Stretched-Grid GCMs

The use of Variable-resolution GCMs with a high-resolution stretched-grid over the region(s) of interest is a well-established technique in regional climate modelling and provides efficient means for regional downscaling to mesoscales (Fox-Rabinovitz *et al*., 2008). Stretched-grids where first used by Schmidt (1977) for spectral models and by Staniforth and Mitchell (1978) for grid-point models. A little over a decade later, the approach was adopted for short-term numerical weather prediction models by various climate modelling agencies in the US, Canada, France and Australia (Fox-Rabinovitz *et al*., 2008). The prevailing advantage of variable-resolution stretched-grid GCMs is that they are not dependant on lateral boundary forcings in comparison to RCMs and are free from the associated computational Lateral Boundary Condition (LBC) limitations (Fox-Rabinovitz *et al*., 2008). As a result, stretched-grid GCMs can be used for straightforward simulations as traditional GCMs and provide self-encompassing interactions between global and regional scales of motion as in traditional GCMs. In addition to that, variable-resolution stretched-grid GCMs are more computationally economical than uniform-grid high-resolution GCMs (Fox-Rabinovitz *et al*. 1997; Côté *et al*. 1998).

Although Variable-resolution stretched-grid GCMs have proven to be an invaluable tool in simulating TCs (Reed *et al*.,2012; Zarzycki *et al*.,2014) , there remains a dearth in literature for long-term studies of regional TC climatology over various basin, with the exception of the Atlantic basin (Chavin *et al*, 2006, Caron *et al*, 2011, Zarzycki and Jablonowki, 2014) . Chauvin *et al.* (2006) investigated the sensitivity of Atlantic TCs to anthropogenic warming

using a very high (0.5°x0.5° stretched-grid over the Atlantic basin) GCM simulation and found that the ARPEGE-Climate stretched-grid could simulate realistic TCs. However, the study did not investigate the intensity of the GCMs simulated TCs. Caron *et al*. (2010) used the Global Environmental Multiscale (GEM) model (increasing model resolution from 2° to 0.3° over the Atlantic basin) and showed an increase in realism of TCs as well as the improvements in the number, geographical distributions and overall track density in higher-resolution stretched-grid simulations. Despite that, none of the GEM model integrations produced storms stronger, based on MSW, than category 1. Zarzycki and Jablonowki (2014) employed the Community Atmosphere Model Spectral Element (CAM-SE) model (a hydrostatic variable-resolution GCM) over the North Atlantic with a stretched-grid nest of 0.25° and found that the 0.25° grid spacing simulates well the distribution of observed TC intensities and statistics. However the model struggled to simulate the interannual variability of TCs in comparison to the observation.

The application of variable-resolution GCMs in studying TCs over the SWIO has been very minimal. The only know study by Malherbe *et al.* (2012) used the conformal-cubic atmosphere model (CCAM) at 60 km horizontal resolution over the SWIO and found that the model captured the general spatial characteristics of observed TCs realistically for the 1961-1990 period. However, Mavume *et al.* (2009) pointed out that observation data before the Satellite era (1979) must be regarded relatively unreliable as it presents many missing values of TCs. Moreover, the realism of the TCs was compared to reanalysis instead of observation. Apart from inconsistencies in the reanalysis due to observational constraints before the satellite era, the changing mix of observations and biases in observation and models, can introduce spurious variability into reanalysis output (Wu *et al*., 2005).

2.5.4 CAM-EULAG MODEL

CAM-EULAG (CEU) has been shown to be a more computationally economical and efficient GCM as compared to GCMs with uniform high-resolution grids (Abiodun *et al*., 2008; Abiodun *et al*., 2011). GCMs are commonly governed by hydrostatic equations in order to simulate circulation dynamics. The grid resolution of these GCMs can be increased by increasing the computing power. As the grid resolution increases, non-hydrostatic dynamics become a factor (Abiodun *et al*., 2008). CAM3 can be run with a resolution of ~20 km but requires immense computational power. However, since all the present dynamical cores of CAM3 are hydrostatic, even at that resolution, CAM3 would struggle to resolve the stratiform region of a mesoscale convective system while the convective areas that require resolution on

the order of a kilometre would remain unresolved (Fritsch and Kain, 1993). Because CEU is a non-hydrostatic GCM, this makes it an optimal choice for future high-resolution runs especially when non-hydrostatic behaviour becomes a determinant.

There have been a handful of studies that have utilized CEU but none of them have done studies in TC simulation. Abiodun *et al*. (2008) conducted three aqua-planet simulations using CAM3 with each of the dynamic cores EULAG (CEU), finite volume (CFV) and Eulerian Spectral (CES). They found out that CEU adequately captured the result of CFV and CES and therefore suitable for climate simulations. Abiodun *et al.* (2011) compared the simulated rainfall between CEU and CFV over West Africa during the boreal summer from 1996 to 2006. The authors found that CEU outperformed CFV even at the same uniform grid of 2° x2.5°. Moreover, when the stretched-grid was applied, the results improved further. Ogier (2013) applied CEU to study the characteristics of inertial gravity waves over southern Africa and observed that CEU seemingly showed that the interaction between horizontal wind and topography is an important cause of inertial gravity wave activity over southern Africa. Driver (2014) studied rainfall variability over southern Africa and found out that CEU captured some of the essential features of rainfall over southern Africa, such as the band of precipitation associated with the ITCZ as well the area of minimum rainfall over the South Atlantic Ocean.

2.6 Numerical Detection and Tracking of Tropical Cyclones

The detection of simulated TCs from model output may be disputable and sometimes subjective. Over the years, a number of studies have been conducted with various climate models in demonstrating their ability in simulating TCs. While there is little dispute on the ability of the climate models in simulating TCs, these studies employed various techniques and threshold criteria for detecting simulated TCs (see Table A.1). In general, a typical TC detection and tracking algorithm starts by locating a minimum MSLP in order to define the centre of a potential TC (Suzuki-Parker, 2011). Potential storms are then filtered by the magnitude of the vorticity which is the minimum (maximum) vorticity field in the southern (northern) hemisphere. The wind speed criterion is also employed including a warm core and structural criteria. Each TC track is then filtered according to a duration criterion.

One of the first studies to employ a TC detection criterion for model TCs was Bengtsson *et al*. (1982) who employed the European Centre for Medium range Weather Forecasting (ECMWF) operational global forecasting model at a horizontal resolution of ~200 km. Their simplistic detection criteria used an 850 hPa wind speed criteria of >25 m/s and an 850 hPa

relative vorticity > $7.00x10^{-5}s^{-1}$ for identifying TCs. A little over a decade later, Haarsma *et al*. (1993) introduced a warm-core and duration (> 3days) criteria for TC detection but excluded the wind speed threshold and reduced the vorticity threshold to $>3.50x10^{-5}s^{-1}$. Bengtsson *et al*. (1995) adopted the same vorticity threshold used by Haarsma *et al.* (1993) as well as the warm-core and duration criteria but with modifications. In addition to that, Bengtsson *et al*. (1995) used a structural criteria in order to present better separation between simulated model TCs and extratropical low-pressure systems, which would have otherwise been detected spuriously as a result of the wind speed and vorticity criteria only.

In past years, many studies have used wind speed, relative vorticity, warm-core and duration criteria for detecting TCs. However, even at the same model resolution, there are notable differences in the threshold values in each parameter, especially for wind speed. For example, Walsh and Watterson (1997), Nguyen and Walsh (2001) and Sugi *et al*. (2002) used models with the same horizontal resolution (125 km) but employed a different wind speed criterion of >6-10 m/s at 10 m, >5m/s at 10 m and >15 m/s at 850 hPa respectively. Moreover, there is no universal agreement as to whether to use 850 hPa winds, near-surface or 10 m winds in TC detection algorithms and the choice is often not well justified in the literature. In an attempt to find a common ground, Walsh *et al*. (2007) suggested that all model wind speeds be corrected to 10-m since observed TCs are measured at a height of 10 m above the surface. However due to limited model resolution, the structure and intensity of simulated TCs are different from real TCs, therefore the selection criteria for model simulated TCs should not be the same as for observed TCs (Sugi *et al*., 2002). Walsh *et al*. (2007) also argued that the wind speed of criteria of >22m/s at 850 hPa corresponded to 17 m/s at 10 m, hence lowering the threshold of 22 m/s to 17 m/s on the 850 hPa winds would lead to an artificial increase in the number of TCs in the detection. However an earlier study by Oouchi *et al*. (2006) found that using 10 m surface winds with a threshold of 17 m/s was very stringent for simulating the observed annual global frequency of TCs and opted to use winds >17 m/s at 850 hPa which showed better agreement with the observation.

The warm-core criterion for detecting TCs also shows variability from one study to another. Some authors use the vertical mean temperature anomalies at various pressure levels (e.g. Chauvin *et al.*, 2006 ; Knutson *et al*., 2007 ; Stowasser *et al*.,2007), while some take the sum of the temperature anomalies at the various pressure levels (e.g. Walsh *et al*., 2004 ; Ouchi *et al*., 2006 ; Murukami and Wang, 2010). Surprisingly, Suzuki-Parker (2011) noted that the simulated frequencies of TCs from the aforementioned studies are very much similar to each

other. This is because the TC parameters in the various studies are tuned in such a way that the detected number of TCs produces a number closer to the observed count.

3 DATA AND METHODS

This chapter provides a description of the data and methods used for the present study. Section 3.1 details all the observation and reanalysis data. The model description and experimental setup is outlined in section 3.2 followed by section 3.3, which discusses the methods employed throughout the course of this study.

3.1 Data

This study analysed observation, reanalysis and model simulation data for the study period 1999-2010. In addition to that, Tropical Cyclones (TCs) are defined when the Maximum Sustained Wind (MSW) is greater than 32.78 m/s (~118 km/h) and storms that are identified as extratropical are excluded from the data used here since this study focuses purely on storms identified as TCs. The Joint Typhoon Warning Centre (hereafter JTWC) best track data observation is obtained online at http://www.usno.navy.mil/JTWC. The JTWC uses the Dvorak technique (Dvorak, 1984) to estimate TC intensity, which is based on the analysis of cloud patterns in visible and infrared satellite imagery. The best track data contains TC centre locations, the minimum centre pressure and Maximum Sustained Winds (MSWs) at 6-hourly intervals and is used to validate CAM-EULAG (CEU) and ERA-Interim (ERAINT) with regards to the spatial patterns of TC tracks, genesis locations, intensities, as well as the variation of TCs on a daily, monthly and annual time scale. Monthly observed precipitation was obtained from the Global Precipitation Climatology Project Version 2.2 (hereafter GPCP) and is obtainable from *http://www.esrl.noaa.gov/ps*. The GPCP data has a global spatial coverage and combines observations and satellite precipitation into 2.5°x2.5° global grids and is used to evaluate the ERAINT and CEU simulated rainfall over the South West Indian Ocean (SWIO) basin.

The Oceanic Niño Index (ONI) used in the study is a three month running mean of the Extended Reconstructed Sea Surface Temperature v4 (ERSST) SST anomalies in the Niño 3.4 region (5°N-5°S, 120°W-170°W) based on a 30-year based period. The El Niño (La Niña) periods are defined when the SST anomalies in the Niño 3.4 region are greater (smaller) than +0.5 (-0.5) °C. For the Indian Ocean Dipole (IOD), the dipole mode index (DMI) data is used to calculate positive/negative IOD phases and is defined as the difference in SST anomalies in the western (50-70°E, 10°S-10°N) and eastern (90-110°E,10°S-0°S) equatorial Indian Ocean.

A positive (negative) DMI event is identified when the SST anomalies are greater (smaller) than 0.47(-0.47) °C. The index is calculated relative to a climatological seasonal cycle based on the years 1982-2005. A more detailed description can be found at Saji *et al*. (1999). The South Atlantic Subtropical Dipole (SASD) mode index data is derived using the ERSST v3b in situ SST data and is defined as the difference in SST anomalies between 30-40°S, 10-30°W and 15-25°S, 0-20°W. Positive (Negative) SASD events are defined when the SST anomaly is 1 standard deviation above (below) the mean. The ERSST monthly analysis is available from January 1854 to the present. However, due to sparse data before 1880, there is a damping of the analysed signal. However, after 1880 the data is more consistent. The ERSST v3b analysis is the same as described in the ERSST v3 paper (Smith *et al*, 2008) with one exception i.e. ERSST v3b does not use satellite SST data. A summary of the indices is shown in Table 3.1. The aforementioned SST indices are used to investigate their potential impacts on TC activity over the SWIO.

Table 3.1: Description of the climate indices used in the study.

Abbreviation	Index Name	Period	Data Source
ONI	Oceanic Niño Index	1950-2015	http://www.cpc.ncep.noaa.gov/products/analysis_monitoring/ensostuff/ensoyears.shtml
IOD	Indian Ocean Dipole	1982-2005	http://stateoftheocean.osmc.noaa.gov/sur/ind/dmi.php
SASD	South Atlantic Subtropical Dipole	1854-present	http://www1.ncdc.noaa.gov/pub/data/cmb/ersst/v3b/netcdf

The monthly and 6-hourly reanalysis precipitation, wind, vorticity, vertical velocity and temperature data, which has a spatial resolution of 80 km (T255 spectral) on 60 vertical levels, is obtained from the ERA-Interim (ERAINT) dataset
(Available online at http://www.ecmwf.int/en/research/climate-reanalysis/era-interim) and is used to validate how well CEU simulates the climatology of the SWIO during TC season (November-April). More information about ERAINT can be found at Berrisford *et al.* (2011).

3.2 Model Description and Experiment

The model evaluated in this study is CEU. CEU is a non-hydrostatic global climate model with grid stretching capabilities that uses the Community Atmospheric Model Version 3 (hereafter CAM3) physics routines and Euler-Lagrangian (EULAG) dynamics. CAM3 is the fifth generation of the atmospheric model component of the Community Climate System Model (CCSM), which also includes land, ocean and thermodynamic sea-ice components. A complete description of CAM3 can be found in Collins *et al.* (2004). The physics package consists of moist processes, cloud and radiation calculations, surface models and turbulent mixing processes. A particular feature of CAM3 is the use of a microphysical parameterization scheme that is similar to cloud resolving models. However, higher grid resolution simulations (~20km) are required in order to take advantage of these advances than what the standard CAM3 offers (~200 km). CAM3 has a clean separation between the dynamics and physics parametrizations, which allows for relatively easier replacement of either set of subroutines. This separation allows for the replacement of the dynamical core by EULAG, a non-hydrostatic, parallel computational model for all-scale geophysical flows. The non-hydrostatic behaviour of EULAG is achieved through the anelastic approximation of the equations of motion which are solved in a EULerian (flux form) or a LAGrangian (advective form) framework. EULAG combines non-oscillatory forward-in-time (NFT) numerical algorithms with a robust elliptic Krylov solver. The key signature of EULAG is that it is formulated in generalized coordinates which in particular, enable grid adaptivity. These features give EULAG a novel advantage over the existing dynamical cores in CAM3 (Abiodun *et al*., 2008).

In the present study, the CEU model grid is stretched to a resolution of 0.5°x 0.5° (meridional x zonal) over the SWIO, 1°x 1° over much of the globe and 2° x 2.5° over the Pacific Ocean and poles (see Figure 3.1). The prevailing advantage of using a stretch grid is the ability to apply very high resolution over the area of interest in a global model without needing a substantial increase in computational power. The model simulation uses 26 vertical levels with an integration time step of 30s and a sample output rate of 6-hourly data. Due to the high resolution of the experiments as well as limitations on computational resources, rather than running one 11-year simulation, eleven 1-year simulations of 11 months each were run to create a climatology for the SWIO TC season. Each 1-year experiment was run from the 1st of August of the previous year until the first of July for each of the years from 1999 to 2010. Abiodun *et al*. (2008) showed that CEU reached statistical stationarity in approximately 40 days by looking at the time evolution of the zonal average of (a) zonal wind, (b) potential

temperature and (c) specific humidity in an aqua-planet simulation (Figure 3.2). In addition, Driver (2014) showed a similar spin-up time (40 days) when CEU was initialised with more realistic atmospheric conditions. Therefore, the first three months were discarded as spin-up (i.e. August, September, and October). The SWIO TC season months (November-April) were used for all the following analyses and discussions.

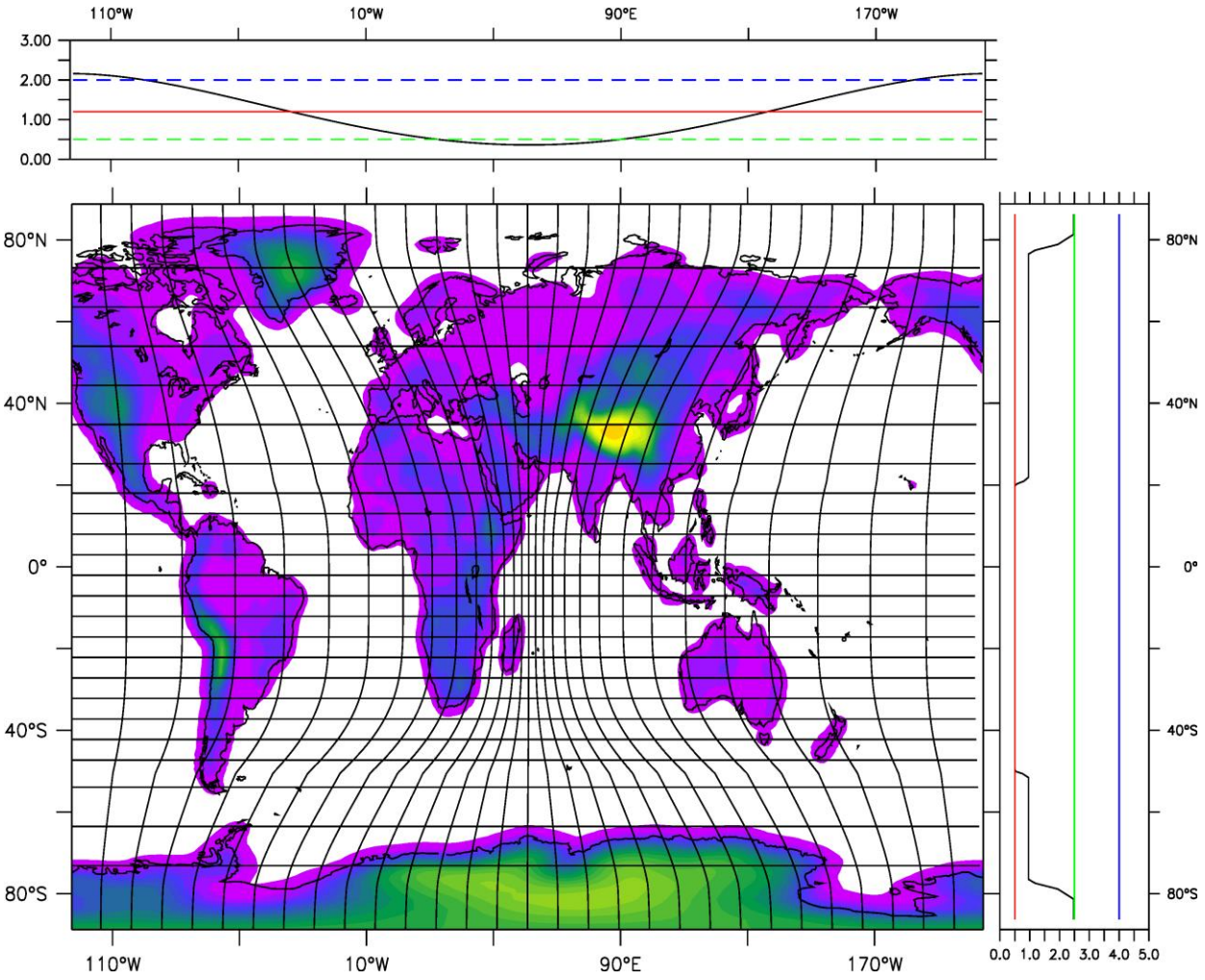

Figure 3.1: The CAM-EULAG model stretch grid setup with the highest resolution (0.5°x0.5°) over the South West Indian Ocean (0-40°S; 30-75°E).

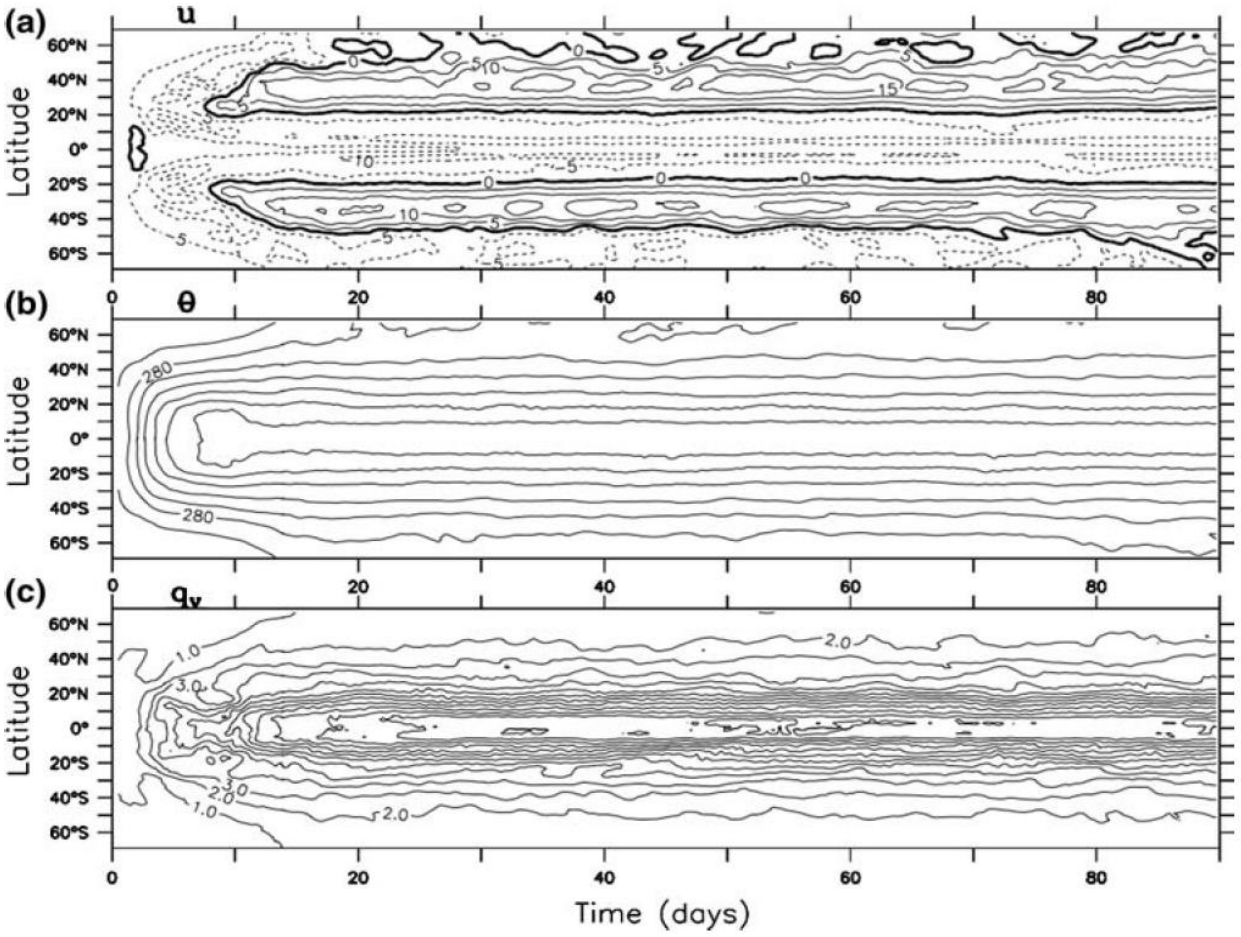

Figure 3.2: Time evolution of zonally averaged (a) Zonal Wind (u in m/s), (b) potential temperature (θ in K) and (c) specific humidity (q_v in g kg^{-1}) at 850 hPa (Source: Abiodun *et al*., 2008).

3.3 Methods

3.3.1 Tropical Cyclone Detection and Tracking Algorithm

An objective procedure for detecting and tracking TCs in this study uses a similar method to that described by Vitart *et al*. (1997), Kleppek *et al*. (2008) and Zarzycki and Jablonowski (2014). Candidate TCs were detected in 6-hourly ERAINT and CEU output as follows:

- The centre of a low-pressure system was detected by finding a closed minimum MSLP around an 8x8 grid. For each low-pressure system, the nearest minimum vorticity smaller than $-3.5 \times 10^{-5} s^{-1}$ was detected. This minimum must occur within 4° of the centre of the low-pressure system.

- The closest local maximum of 850 – 300 hPa average temperature is defined as the centre of the warm core. The average temperature must be greater than 0°C. The warm core is defined within 3° from the centre of the low pressure.

- If TCs make landfall, they weaken, which in turn complicates their tracking (Kleppek *et al.*, 2008). Therefore the wind speed at 850 hPa is used as the fourth parameter which is the same wind speed level chosen by Kleppek *et al.* (2008). The maximum wind speed within 5 degrees of the storms centre must be greater than 61.20 km/h (17 m/s) and must reach at least 118 km/h (32.73 m/s) during its lifespan. Furthermore, the wind speed threshold was scaled according to the resolution of the gridded data following the suggestion of Walsh *et al.* (2007).

Once the candidate TCs have been detected using the above mentioned criteria, TC tracks were computed as follows:

- Look for the closest storm within 500 km following the 6-hour period. (This translates to an average forward velocity of 83.33 km/h or 23.15 m/s). If no storm is detected, then the track of the detected storm is considered to have stopped. To be considered a full trajectory, the storm must persist for at least 2 days. Note, these do not have to be consecutive (Zarzycki and Jablonowski, 2014). In order to reduce broken tracks associate with weakening TCs, storms originating within 24-hours and 500 km of the previous storm's termination point are merged with preceding storm. These merged systems tend to be weakening TCs which fail to meet the TC detection criteria during intermittent 6-hourly intervals.

3.3.2 Performance Measures

The anomalous interannual trend in TC counts, which can either be positive or negative, can be regarded as a simple binary (dichotomous) event. These kinds of events are referred to as yes/no forecasts and represent the simple type of decision-making situation (Jolliffe and Stephenson, 2003). In the present study, the (2 x 2) contingency table of simulations (CEU and ERAINT) and observation is constructed for the TC anomaly binary event (see Table 3.2). The cell counts for each of the four possible combinations (hit, false alarm, miss and correct rejection) of the simulation and observed event are represented by *a, b, c* and *d* respectively (Table 3.3). The sum of all the events, $n = a + b + c + d$, is known as the sample size and according to Jolliffe and Stephenson (2003), is important for determining the amount of sample uncertainty in the verification statistics . The counts in Table 3.2 may be converted to relative frequencies by dividing by *n*, and then show the results as estimates of joint probabilities. However, it is better to use raw cell counts rather than relative frequencies since raw counts provide useful information about the number of events and are unlikely to be misinterpreted (Hoffrage *et al*., 2000). The approach in the present study uses raw counts.

A verification measure is any function of a forecast, observation, or their relationship. A performance measure is a verification measure that focuses on the correspondence between the forecast (simulation for the present study) and observation, either on an individual or collective basis Murphy (1997). With the aid of the abovementioned (2 x 2) contingency table, 8 performance measures (see Table 3.4) were used in the present study in order to evaluate the ability of the CEU and ERAINT in capturing the interannual variability of SWIO TCs. The performance measures include:

- **Hit rate:** *The fraction of observed "yes" events that were correctly forecast. Range: 0 to 1. Perfect score: 1.*

- **False alarm rate:** *The fraction of the observed "no" events that were incorrectly forecast as "yes". Range: 0 to 1. Perfect score: 0.*

- **Proportion correct:** *Measures the overall fraction of simulations that were correct. Range: 0 to 1. Perfect score: 1.*

- **False alarm ratio:** *The fraction of predicted "yes" events that did not occur. Range: 0 to 1. Perfect score: 0.*

- **Heidke skill score:** *Measures the fraction of correct forecasts after eliminating those forecasts which would be correct due purely to random chance. Range: -1 to 1. 0 indicates no skill. Perfect score: 1.*

- **Pierce's skill score:** *Measures how well did the forecast separate the "yes" events from the "no" events. Range: -1 to 1. 0 indicates no skill. Perfect score: 1.*

- **Gilbert's skill score:** *Measures the fraction of observed and/or forecast events that were correctly predicted and adjusted for hits associated with random chance. Range:-1/3 to 1. 0 indicates no skill. Perfect score: 1.*

- **Yule's Q (Odds ratio skill score):** *Measures the improvement of the forecast over random chance. Range: -1 to 0. 0 indicates no skill. Perfect score: 1.*

A complete description of the skill scores can be found at Jolliffe and Stephenson (2003).

Furthermore, the interannual variability of the observed, reanalysis and simulated TC anomaly patterns were also computed using phase Synchronization (η), defined by Misra (1991) as

$$\eta = \left(\frac{n'}{n}\right) \times 100\%$$

and is used to quantify how well the model simulates or capture the timing of each patterns. n' is defined as the number of years in which the simulations are in phase with the observation (i.e. both observed and simulated annual TC count anomalies are simultaneously positive or negative), while **n** is the total number of years in the study (i.e. 11 years). If the reanalysis or simulated TC occurrence anomalies are out of phase with the observation, **η** will be 0% (i.e. no synchronisation), while **η** will be 100% if all the simulations are in phase with the observation (i.e. perfect synchronisation). Several studies e.g. Araujo *et al*. (2014), Tozuka *et al*. (2014) have used synchronisation to evaluate the accuracy of phase changes between model and observed datasets.

The Accumulated Cyclone Energy (ACE) is used in this study to calculate the interannual variability of TC activity over the SWIO. ACE is an integrated measure of TC activity which combines intensity and duration (Bell *et al.*, 2000). ACE is defined as

$$\text{ACE} = 10^{-4} \sum v_{max}^2$$

Where v_{max} is the MSW (in knots) for a TC at a given time. The sum is taken over all 6-hourly time-steps during a TC's lifetime. ACE from individual TCs can be summed regionally in order to produce basin-wide statistics.

The non-parametric Spearman rank correlation was used in this study to calculate the correlation of ERAINT and CEU with respect to observation on the interannual variability of TC occurrence and TC days. Spearman's rank correlation was chosen since it does not assume that data is described by normal distribution. Furthermore, Spearman's rank correlation overcomes the effect of outliers and skewness by considering the rank of the data instead of the magnitude. The rank correlation is defined as

$$\rho = 1 - \frac{6\sum d_i^2}{n(n^2-1)}.$$

Where $\boldsymbol{n}$ is the sample size in each dataset and $\boldsymbol{d_i}$ is the difference between the ranks of corresponding values of two datasets.

Table 3.2: Contingency table for the number of CEU (black) and ERAINT (red) categorical events with respect to the observation (JTWC) in the study.

CEU (ERAINT)	Observation		
	Positive Anomaly	Negative Anomaly	Total
Postive Anomaly	*5 (4)*	*2 (2)*	*7 (6)*
Negative Anomaly	*1 (2)*	*3 (3)*	*4 (5)*
Total	*6 (6)*	*5 (5)*	*11 (11) = n*

Table 3.3: Schematic contingency table for a categorical binary event (positive/negative anomaly). The numbers of observations in each category are represented by *a, b, c* and *d* and *n* is the total.

Simulation	Observation		
	Positive Anomaly	Negative Anomaly	Total
Postive Anomaly	*a*	*b*	*a + b*
Negative Anomaly	*c*	*d*	*c + d*
Total	*a + c*	*b + d*	*a + b + c + d = n*

Table 3.4: A summary of the performance measures used in the study. A more complete description of each measure can be found at Joliffe and Stephenson (2003).

Performance Measure	Definition	Range of values
Hit rate, ***H***	$\boldsymbol{H} = \frac{a}{a+c}$	[0,1]
False alarm rate, ***F***	$\boldsymbol{F} = \frac{b}{b+d}$	[0,1]
False alarm ratio, **FAR**	$\mathbf{FAR} = \frac{b}{a+b}$	[0,1]
Proportion correct, **PC**	$\mathbf{PC} = \frac{a+d}{n}$	[0,1]
Heidke skill score, **HSS**	$\mathbf{HSS} = \frac{\mathrm{PC}-E}{1-E}$ $\quad \boldsymbol{E} = \frac{(a+c)(a+b)}{n^2} + \frac{(b+d)(c+d)}{n^2}$	[-1,1]
Peirce's skill score, **PSS**	$\mathbf{PSS} = \frac{ad-bc}{(b+d)(a+c)}$	[-1,1]
Gilberts skill score, **GSS**	$\mathbf{GSS} = \frac{a - \frac{(a+b)(a+c)}{n}}{a - \frac{(a+b)(a+c)}{n} + b + c}$	[-1/3,1]
Yule's **Q** (Odds ratio skill score)	$\mathbf{Q} = \frac{ad-bc}{ad+bc}$	[-1,1]

4 RESULTS AND DISCUSSION

This chapter presents the results of this study. Section 4.1 presents the model validation over the South West Indian Ocean (SWIO) followed by section 4.2 and 4.3 which discusses the structure and intensity of the simulated Tropical Cyclone (TC) respectively. Section 4.4 looks at the spatial patterns of TCs over the SWIO, which include tracks and genesis locations. The Monthly and Annual variation of TCs are discussed in section 4.5 and 4.6 respectively followed by section 4.7, which reports on the influence of large-scale sea surface temperature (SST) parameters.

4.1 Climatology of Tropical Cyclones over the South West Indian Ocean

Although previous studies have established the capability of CEU in simulating the climate over various regions (Abiodun *et al*., 2011; Ogier, 2012; Driver, 2014), none of them have evaluated the model over the SWIO region. Therefore, before examining the ability of the model in simulating TCs over SWIO, it is necessary to investigate how well the model reproduces the regional climate over the SWIO. For this, we compare the CEU simulation with GPCP and ERAINT. The validation focuses on how well CEU simulates the temporal and spatial variation of essential climatic features in temperature, rainfall, Mean Sea Level Pressure (MSLP), vorticity, vertical velocity and wind fields over the SWIO during the TC season (November-April).

4.1.1 Surface Temperature

There is a good agreement between CEU and ERAINT on the spatial distribution of temperature over the SWIO (Figure 4.1). The model captures the temperature gradient between the Tropics and Mid-latitude, and reproduces the temperature contrast between the continent and the ocean, as in ERAINT. There is a good agreement between CEU and ERAINT temperature values over the ocean. However, there are notable discrepancies between the simulated (CEU) and reanalysed (ERAINT) temperatures over the land, especially over the areas with high topography. The major discrepancies in the temperature field occur over Madagascar and over Lake Victoria (Figure 4.1), where CEU exhibits a cold bias (about -5^{o}C) and warm a bias (up to 4^{o}C), respectively. These discrepancies may be due to differences in how CEU and ERAINT resolve the topography over the continent. A

comparison of ERAINT results with Climatic Research Unit (CRU) observation of land temperatures show a close relationship between ERAINT and CRU (figure not shown), which further increases confidence in the ERAINT dataset as adequate for temperature validation.

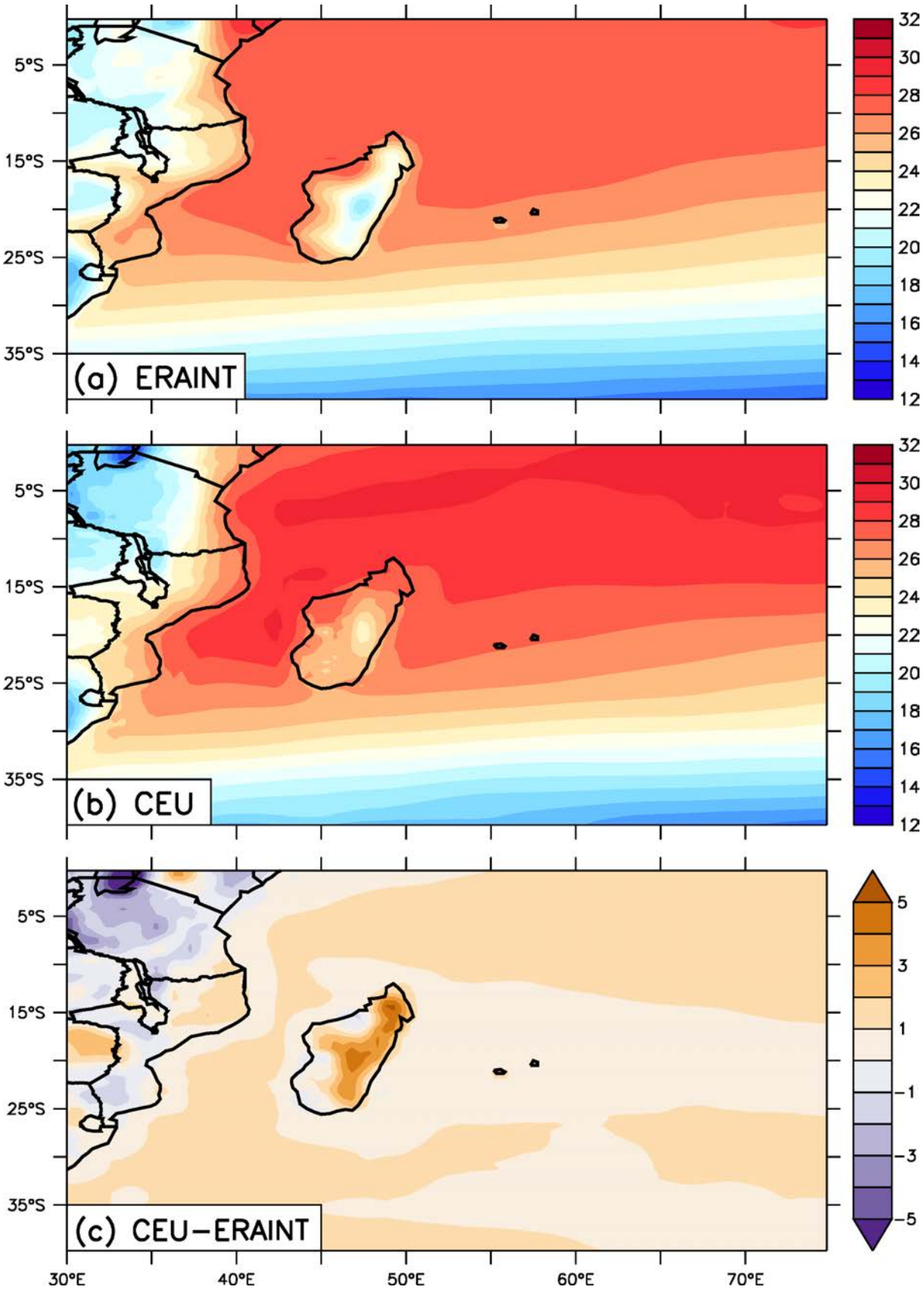

Figure 4.1: Surface climatological temperature over the South West Indian Ocean for Tropical Cyclone season November-April (1999-2010) in °C. Panel (c) shows the difference between CEU and ERAINT.

4.1.2 Rainfall

There are common features in the rainfall distributions produced by the CEU simulation, ERAINT, and GPCP observation over the SWIO (Figure 4.2). GPCP shows a band of maximum rainfall (associated with the Inter Tropical Convergence Zone, ITCZ) around 5-20°S and an area of minimum rainfall over the Mozambique Channel (around 70-75°E; 20-35°S) (Figure 4.2a). The rainfall band shows a local maximum over Mozambique (about 12 mm day^{-1}) and over Madagascar (about 12 mm day^{-1}). Both ERAINT and CEU reproduce the tropical rainfall band, but they fail to capture the local maximum over Mozambique. While ERAINT reproduces the local maximum over Madagascar, CEU simulates local minimum over the island. In addition, ERAINT does not reproduce the minimum rainfall over the Mozambique Channel (MC), while CEU simulates a local maximum over the area. The rainfall bias is within ±1 mm day^{-1} in ERAINT but up to 9 mm day^{-1} in CEU. CEU produces its maximum dry bias over Madagascar and its maximum wet bias (9 mm day^{-1}) over the MC. The wet bias could be due to the convective parameterization in the model; the parameterization may too sensitive to the warm boundary layer over this area. The overestimation of the deep convection in this area may be responsible for the inability of CEU to simulate the local maximum rainfall over the Madagascar area, because deep convections usually suppress convection around them. However, the CEU dry bias over Madagascar is consistent with the warm bias over the area (Figure 4.1b), because lesser rainfall means lesser cloud albedo, more incoming solar radiation, and more heat. Another contributing factor would be topography that is too low over Madagascar, so tropical easterlies do not produce orographic precipitation as strongly in CEU as in the other data sources. This could also yield temperatures warmer than observed (by being at lower elevation).

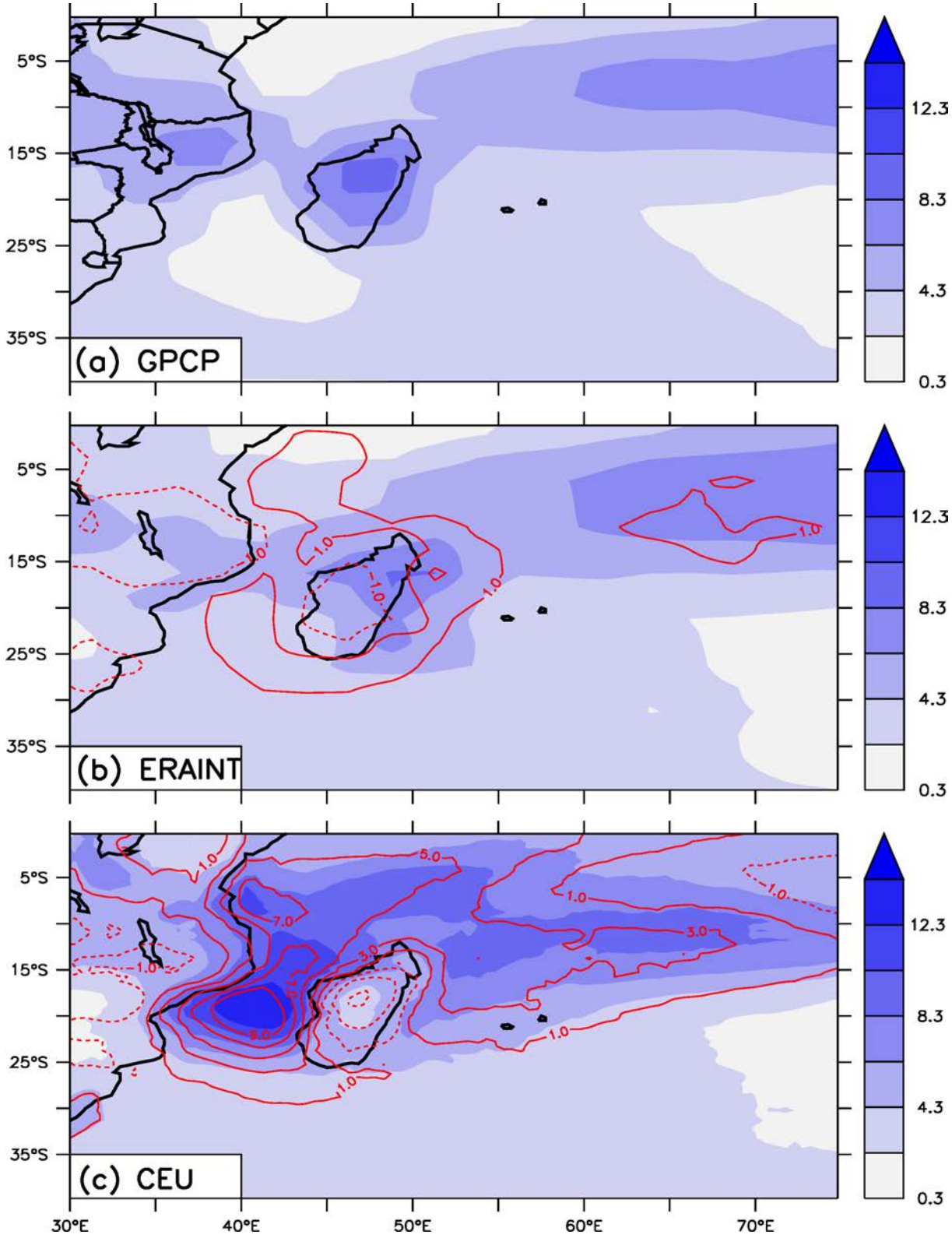

Figure 4.2: Climatological rainfall over the South West Indian Ocean for Tropical Cyclone season November-April 1999-2010 in mm/day. The red contours shown in (b) and (c) show the bias between the ERAINT and CEU rainfall with respect to GPCP i.e. CEU-GPCP and ERAINT-GPCP. Solid contours denote a wet bias and dashed contours show areas where there is a dry bias.

4.1.3 Mean Sea Level Pressure and 850 hPa Winds

In general, CEU gives a remarkable simulation of the mean sea level pressure (MSLP) over the SWIO when compared with ERAINT (Figure 4.3). The model simulates well the temporal low trough over the SWIO and reproduces the Mascarene High (South Indian High Pressure System) as in ERAINT. These are well known features over the region. The model captures the location and structure of the South Indian High Pressure System, but overestimates with a higher MSLP centre (by about 6 hPa) when compared to that of ERAINT and locates the South Atlantic High Pressure System slightly more east than that of ERAINT. In addition, the model correctly simulates the location of the low pressure through, but with a higher value than that of ERAINT. However, the gradient of the mean sea level pressure is stronger in CEU than in ERAINT. This implies that the Hadley circulations would be stronger in the CEU simulation than in the ERAINT results. The stronger MSLP gradient in CEU translates into a strong easterly flow in the model.

Although, the general patterns of the 850 hPa wind-fields are similar in CEU and ERAINT, the wind speeds are stronger in CEU (Figure 4.4). The major discrepancy between the CEU and ERAINT wind patterns occurs over Mozambique, where CEU simulates a cyclonic flow but ERAINT shows an easterly flow. The simulated cyclonic flow is consistent with the observed local maximum rainfall over the MC, but it is not producing rainfall in the area of occurrence because it draws in dry continental air into the area and deflects moist maritime air away from the area, meanwhile, ERAINT allows the moist air flow through the area.

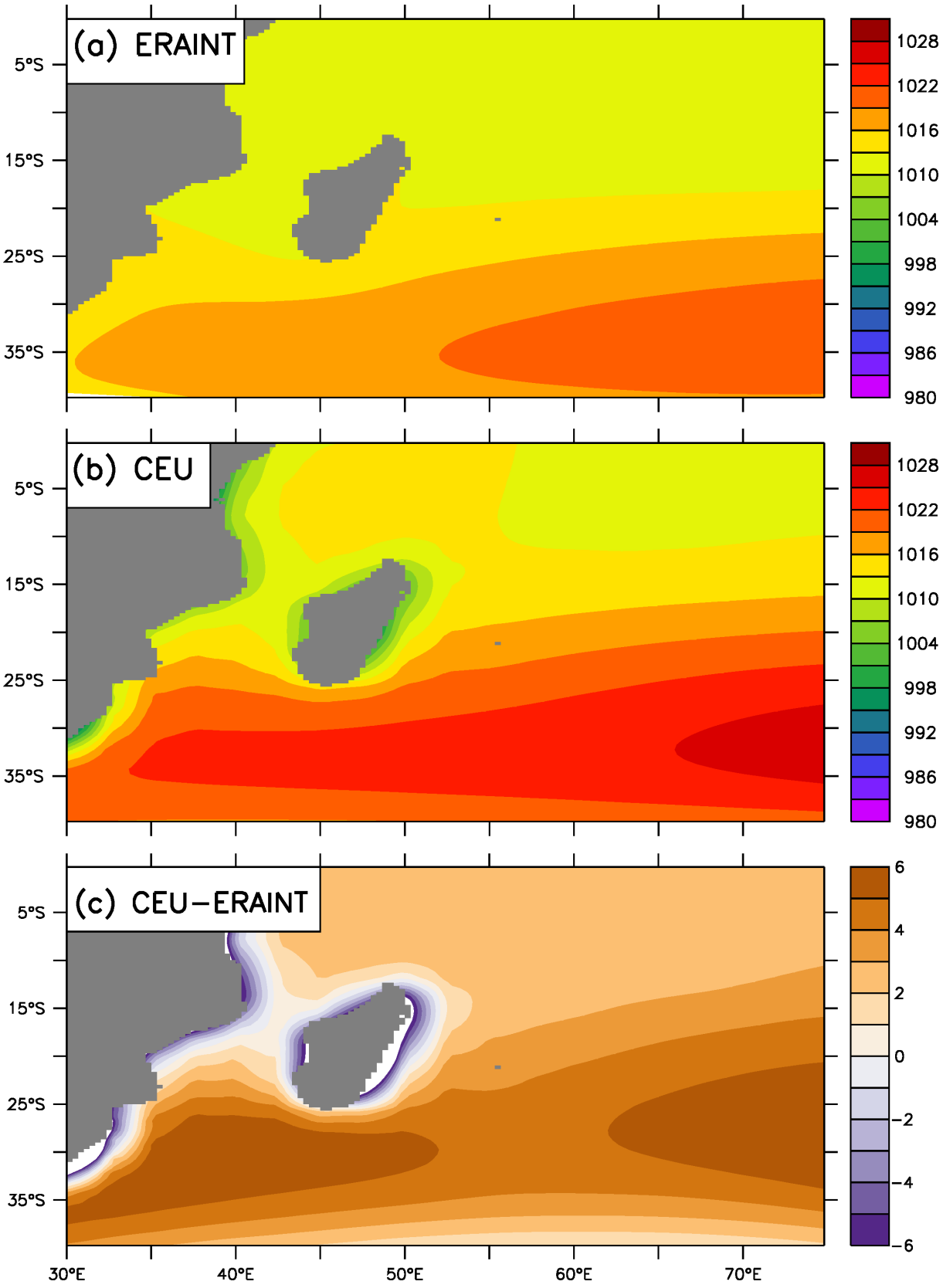

Figure 4.3: Surface climatological Mean Sea Level Pressure over the South West Indian Ocean for Tropical Cyclone season November-April 1999-2010 in hPa. Panel (c) shows the difference between CEU and ERAINT.

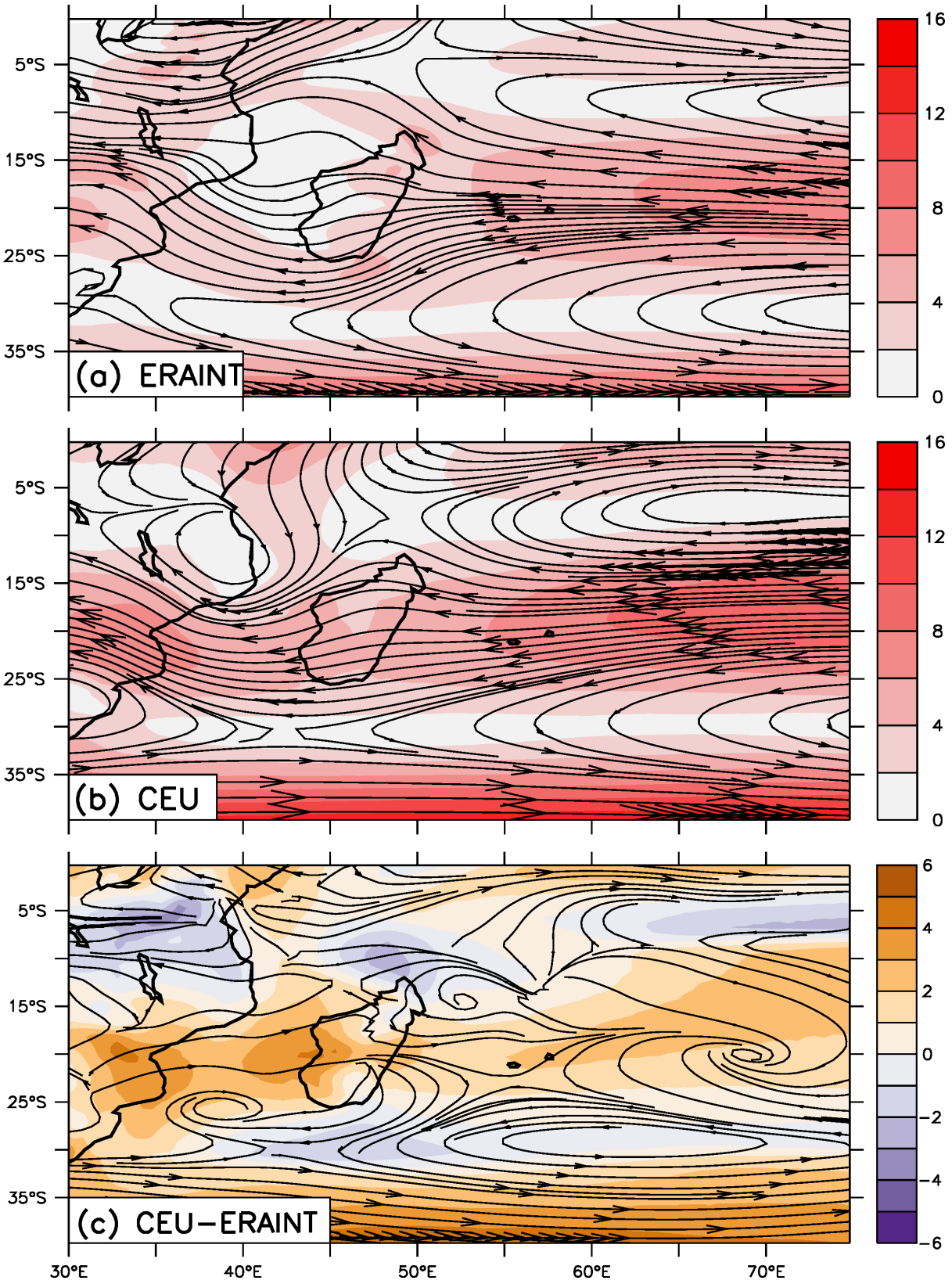

Figure 4.4: 850 hPa climatological winds for Tropical Cyclone season November-April 1999-2010 for (a) CEU and (b) ERAINT in m/s. Panel (c) shows the difference between CEU and ERAINT.

4.1.4 Vorticity

The CEU simulated 850 hPa vorticity field has common features with those in ERAINT results (Figure 4.5). ERAINT shows a large area of negative vorticity approximately 50-75°E; 0-20°S, which is consistent with the ITCZ since negative vorticity values in the southern hemisphere lead to surface convergence. Moreover, this result is consistent with the observed GPCP precipitation (Figure 4.2a) since areas of high surface convergence are favourable to the formation of convective precipitation. Below 25°S, ERAINT shows positive vorticity values which are associated with the South Indian High Pressure System. Moreover, positive vorticity values associated with the South Indian High Pressure System indicate areas of subsidence where convective rainfall is often inhibited. Therefore, this result further highlights the difference in rainfall patterns between areas in the vicinity of the ITCZ and South Indian High Pressure System (see Figure 4.2). CEU is in agreement with ERAINT with regards to the spatial pattern of the ITCZ as well as areas of subsidence. However, the CEU vorticity field over the MC is much stronger than the reanalysis. This strong bias is consistent with the models wet bias over that region.

4.1.5 Vertical Velocity

The location of the Hadley Cell is well captured by CEU where the zonally averaged vertical velocity compares well with the ERAINT (Figure 4.6). The reanalysis shows areas of strong convergence between 5-10°S which is where Hadley Cells meet and form the ICTZ and ultimately the area of maximum precipitation in the tropics as seen in the GPCP observation (Figure 4.2a). The reanalysis shows well the descending arm of the Hadley Cell between 25-40°S which is consistent with the low rainfall rate in that area as seen in the observation (Figure 4.2a). Although the positions of the CEU simulated convergence and divergence zones compare well with ERAINT, the speed at which air ascends or descends is higher in the model. In the area of dominant convergence (0-20°S), CEU exhibits a stronger negative vertical velocity bias, especially in the lower levels. As a result, this causes the model to produce more convective rainfall in comparison to the observation, which is consistent with the anomalous CEU rainfall over the MC. In the descending arm of the Hadley Cell, the model underestimates the speed of the subsidence motion especially in the higher levels (>600 hPa), but overestimates below 800 hPa, which is consistent with the stronger MSLP values in the CEU simulation.

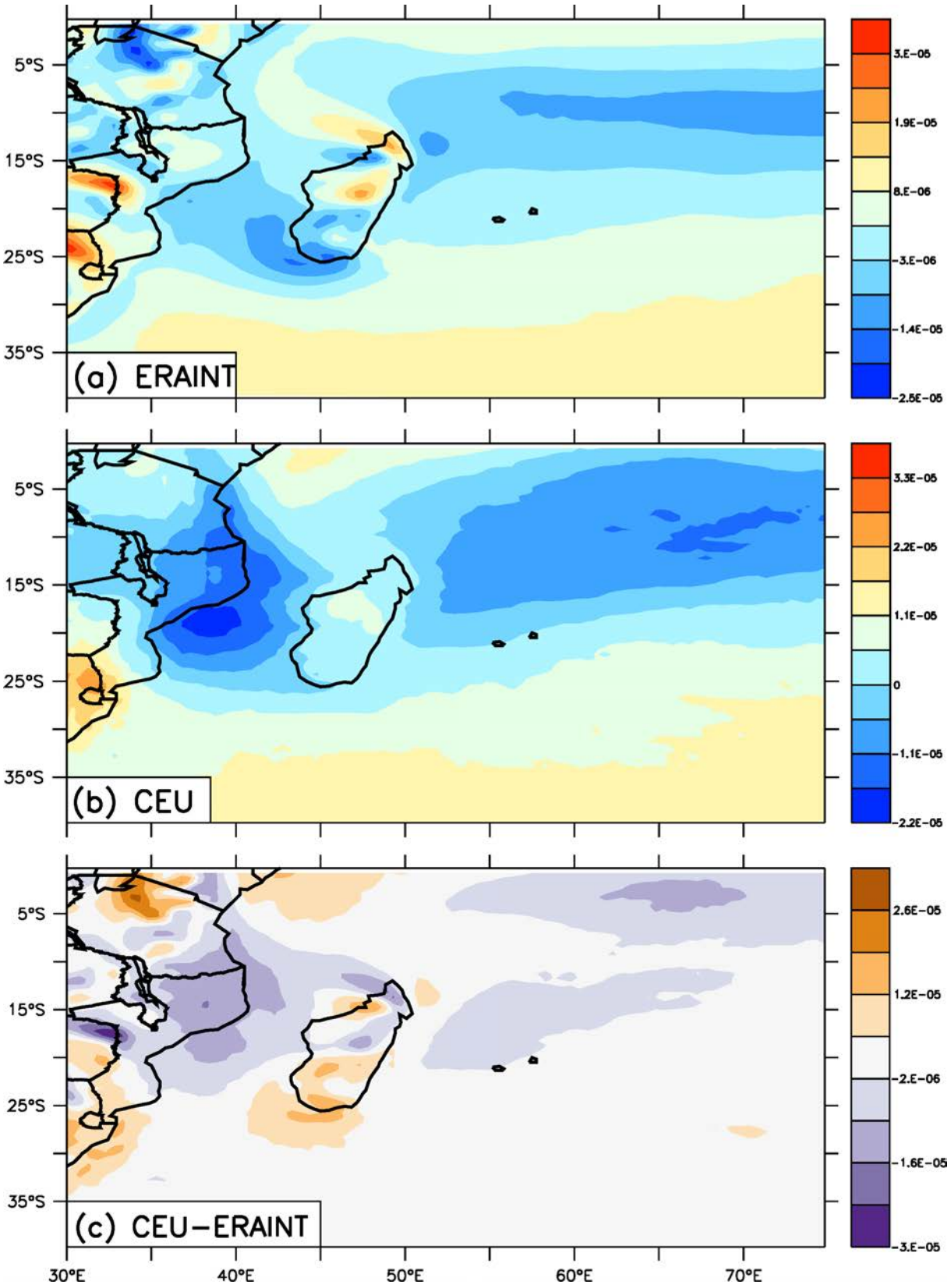

Figure 4.5: 850 hPa climatological vorticity over the South West Indian Ocean for TC season November-April 1999-2010 in s^{-1}. Panel (c) shows the difference between CEU and ERAINT.

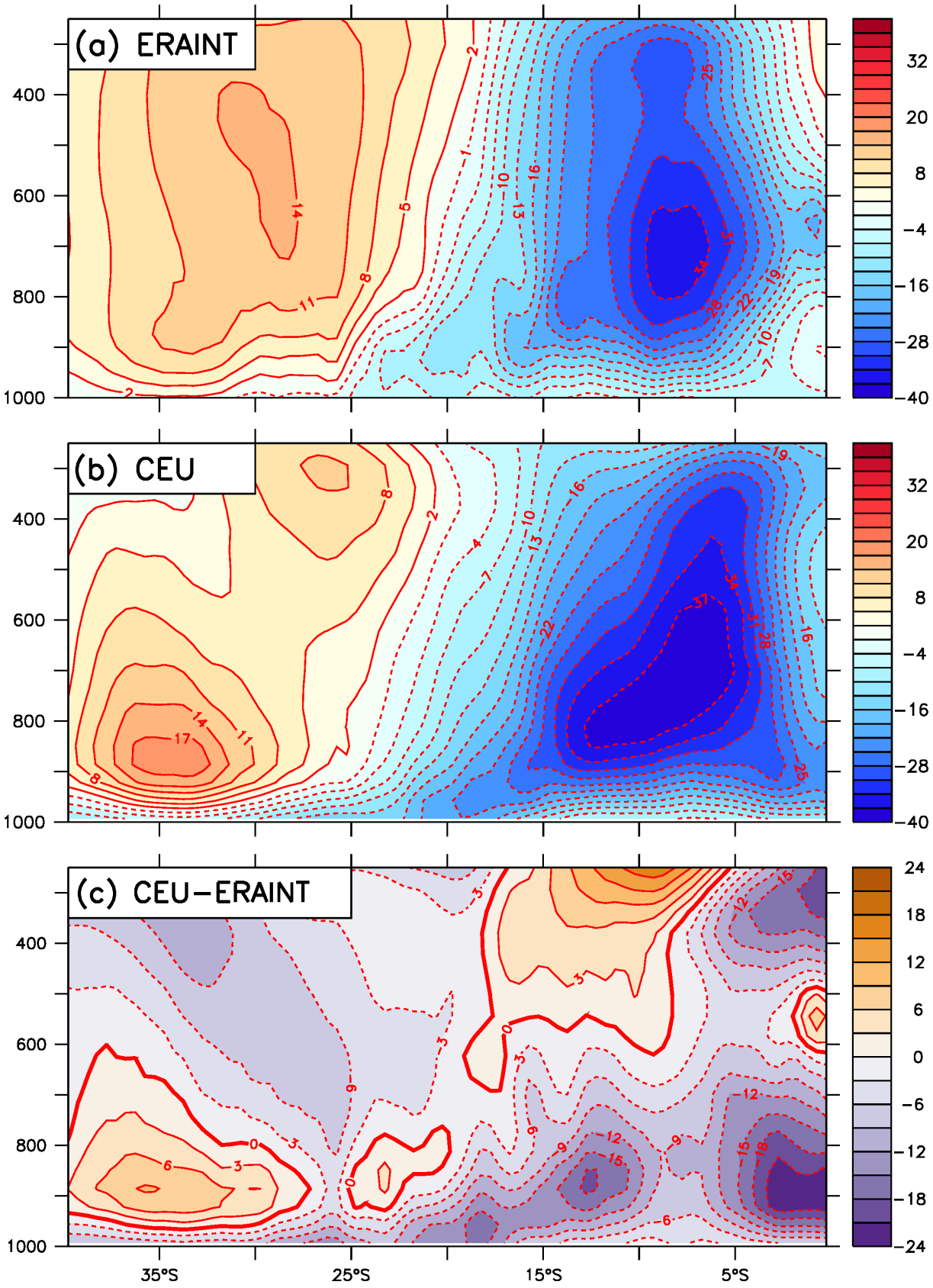

Figure 4.6: Zonally averaged vertical velocity (30-75°E) over the South West Indian Ocean for TC season November-April 1999-2010 in 10^3Pa/s. Height in pressure levels (hPa). Panel (c) shows the difference between CEU and ERAINT.

4.2 Simulated Tropical Cyclone Structure

The structural characteristics of an observed TC are well simulated by CEU. This includes a calm eye in the centre of the storm, strong winds near the eye wall and a warm core in the centre of the storm (Figure 4.7). The genesis of the CEU simulated TC began on the 21st of January 2000 in the SWIO as a Tropical Depression (hereafter TD) with a maximum 850 hPa wind intensity of 90 km/h. The storm strengthened into a TC, reaching a maximum wind intensity of approximately 140 km/h (minimum MSLP of 973 hPa) on the 24th of January 2000. Figure 4.7a shows the 850 hPa horizontal wind at the storms peak with a clearly defined eye (highlighted with a box) and strong cyclonic winds surrounding the eye. The TC exhibits a strong warm core between 900 and 200 hPa which is associated with diabatic heat release (Figure 4.7b) and a local maximum 850-300 hPa average temperature of 6 degrees as computed by the TC detection algorithm (see section 3.3.1). Figure 4.7c and 4.7d show the longitude-pressure level cross sections of the wind speed and vorticity respectively. The TC exhibits a calm eye (diameter ~100 km) at all pressure levels and maximum wind speeds in the lower levels (Figure 4.7c). The CEU model simulates well the relative vorticity in the centre of the storm with the largest values of negative relative vorticity in the lower levels (Figure 4.7d). The negative low-level vorticity (positive in the Northern Hemisphere) represents the "spin" of the atmosphere that is needed to form a cyclonic rotating storm in the southern hemisphere.

ERAINT shows a broad skill in exhibiting the dynamical structure of a TC but less detailed in comparison to the simulated CEU TC. The ERAINT TC (shown in Figure 4.8) formed in the SWIO on the 8th of March 2002 as a TD (minimum MSLP of 1003 hPa) reaching TC strength (130 km/h) on the 10th of March when it brushed the north eastern parts of Madagascar. The TC reached a wind intensity of 140 km/h (minimum MSLP of 973 hPa) on 12 March 2002 and transitioned into an extra-tropical cyclone on the 17th of March. It is worth noting that this ERAINT TC corresponds to TC Hary which developed on March 5 2002 and dissipated on the March 17 2002. Figure 4.9 shows the ERAINT TC (red) tracks which are very similar to the observed JTWC (blue) tracks for TC Hary. This result increases confidence in the ability of the objective TC detection algorithm in tracking TCs in gridded datasets. In comparison to the simulated CEU TC (Figure 4.7a), the reanalysis storm shows a broader and less detailed wind field (Figure 4.8a). This lack in representation may be attributed to the low ERAINT horizontal resolution (80km) in Comparison to CEU (50km), which shows that the dynamical structure of a model TC is intrinsic on the model resolution.

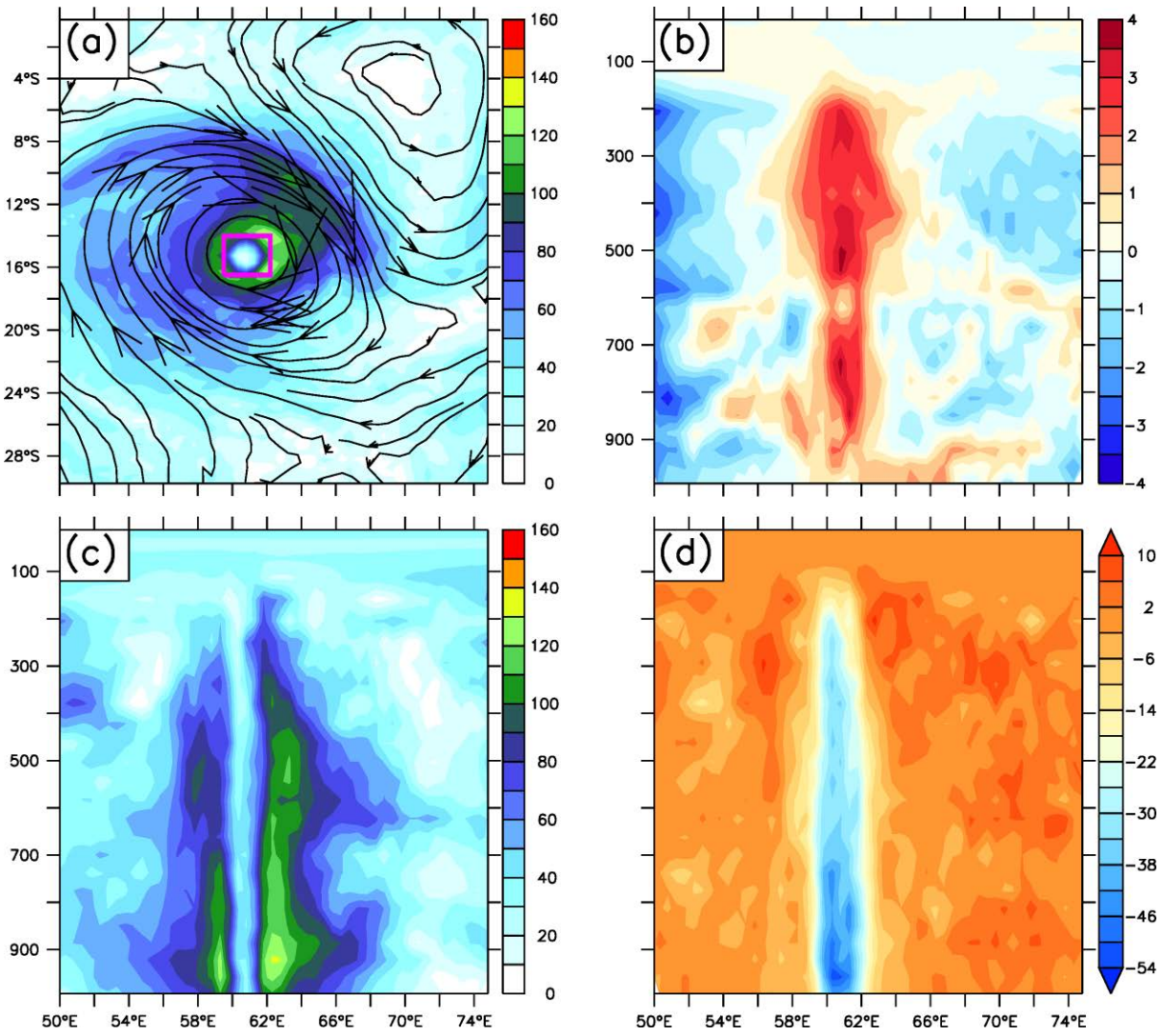

Figure 4.7: Dynamical structure of a Tropical Cyclone as simulated by CAM-EULAG. Panel (a) shows the 850 hPa horizontal wind distribution in m/s, (b) shows the temperature anomaly associated with the warm core in °C, (c) and (d) shows the vertical cross-section of the wind speed (in m/s) and vorticity (in $10^{-5}s^{-1}$) respectively.

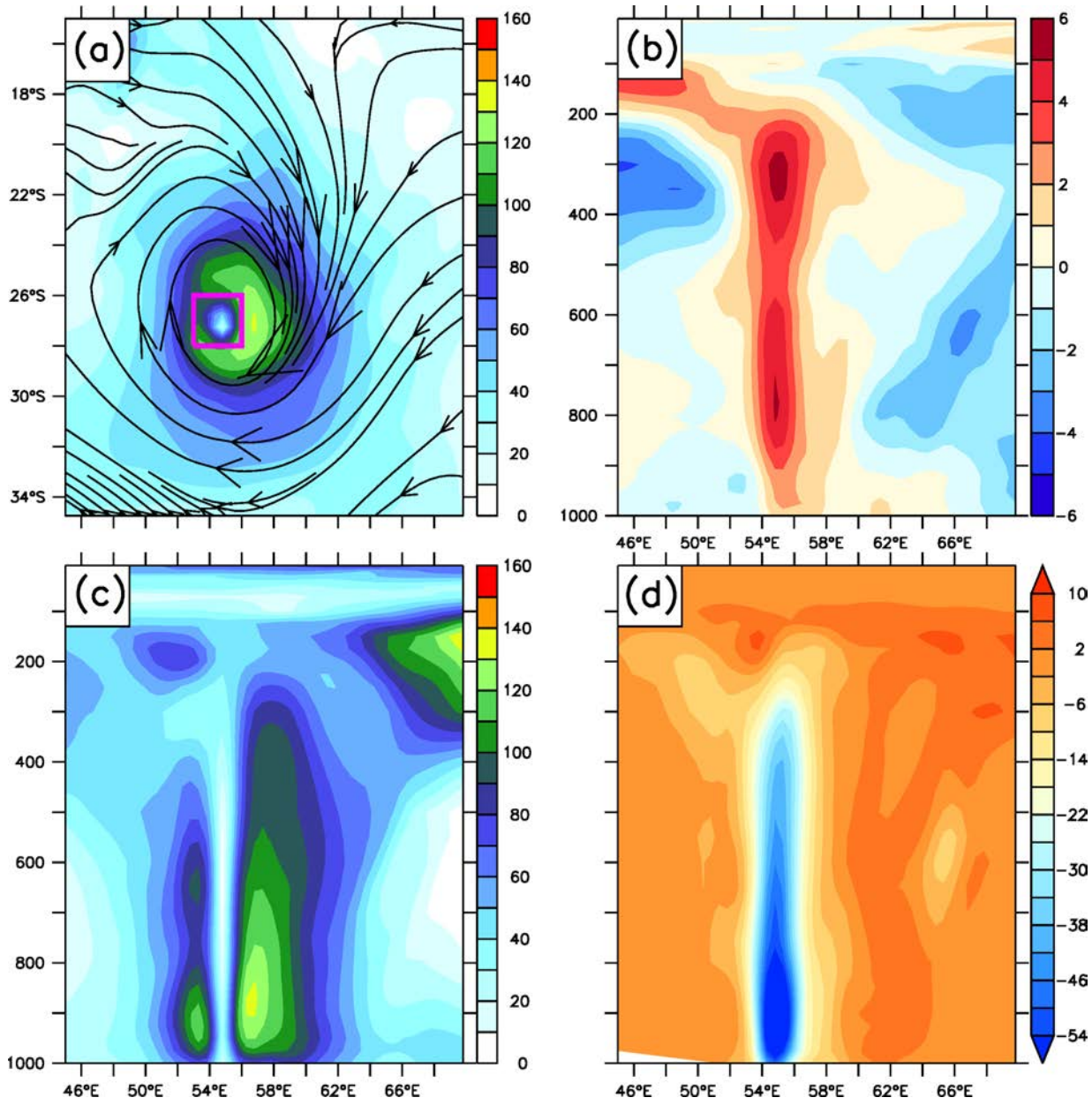

Figure 4.8: Dynamical structure of a Tropical Cyclone as simulated by ERAINT. Panel (a) shows the 850 hPa horizontal wind distribution in m/s, (b) shows the temperature anomaly associated with the warm core in °C, (c) and (d) shows the vertical cross-section of the wind speed (in m/s) and vorticity (in $10^{-5}s^{-1}$) respectively.

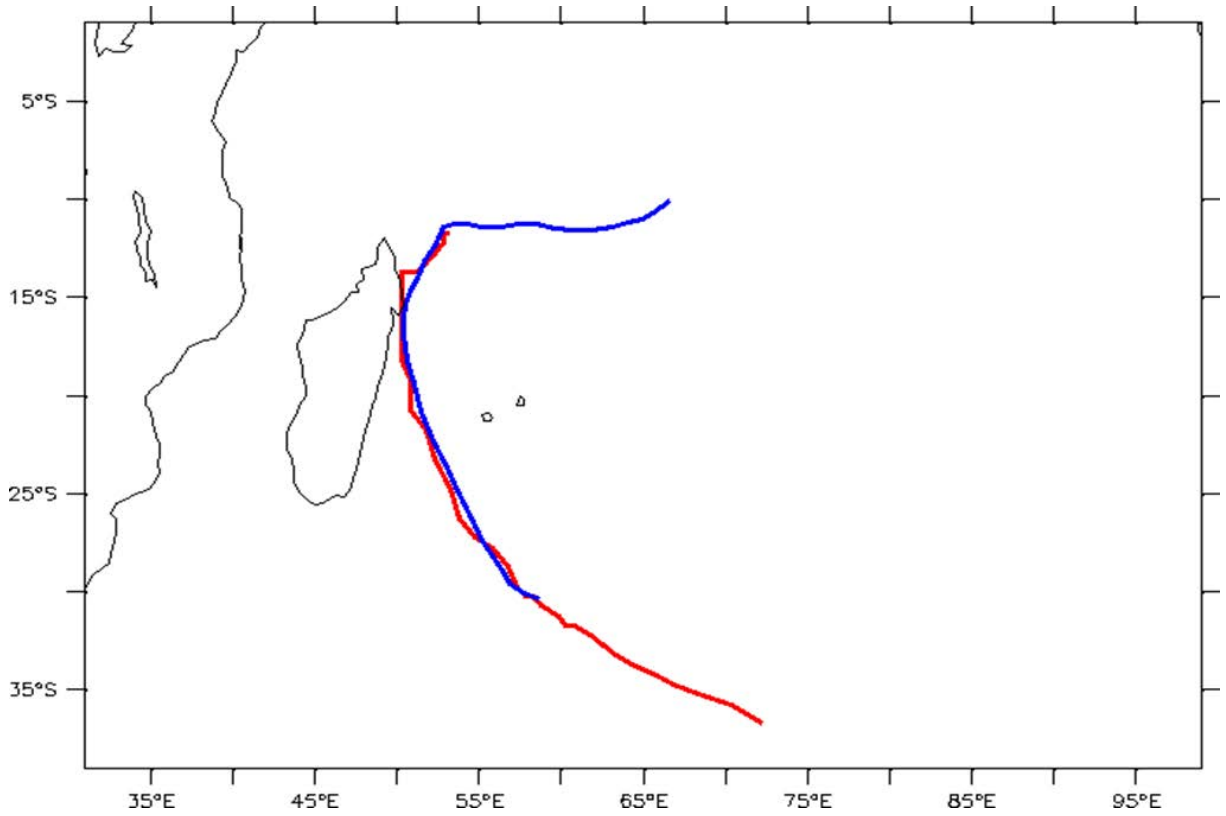

Figure 4.9: Observed JTWC (blue) and ERAINT (red) Tracks for Tropical Cyclone Hary which developed on the 5th of March 2002.

4.3 Simulated Tropical Cyclone Intensity

4.3.1 Accumulated Cyclone Energy

ERAINT correlates (spearman) better with the observation (ρ = 0.63) in comparison to CEU (ρ = -0.29) on the interannual variability of Accumulate Cyclone Energy (ACE). However, it underestimates more the annual mean ACE over the basin in comparison to CEU (Figure 4.10). The observed annual mean ACE over the SWIO basin is 161.93 $10^4 kn^2$. ERAINT shows an annual mean ACE of 52.35 $10^4 kn^2$ which is 32% of the observation mean while the CEU simulation shows better performance with an annual mean ACE of 62% of the observation. However, this result suggests that even at 0.5° x 0.5° horizontal resolution, CEU struggles to sustain more intense TCs. Moreover, this is further highlighted by the highest but coarser 80 km grid spacing in ERAINT which produced a low annual mean ACE. However, applying Walsh *et al*. (2007) technique by scaling the CEU and ERAINT simulated data to 25 km resolution, the ACE increases to 102.94 $10^4 kn^2$ and 53.89 $10^4 kn^2$ respectively. Therefore, this result emphasizes the deficiency of coarser horizontal resolutions in generating and sustaining realistic TC intensities during a climate simulation and better resolution is needed in order to increase the realism of simulated TC intensities.

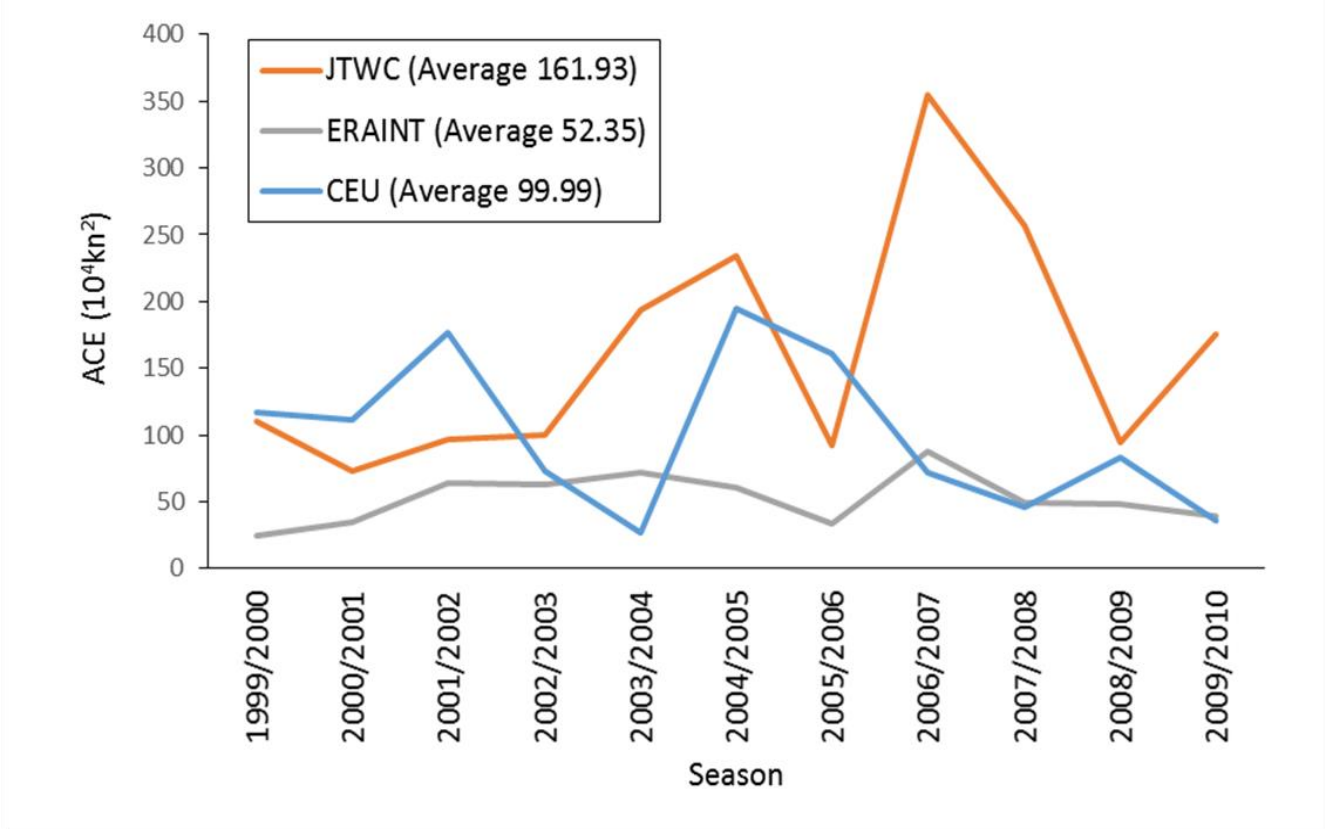

Figure 4.10: Interannual variability of the Accumulated Cyclone Energy for Observed (JTWC), ERAINT and CEU Tropical Cyclones over the South West Indian Ocean.

4.3.2 Wind-Pressure Relationship

There is a good agreement between observation, ERAINT and CEU on the wind-pressure relationship, with a few discrepancies (Figure 4.11). Both CEU and ERAINT show the highest wind speeds corresponding with the lowest minimum MSLP centres, which is consistent with the observation. However, both the model and reanalysis exhibit stronger wind speeds with relatively higher MSLP centres in comparison to the observation. For example, ERAINT TCs reach wind speeds of approximately 250 km/h with MSLPs of 960 hPa, but for observed TCs, it takes lower MSLPs of approximately 920 hPa in order to reach the same wind speed threshold. According to Manganello *et al.* (2012), this deficiency may arise due to unrealistic surface roughness parameterizations in intense storms as well as the lack of explicitly resolved convection. In addition to that, the wind-pressure relationship is highly sensitive to the manner in which surface winds are derived in model output (Zarzycki and Jablonowski, 2014). The observed wind-pressure relationship exhibits a strong linear relationship with a R^2 value of 0.98 while ERAINT and CEU showed linearly regressed R^2 values of 0.68 and 0.70 respectively, which shows adequate skill in the gridded datasets. However both the model and reanalysis struggle to adequately produce the overall spread seen in the observation. This is especially prevalent in MSLP values lower than 960 hPa for ERAINT and 940 hPa for CEU where there is no TC representation. This lack of representation may be due to the lack of coarser horizontal resolution model output in producing storms with minimum MSLP centres deeper than 930 hPa.

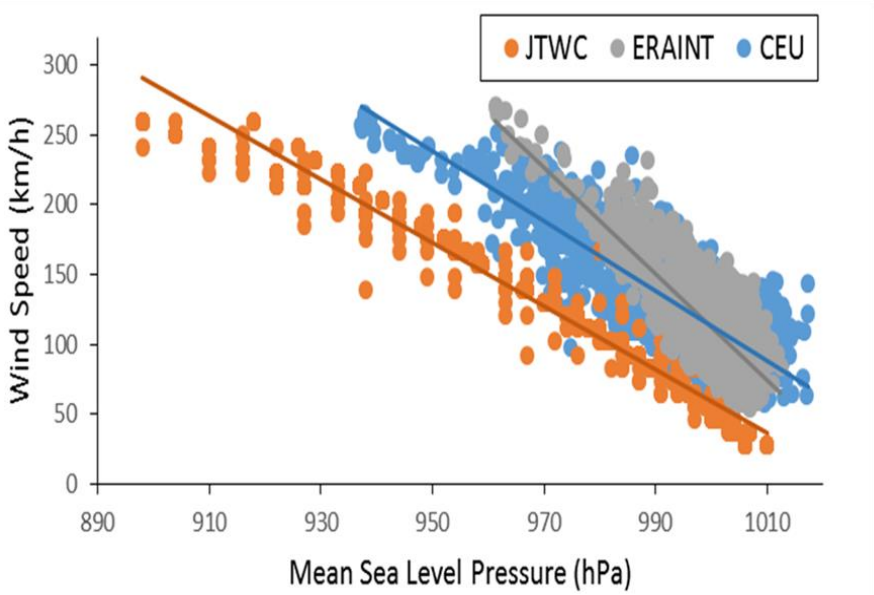

Figure 4.11: Wind-pressure relationship of Observed (JTWC), ERAINT and CEU Tropical Cyclones over the South West Indian Ocean (0-40°S; 30-75°E) for November to April, 1999-2010.

4.4 Spatial patterns of Tropical Cyclone Tracks and Genesis locations

There is some agreement between the observation (Figure 4.12a), reanalysis (Figure 4.12b) and model (Figure 4.12c) on the spatial characteristics of TC tracks over the SWIO. The observation shows the largest concentration of TC activity approximately between 10-30°S and no TC activity near the equator. This result is consistent with earlier studies by Vitart *et al*. (2003) and Mavume *et al.* (2009). Near the Horse Latitudes (30-35°S), observed TCs tend to recurve westward due to the prevailing westerlies which are characteristic of the mid-latitude atmospheric circulation. What is more is more interesting is that both the ERAINT and CEU capture the spatial pattern of TC tracks very well. However, the reanalysis and model show land falling TCs over Madagascar with discrepancies as well as the land fall of TCs over the eastern parts of Mozambique. Furthermore, the model shows a prevalence of TC activity over the Mozambique Channel in comparison to the observation and ERAINT. This can be attributed to the anomalous 850 hPa vorticity over the area (Figure 4.5b) which is stronger than the ERAINT and may lead to a more substantial cyclonic feature over the channel. In addition, the models anomalous TC count over the MC may artificially increase the ACE over the basin since there are more TCs forming in comparison to the observation. Although the model over simulates tracks above 10°S in comparison to the observation and ERAINT, it does very well between (30-40°S; 30-40°E) by not simulating them at all.

There are notable discrepancies between the observation (Figure 4.13a), reanalysis (Figure 4.13b) and CEU (Figure 4.13c) on the number of TCs formed directly over the SWIO basin (0-40S°; 30-75°E). Approximately 54% of all observed SWIO TCs form outside the basin compared to CEU which only has 5% outside the domain. The observed TCs form east of 75°E and propagated west into the SWIO with the aid of the South-East trade winds (zonal steering flow in Vitart *et al.* (2003)), this pattern is similar to the findings of Mavume *et al*. (2009). Approximately 35% of all CEU TCs formed over the MC compared to only 6% in the observation. This finding suggests that the strong model bias present in CEU over the MC needs to be investigated further but it is not within the scope of the present study. Figure 4.5b strongly supports the claim that the 850 hPa vorticity anomaly present in CEU may be the chief cause of the substantial TC genesis over the MC since large values of vorticity aid in the formation of TCs (Gray, 1968; Henderson-Sellers *et al*., 1998). From the anomalous CEU TC genesis over the MC, It is without recourse that large values of low-level relative vorticity are one of the key ingredients favouring tropical cyclogenesis. Although the model simulation shows incongruity on the number of TCs that form over the basin, it exhibits some skill in the spatial distribution of genesis locations. For example, the TC genesis is mostly concentrated

between 5°-20°S and no TCs are simulated below 30°S, which is in agreement with the observation. Furthermore, CEU is in coherence with the observation and ERAINT with regards to the lack of TCs forming close to the equator. Near the equator, the Coriolis parameter tends to zero and the development of strong organized vortices is inhibited.

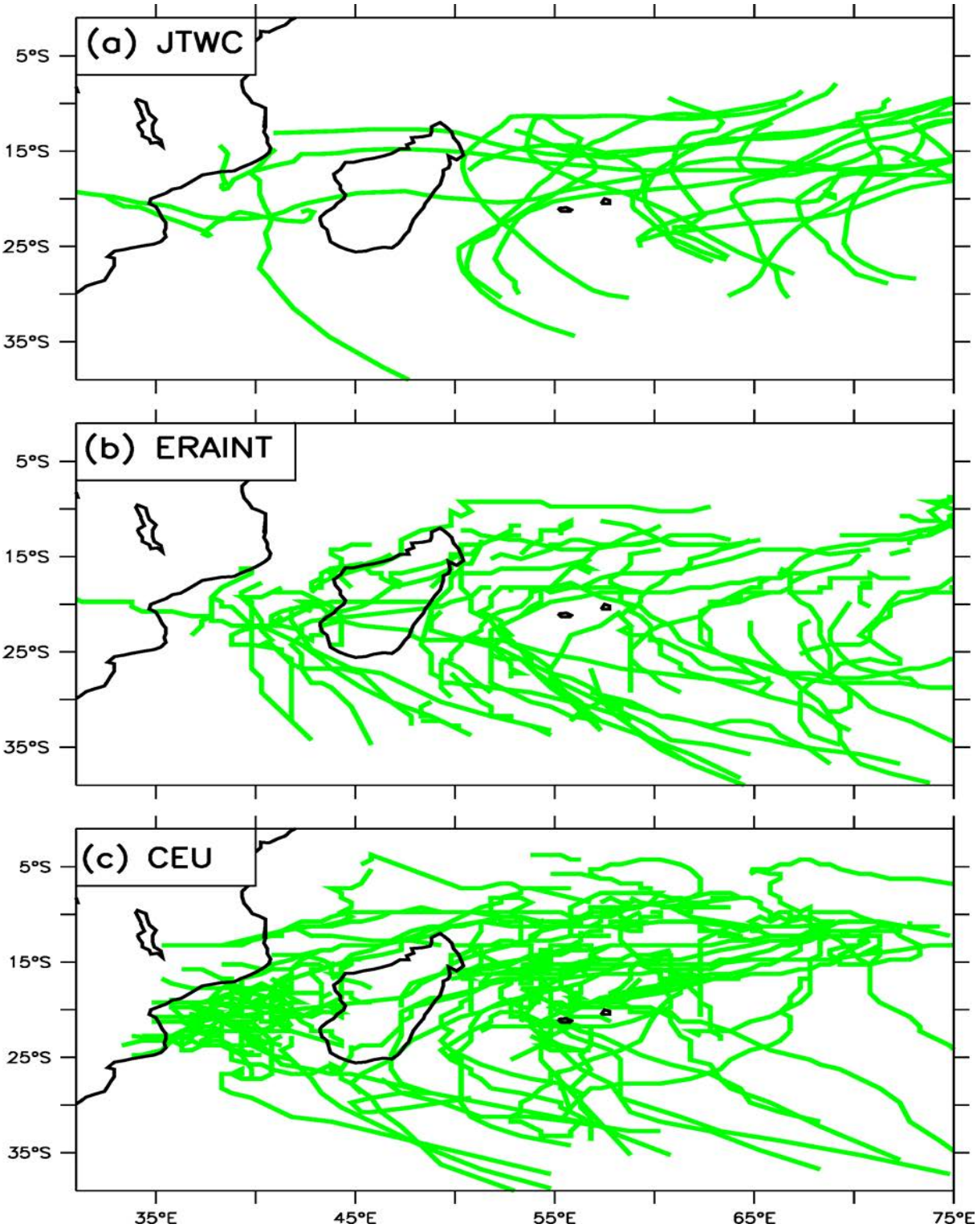

Figure 4.12: TC Tracks over the South West Indian Ocean for Tropical Cyclone seasons (November – April) from 1999 to 2010 for (a) JTWC Best Track data (Observation), (b) ERAINT and (c) CEU Tracks.

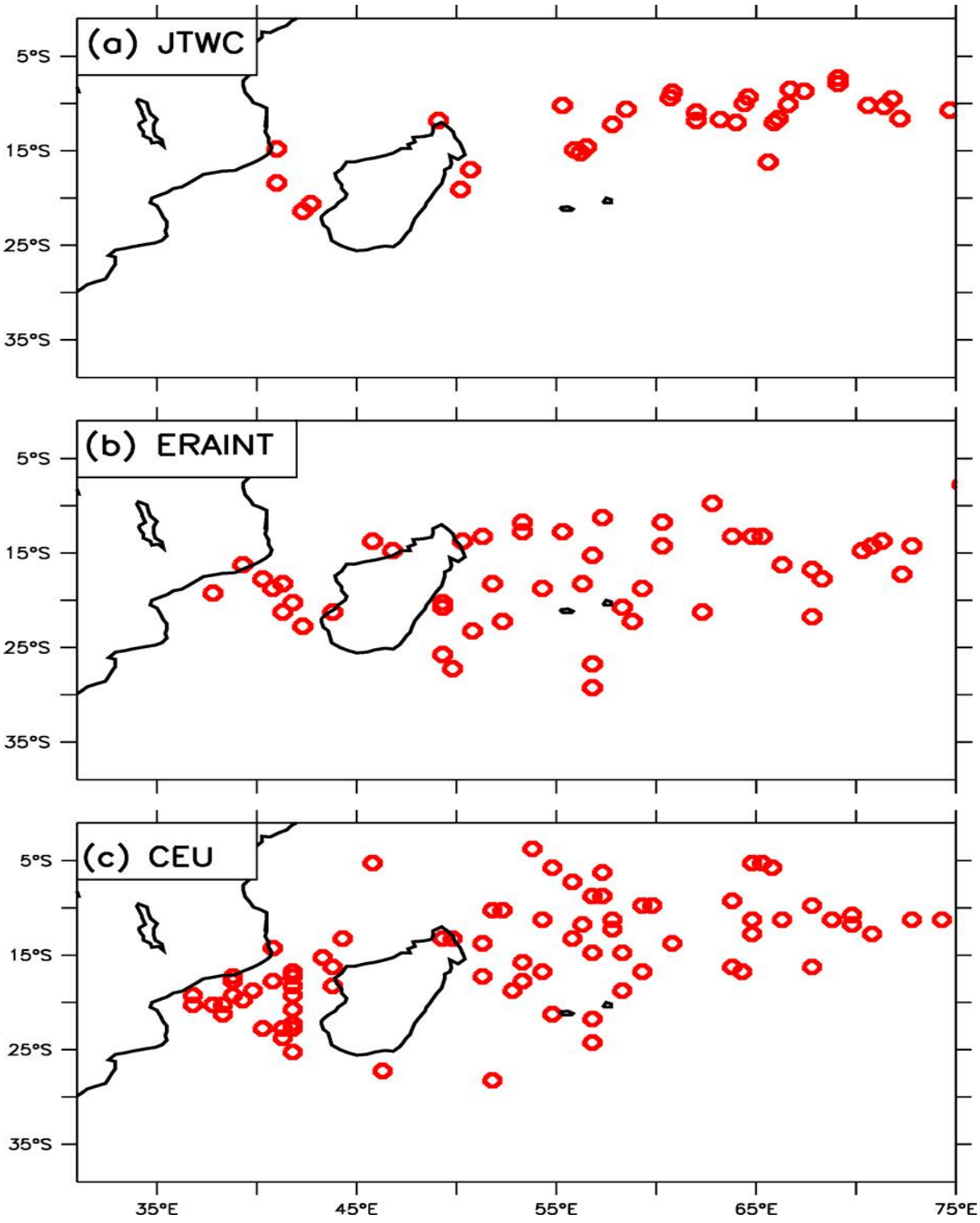

Figure 4.13: Tropical Cyclone genesis locations over the South West Indian Ocean for Tropical Cyclone seasons (November – April) from 1999 to 2010 for (a) JTWC Best Track data (Observation), (b) ERAINT and (c) CEU Tracks.

4.5 Monthly Variation of Tropical Cyclone occurrence

CEU captures well the monthly variation of the observed TCs over the SWIO with a few discrepancies (Figure 4.14). The observation shows peak TC activity in January and February which is consistent with the peak of summer in the southern hemisphere. Moreover, this time is simultaneous with high SSTs; hence the formation of TCs more favourable. The model and reanalysis is able to adequately capture the peak of TC activity in January and February which is in agreement with the observation. However, both the model and ERAINT overestimates the number of TCs for each of the two peak months (January and February) in comparison to the observation. The ERAINT bias can be attributed to the bias in TC formation over the MC during the two peak austral summer months where a total of 11 TCs, 6 more that the observation, formed directly over the channel. Furthermore, this finding suggests that ERAINT may also exhibit a bias in climate conditions necessary for cyclogenesis over the MC.

Despite that, ERAINT shows good agreement with the observation for November, December, March and April. For CEU, a good number of anomalous TCs in January and February formed over the MC which is consistent with the models vorticity bias over that area. Of the total CEU TCs that formed over the channel (i.e. 30), 14 (~47%) formed in January, 8 (~26 %) in February and 8 in other months. This firmly suggests that the MC bias in CEU is strongly exhibited in January and February where it shows a prevalence of TC genesis. Of the 5 observed TCs that formed in the MC (Figure 4.13a), 3 (60%) formed in January and February. Although the time period of the study (11 years) is too short to have robust statistics of the variability of MC TCs, Mavume *et al*. (2009) analysed TC data for 27 years (1980-2007) and showed that the majority of MC TCs (60%) formed in January and February which is consistent with the results of this study. The model shows some skill in simulating TC numbers during December and March with marginal differences in comparison to the observation but struggles to adequately simulate TC counts for November and April.

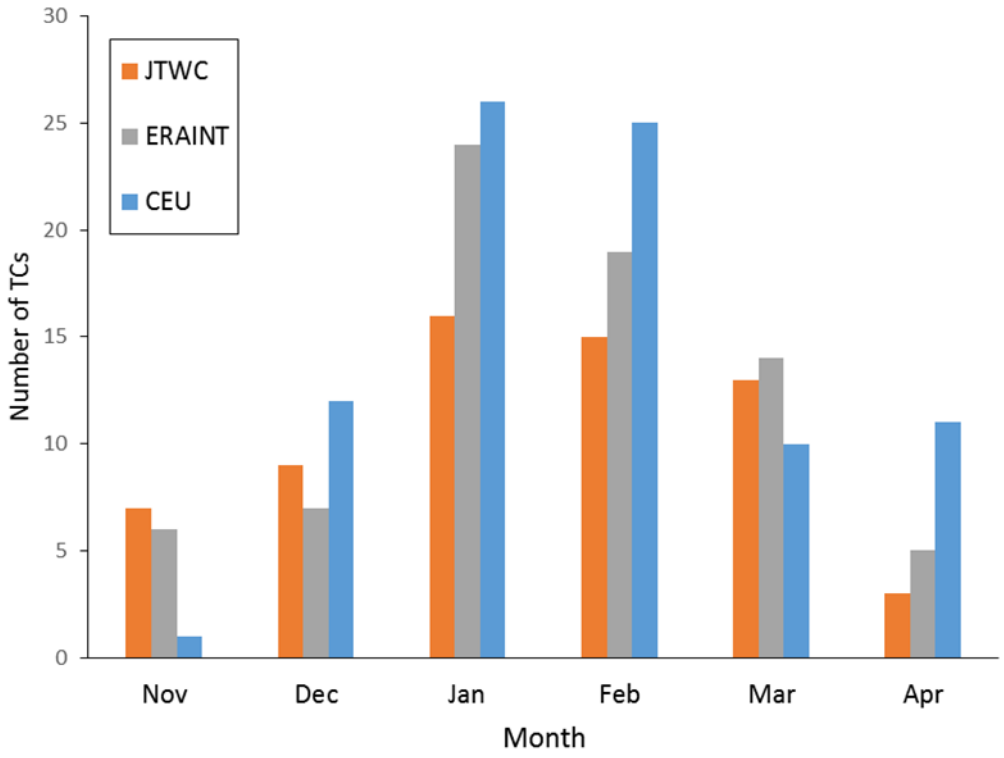

Figure 4.14: Monthly Variability of Tropical Cyclones over the South West Indian Ocean for the study period 1999-2010.

4.6 The Interannual Variability of Tropical Cyclones

In the SWIO, TCs show variability on an annual basis with an average of 5.72 observed TCs occurring per season, which is similar with the findings of Mbedzi (2010) but disagrees with Henderson-Sellers *et al.* (1998) and Mavume *et al.* (2009). Henderson-Sellers *et al*. (1998) reported an annual mean of 10.6 TCs between 1970 and 1995. However, data before the satellite era (i.e. 1980) must be regarded as relatively unreliable. The inconsistency with the results of Mavume *et al*. (2009) who found an Annual mean of 10.5 can be attributed to the fact that the authors combined Tropical Storms and TC in constructing the basin statistics, hence the discrepancy. Figure 4.15 demonstrates that the observed TC counts showed a large variation in the 2005/2006 and 2006/2007 TC season. The 2005/2006 had the lowest number of TCs while the 2006/2007 season showed the highest. In light of that, it is thought-provoking that the anomalous low (high) number of TCs in 2005/2006 (2006/2007) were simultaneous with an all negative (positive) ENSO, IOD and SASD phase. However, the 2002/2003 as well as the 2009/2010 TC season were both simultaneous with neutral SASD and positive ENSO and IOD, but had an almost equal, but opposite, anomaly of TC counts. CEU shows a large anomaly for 2005/2006 but in reverse in comparison to observation. Another CEU anomaly is in the 2007/2008 season which is marked by a positive IOD and

SASD phase coupled with a negative ENSO mode. It is interesting to note that the highest (lowest) CEU anomaly was simultaneous with negative (positive) IOD and SASD phase. However it is beyond the scope of this study to investigate what brings about these anomalous trends with regards to the SST indices.

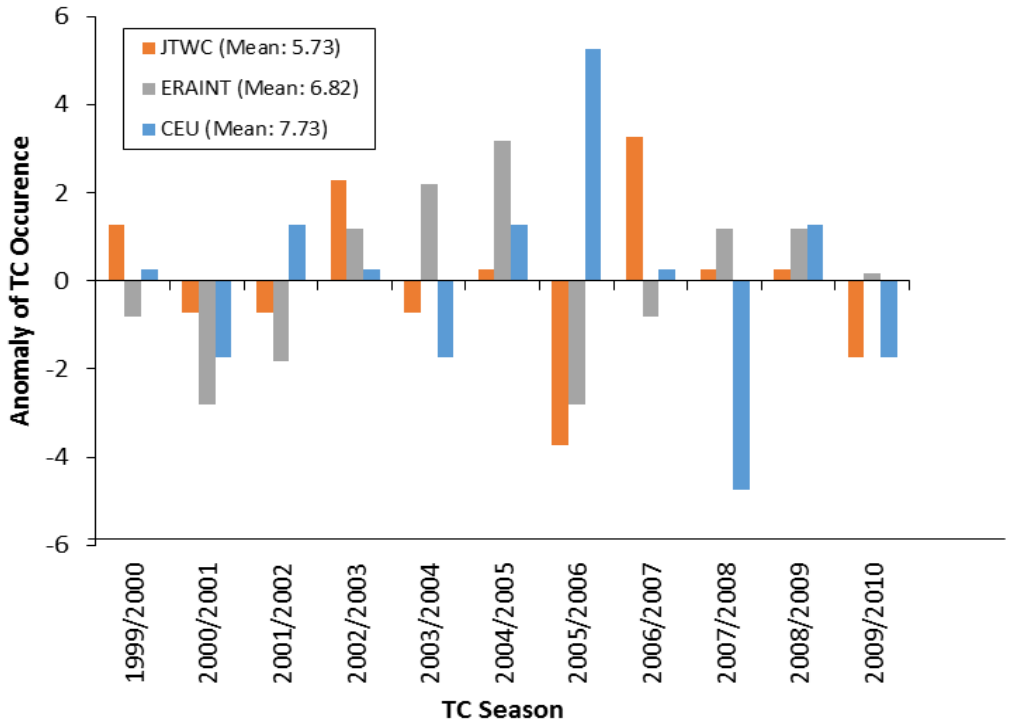

Figure 4.15: Interannual variability of Tropical Cyclone occurrence over the South West Indian Ocean for study period 1999-2010.

In comparison to ERAINT, CEU struggled to correlate better with observation in the interannual variability of TC counts but showed better performance in comparison to ERAINT when other various performance measures where used (see Table 4.1). ERAINT showed some skill with a spearman correlation of ρ = 0.32 with observation and CEU displayed poor spearman correlation with ρ = -0.06. However, using phase synchronization (defined in section 3.3.2), CEU showed better agreement (η = 73%) in comparison to ERAINT (η = 64%) with regards to the TC anomaly patterns in the observation (Figure 4.15). Applying the Proportion Correct (PC) skill measure, the overall fraction of simulations that were correct was 64% in ERAINT and 73% in CEU. CEU and ERAINT showed a good hit rate (*H)* of 0.83 and 0.67 respectively; with a False Alarm rate (F) of 0.40 in capturing the positive/negative anomaly binary events (see Table 4.1). Both the model and reanalysis show good performance in exhibiting a low probability of false detection (FAR) of 0.29 and 0.33 respectively. The Heidke skill score (HSS) for CEU and ERAINT is 0.44 and 0.27 respectively, which shows that CEU presents more skill in measuring the fraction of correct simulations after eliminating those simulations that would have been correct due to random chance. CEU and ERAINT scored Pierce's skill score (PSS) values of 0.43 and 0.27 respectively. This means that the CEU model performed much better than ERAINT in separating "positive anomaly" events from "negative anomaly" events. According to Gilberts skill score (GSS), ERAINT showed less skill (0.15) in predicting positive anomaly events corresponding to observation (adjusting for hits associated with random chance) in comparison to CEU (0.28). CEU and ERAINT scored Q (Odds and ratio skill score) values of 0.76 and 0.50 respectively, which shows that the model and reanalysis shows some skill in the improvement of the simulations over random chance.

Table 4.1: Summary of performance results between CEU and observation as well as ERAINT and observation in simulating the interannual anomalous binary event (positive/negative) in TC counts over the SWIO.

	H	*F*	FAR	PC	HSS	PSS	GSS	Q
CEU	0.83	0.40	0.29	0.73	0.44	0.43	0.28	0.76
ERAINT	0.67	0.40	0.33	0.64	0.27	0.27	0.15	0.50

The number of TC days shows variability from one year to another (Figure 4.16). What is more interesting is that the observation shows a downward and upward trend in TC days between 1999 and 2010. This happens approximately every three years, with some exceptions. A similar pattern has also been observed in Mavume *et al.* (2009) who used a longer time series (1980-2007), but the authors did not make any mention of it. Remarkably, the CEU simulation resembles a comparable pattern as well. It would be interesting for future studies to look if there is any significance to this pattern. Figure 4.16 shows the largest number of observed TC days in 2006/2007, which may be due to the high anomalous TC counts during that season (Figure 4.15). Moreover, the TC days in 2005/2006 are the least which correspond to the anomalously low TC counts for that season.

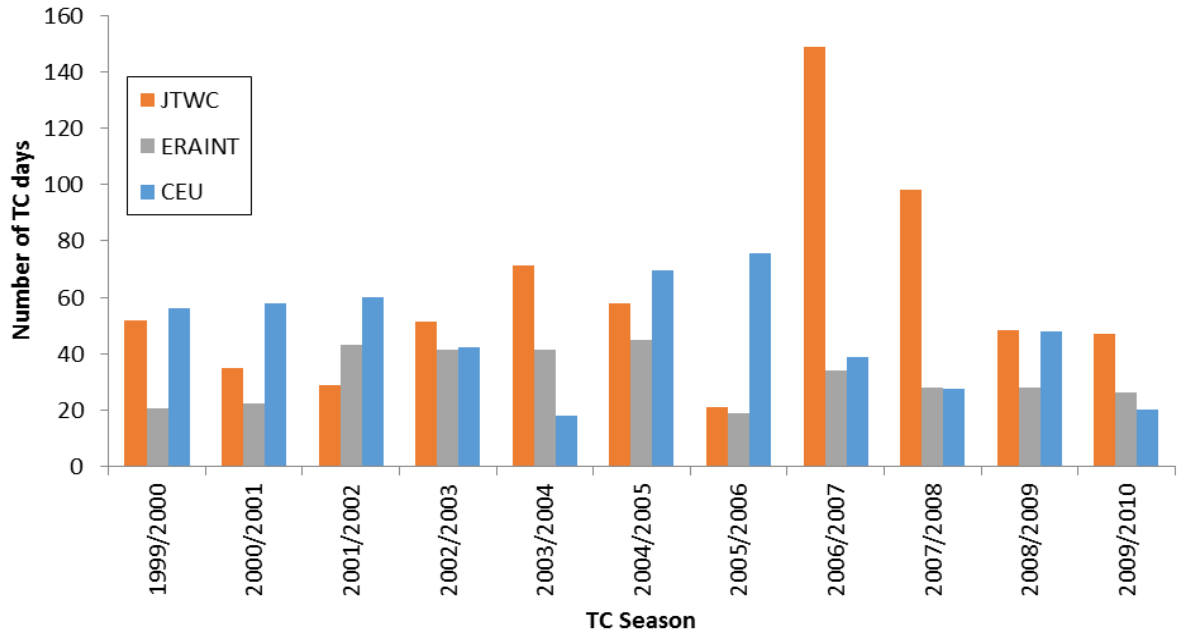

Figure 4.16: Interannual variation of Tropical Cyclone days over the South West Indian Ocean for study period study period 1999-2010.

4.7 Influence of Large Scale Sea Surface Temperature Parameters

4.7.1 El Niño Southern Oscillation

During the 11 TC seasons (November-April 1999-2010), there were 4 El Niño periods (2002/2003, 2004/2005, 2006/2007 and 2009/2010), 2 neutral periods (2001/2002 and 2003/2004) and 5 La Niña periods (1999/2000, 2000/2001, 2005/2006, 2007/2008 and 2008/2009). In 2001/2002, ERAINT is in accordance with the observation on the negative TC anomaly trend whilst CEU simulates a positive anomaly and the reverse occurs in the 2003/2004 TC season (Figure 4.15). However, there is no obvious correlation for this. The 2005/2006 and 2007/2008 season showed the largest disparity between CEU and the observation while ERAINT showed a good agreement with observation. Both of these TC seasons were concurrent with La Niña conditions. The 2005/2006 TC season was a weak La Niña year with only 2 observed TCs forming in the basin. Other weak La Niña TC seasons were 2000/2001 as well as 2008/2009 with 6 and 9 observed TCs respectively. However, there is no obvious correlation between the weak La Niña TC counts. Moreover there is no interrelationship in the number of TCs that form during a weak, moderate or strong La Niña/ El Niño event. This shows that ENSO alone cannot be used to explain the interannual variation of TCs over the SWIO which is in agreement with the suggestion of Mavume *et al*. (2009). ERAINT shows agreement with observation with regards to more TCs forming during El Niño periods (Figure 4.17). However, CEU does not show any notable differences in TC counts during an El Niño, La Niña or the neutral phase of ENSO. Moreover, ENSO alone may not explain the interannual variability of TCs over the SWIO, but in combination with other indices, may be useful.

4.7.2 Indian Ocean Dipole

There is a good agreement between observation, ERAINT and CEU in the annual relative frequencies (ARFs) of TC occurrence during positive IOD years, but the same cannot be said for negative IOD phases (Figure 4.17). During the study period, there were 7 positive IOD-TC seasons (1999/2000, 2000/2001, 2002/2003, 2006/2007, 2007/2008, 2008/2009 and 2009/2010) in comparison to only 3 negative IOD-TC seasons (2003/2004, 2004/2005, 2005/2006). This finding suggests that a longer time period may be necessary in order to have a more accurate analysis of IOD-TC occurrence. Nevertheless, using relative frequencies of annual TC counts, ERAINT and CEU shows good similarity (ARF of 6.71 and 6.86 respectively) with observation (6.43) during positive IOD phases. However, both ERAINT and CEU exhibit a prevalence of TC occurrence (ARF of 7.67 and 9.33 respectively) during

the cold phase of IOD which is in disagreement with the observation ARF of 4.33 (Figure 4.17). This bias in TC occurrence during negative IOD can be attributed to the high anomalous ERAINT and CEU TC counts during the 2003/2004, 2004/2005 and 2005/2006 TC seasons which correspond to the 3 negative IOD years. CEU shows a large disparity in the ARFs during the neutral phase of IOD in comparison to observation and ERAINT. When considering ENSO, the observation favours more TC activity during a simultaneous positive ENSO and IOD phase. However, both ERAINT and CEU favour more TC activity during positive ENSO and negative IOD events.

4.7.3 South Atlantic Subtropical Dipole

There are more neutral SASD TC seasons in comparison to positive or negative SASD phases during the study period (1999-2010). The 3 positive SASD TC seasons are 2001/2002, 2006/2007 and 2007/2008 and the 2 negative SASD TC seasons are 2003/2004 and 2005/2006 while the rest of the TC seasons are neutral SASD phases. Both CEU and ERAINT have a good agreement with regards to the ARFs of TC occurrences during positive SASD phases (Figure 4.17). Both the observation and CEU had an ARF of 6.67 and ERAINT presented an ARF of 6.33. There is similarity between observation, ERAINT and CEU ARFs during neutral SASD periods with minor discrepancies. CEU and ERAINT showed ARFs of 7.67 and 7.17 respectively in comparison to the observed ARF of 6 during a neutral phase of SASD. There are notable disagreements between CEU and ERAINT ARF's during negative SASD phases in relation to the observation. ERAINT shows an ARF value of 6.50 while CEU exhibits a larger ARF of 9.50 in comparison to observation (3.50). It is interesting to note that the largest TC occurrence in ERAINT and CEU (Between 2003/2004 and 2005/2006 TC Season) happened roughly at the same time with the negative SASD. In combination with ENSO, the observation shows more TC activity during a positive ENSO and positive SASD phase over the SWIO. However, CEU shows an opposite SASD pattern to the observation whilst ERAINT favours TC genesis during El Niño and neutral phases of the SASD.

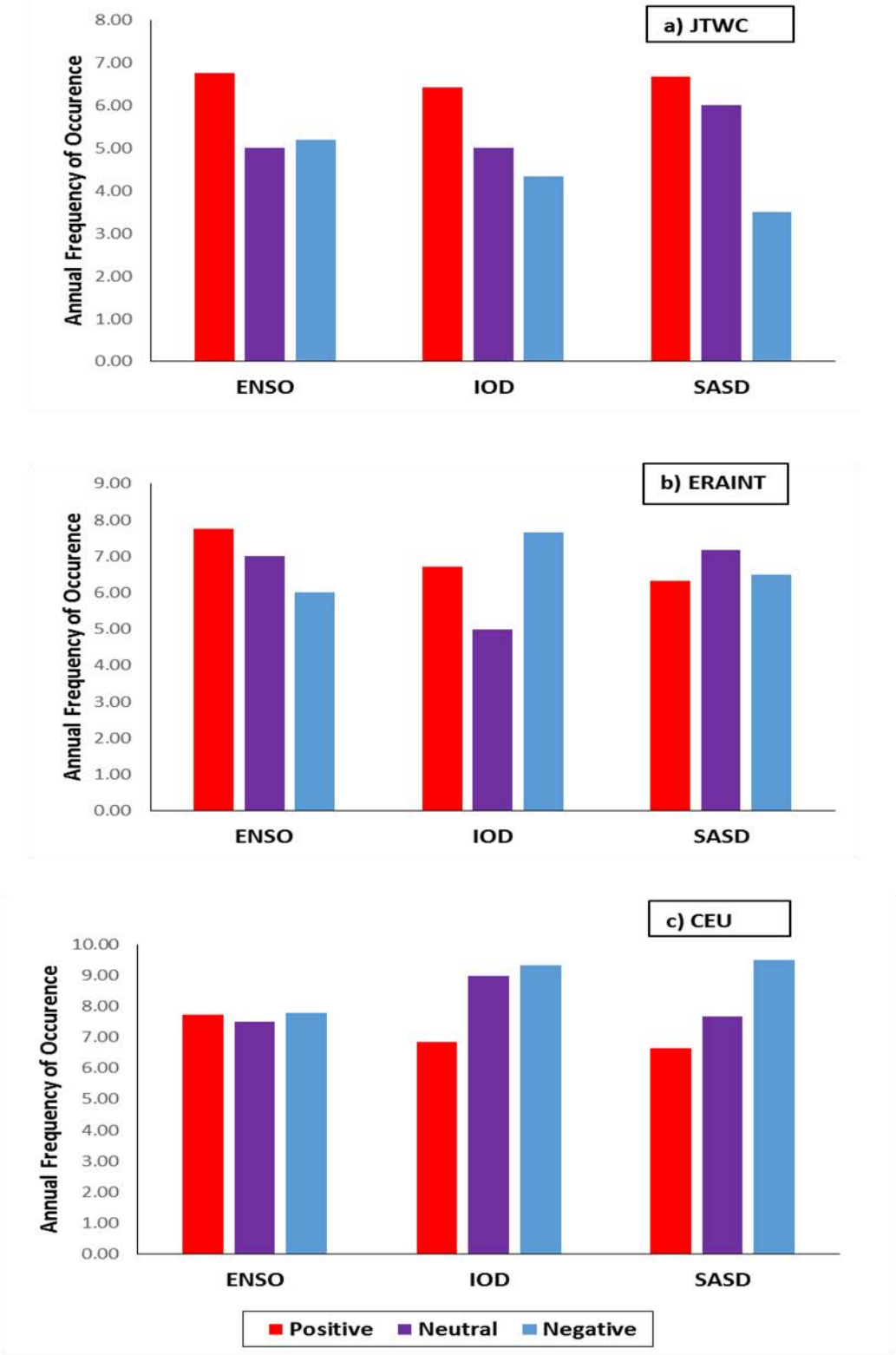

Figure 4.17: Annual frequency of occurrence of South West Indian Ocean Tropical Cyclones during different phases (positive, neutral, negative) of El Niño Southern Oscillation, Indian Ocean Dipole and South Atlantic Subtropical Dipole.

5 CONCLUSIONS

5.1 Summary

This study investigated the skill of a GCM with adaptive grid stretching (CEU) in simulating the characteristics of Tropical Cyclones (TCs) over the SWIO (South West Indian Ocean). The simulation was conducted over a period of 11-years (1999-2010) for the SWIO TC Season (November-April). The model simulation was compared to observation and ERA-Interim (ERAINT) reanalysis data in order to evaluate the skill of the model in simulating the temporal and spatial variation of the regional climate over the SWIO. An objective TC Tracking Algorithm was used in order to detect and track TCs.

In general, CEU showed good agreement with ERAINT in simulating climatic features over the SWIO for the study period. CEU displayed skill in simulating the surface temperature as well as the Mean Sea Level Pressure (MSLP). Other variables such as wind speed, vorticity and rainfall were in good agreement with the observation and ERAINT but had a notable discrepancy over the Mozambique Channel (MC) due to the strong cyclonic features present in the CEU simulation over the region.

The model and reanalysis produced well the spatial tracks of TCs over the SWIO but the model overestimated on the number of TCs over the MC. Both CEU and ERAINT overestimated TC genesis directly over the basin as well as for the MC. However they both showed some skill in showing the spatial distribution of genesis locations.

The CEU model adequately reproduced the dynamical structure of an observed TC but exhibited a larger eye (~100 km) in comparison to a typical observed TC eye (32-64 km). ERAINT could capture some features like the calm eye in the centre of the storm as well as a warm core.

CEU showed better agreement with observation in comparison to ERAINT on the intensity of TCs. However, even at 0.5°x0.5°, CEU struggled to sustain stronger wind speeds as well as producing storms with minimum MSLP centres deeper than 930 hPa.

Both CEU and ERAINT reproduced well the monthly variation of TCs although TCs were

overestimated during the peak months (i.e. January and February) in comparison to the observation. This was due to the strong vorticity bias over the MC which is favourable to Tropical Cyclogenesis. The model was able to show reliability in simulating the interannual variability of SWIO TCs. It captured most of the anomaly trends with a *H* score of 0.83 and a FAR of 0.40 in relation to the observation. ERAINT scored a *H* value of 0.67 which showed some skill.

ERAINT favoured more TC occurrence during a positive phase of ENSO which is agreement with the observation while CEU showed no notable difference in TC counts during El Niño, La Niña or neutral periods. Both CEU and ERAINT showed similarity with observation in ARFs during warm phases of IOD and SASD but showed notable disparities during the neutral and cold phase.

5.2 Recommendations

The results of this study shows that CEU has an application for seasonal forecasting over the SWIO. However, further development is planned in order to improve the performance of the model over the SWIO. The first improvement would be updating the CEU physics package from CAM3 to the newer CAM5.2, which offers improvements on the physics parameterizations. These improvements on parameterization schemes would hopefully improve the CEU simulation over the MC. Moreover, future studies are planned on studying the impacts of various parameterization schemes on TCs over the SWIO, since moist processes have been shown to play an important role in strengthening TCs.

Potential work following from this study should also consider performing ensemble runs in order to provide a more robust climatological analysis of the SWIO, which may improve the TC simulation statistics over the basin. Another possible study could also look at the comparison of uniform grid vs. stretched-grid on TC characteristics. In this study, TCs were simulated using a static stretch grid but the next planned study will look at dynamic grid stretching, which allows for dynamic tracking of features of interest (e.g. storms) whilst increasing resolution locally.

The objective algorithm for detecting and tracking algorithms also needs further improvement. The first improvement would be employing a structural criteria on candidate cyclones in order to remove spurious detection associated with extra-tropical lows. Another improvement could be using standard deviations instead of absolute values with regards to the

temperature, vorticity and wind speed thresholds. This would allow the algorithm to be more robust and objective in detecting TCs in gridded datasets.

With regards to SST parameters, future avenues of research should consider doing more investigation on the role of the IOD and SASD mode on TC activity over the SWIO. Moreover, this investigation should be done in association with ENSO and MJO, since they have been shown to modulate TC activity in various basins.

6 REFERENCES

Abiodun, B.J., Gutowski, W.J., Abatan, A.A. & Prusa, J.M. 2011, "CAM-EULAG: A non-hydrostatic atmospheric climate model with grid stretching", *Acta Geophysica,* vol. 59, no. 6, pp. 1158-1167.

Abiodun, B.J., Prusa, J.M. & Gutowski Jr, W.J. 2008, "Implementation of a non-hydrostatic, adaptive-grid dynamics core in CAM3. Part I: comparison of dynamics cores in aqua-planet simulations", *Climate Dynamics,* vol. 31, no. 7-8, pp. 795-810.

Al-Imdaad Foundation. 2015, Cyclone Giovanna – Madagascar. [image] Retrieved from http://www.alimdaad.com/html/Public/ImageGalleryDetails.aspx?id=222

Araujo, J.A., Abiodun, B.J. & Crespo, O. 2014, "Impacts of drought on grape yields in Western Cape, South Africa", *Theoretical and Applied Climatology,* , pp. 1-14.

Ash, K.D. & Matyas, C.J. 2010, "The influences of ENSO and the subtropical Indian Ocean Dipole on tropical cyclone trajectories in the southwestern Indian Ocean", *International Journal of Climatology,* vol. 32, no. 1, pp. 41-56.

Ashok, K., Guan, Z. & Yamagata, T. 2001, "Impact of the Indian Ocean dipole on the relationship between the Indian monsoon rainfall and ENSO", *Geophysical Research Letters,* vol. 28, no. 23, pp. 4499-4502.

Australia Bureau of Meteorology. 2013*, Tropical Cyclone Intensity and Impacts* [Homepage of ustralian Government Bureau of Meteorology], [Online]. Available: http://www.bom.gov.au/cyclone/about/intensity.shtml [2013].

Badarinath, K.V.S., Mahalakshmim, D.V. & Ratna, S.B. 2012, "Influence of Land Use Land Cover on Cyclone Track Prediction - A study during Ailia Cyclone", *The open Atmospheric Science Journal,* [Online], vol. Vol. 6, , pp. 6 February 2013. Available from: http://benthamopen.com/toascj/articles/V006/33TOASCJ.pdf.

Bell, G.D., Halpert, M.S., Schnell, R.C., Higgins, R.W., Lawrimore, J., Kousky, V.E., Tinker, R., Thiaw, W., Chelliah, M. & Artusa, A. 2000, "Climate assessment for 1999", *Bulletin of the American Meteorological Society,* vol. 81, no. 6, pp. s1-s50.

Bell, J., Hodges, K., Vidale, P.L., Strachan, J. & Roberts, M. 2014, "Simulation of the Global ENSO–Tropical Cyclone Teleconnection by a High-Resolution Coupled General Circulation Model", *Journal of Climate,* [Online], vol. Vol. 27, no. 17, pp. 14 November 2014-6404-6422. Available from: journals.ametsoc.org/doi/pdf/10.1175/JCLI-D-13-00559.1.

Bengtsson, L., Böttger, H. & Kanamitsu, M. 1982, "Simulation of hurricane type vortices in a general circulation model", *Tellus,* vol. 34, no. 5, pp. 440-457.

Bengtsson, L., Botzet, M. & Esch, M. 1995, "Hurricane-type vortices in a general circulation model", *Tellus,* [Online], vol. 47A, no. 2, pp. 175-196. Available from: http://envsci.rutgers.edu/~toine379/extremeprecip/papers/bengtsson_et_al_1995.pdf. [4 November 2014].

Bengtsson, L., Hodges, K.I., Esch, M., Keenlyside, N., Kornblueh, L., LUO, J. & Yamagata, T. 2007, "How may tropical cyclones change in a warmer climate?", *Tellus A,* vol. 59, no. 4, pp. 539-561.

Bengtsson, L. 2001, "Weather. Hurricane threats", *Science (New York, N.Y.),* vol. 293, no. 5529, pp. 440-441.

Bengtsson, L., Botzet, M. & Esch, M. 1996, "Will greenhouse gas-induced warming over the next 50 years lead to higher frequency and greater intensity of hurricanes?", *Tellus,* [Online], vol. 4A, no. 1, pp. 3 November 2014-57-73. Available from: http://pubman.mpdl.mpg.de/pubman/item/escidoc:1852493:2/component/escidoc:1852573/11632-38420-1-SM.pdf.

Berrisford, P., Kallberg, P., Kobayashi, S., Dee, D., Uppala, S., Simmons, A., Poli, P. & Sato, H. 2011, "The ERA-Interim archive version 2.0", *European Centre for Medium-Range Weather Forecasts ERA Tech.Rep,* vol. 1, pp. 23.

Bessafi, M. & Wheeler, M.C. 2006, "Modulation of South Indian Ocean tropical cyclones by the Madden-Julian oscillation and convectively coupled equatorial waves", *Monthly Weather Review,* vol. 134, no. 2, pp. 638-656.

Betts, A.K., Ball, J.H., Beljaars, A.C.M., Miller, M.J. & Viterbo, P.A. 1996, "The land surface-atmosphere interaction: A review based on observational and global modeling perspectives", *Journal of Geophysical Research: Atmospheres,* vol. 101, no. D3, pp. 7209-7225.

Bove, M.C., O'Brien, J.J., Eisner, J.B., Landsea, C.W. & Niu, X. 1998, "Effect of El Niño on US landfalling hurricanes, revisited", *Bulletin of the American Meteorological Society,* vol. 79, no. 11, pp. 2477-2482.

Camargo, S.J., Emanuel, K.A. & Sobel, A.H. 2007, "Use of a genesis potential index to diagnose ENSO effects on tropical cyclone genesis", *Journal of Climate,* vol. 20, no. 19, pp. 4819-4834.

Camargo, S.J. & Sobel, A.H. 2005, "Western North Pacific tropical cyclone intensity and ENSO", *Journal of Climate,* vol. 18, no. 15, pp. 2996-3006.

Caron, L., Jones, C.G. & Winger, K. 2011, "Impact of resolution and downscaling technique in simulating recent Atlantic tropical cylone activity", *Climate Dynamics,* vol. 37, no. 5-6, pp. 869-892.

Chauvin, F., Royer, J. & Déqué, M. 2006, "Response of hurricane-type vortices to global warming as simulated by ARPEGE-Climat at high resolution", *Climate Dynamics,* vol. 27, no. 4, pp. 377-399.

Chen, Y. & Yau, M. 2001, "Spiral bands in a simulated hurricane. Part I: Vortex Rossby wave verification", *Journal of the Atmospheric Sciences,* vol. 58, no. 15, pp. 2128-2145.

Chu, P. 2004, "ENSO and tropical cyclone activity", *Hurricanes and typhoons: Past, present, and potential*, pp. 297-332.

Ciasto, L.M., Simpkins, G.R. & England, M.H. 2014, "Teleconnections between tropical Pacific SST anomalies and extratropical Southern Hemisphere climate", *Journal of Climate,* vol. 28, no. 1, pp. 56-65.

Collins, W.D., Rasch, P.J., Boville, B.A., Hack, J.J., McCaa, J.R., Williamson, D.L., Kiehl, J.T., Briegleb, B., Bitz, C. & Lin, S. 2004, "Description of the NCAR community atmosphere model (CAM 3.0)", .

Côté, J., Gravel, S., Méthot, A., Patoine, A., Roch, M. & Staniforth, A. 1998, "The operational CMC-MRB global environmental multiscale (GEM) model. Part I: Design considerations and formulation", *Monthly Weather Review,* vol. 126, no. 6, pp. 1373-1395.

Dee, D., Uppala, S., Simmons, A., Berrisford, P., Poli, P., Kobayashi, S., Andrae, U., Balmaseda, M., Balsamo, G. & Bauer, P. 2011, "The ERA-Interim reanalysis: Configuration and performance of the data assimilation system", *Quarterly Journal of the Royal Meteorological Society,* vol. 137, no. 656, pp. 553-597.

Didlake Jr, A.C. & Houze Jr, R.A. 2009, "Convective-scale downdrafts in the principal rainband of Hurricane Katrina (2005)", *Monthly Weather Review,* vol. 137, no. 10, pp. 3269-3293.

Driver, P. 2014, *Rainfall Variability over Southern Africa*, University of Cape Town.

Dvorak, V.F. 1984, Tropical cyclone intensity analysis using satellite data, US Department of Commerce, National Oceanic and Atmospheric Administration, National Environmental Satellite, Data, and Information Service.

Evans, J.L. 1993, "Sensitivity of tropical cyclone intensity to sea surface temperature", *Journal of Climate,* vol. 6, no. 6, pp. 1133-1140.

Fauchereau, N., Trzaska, S., Richard, Y., Roucou, P. & Camberlin, P. 2003, "Sea-surface temperature co-variability in the southern Atlantic and Indian Oceans and its connections with the atmospheric circulation in the Southern Hemisphere", *International Journal of Climatology,* vol. 23, no. 6, pp. 663-677.

Fitzpatrick, P.J. 2006, *Hurricanes: A reference handbook,* Abc-clio.

Fox-Rabinovitz, M.S., Stenchikov, G.L., Suarez, M.J. & Takacs, L.L. 1997, "A finite-difference GCM dynamical core with a variable-resolution stretched grid", *Monthly Weather Review,* vol. 125, no. 11, pp. 2943-2968.

Fox-Rabinovitz, M., Cote, J., Dugas, B., Deque, M., McGregor, J.L. & Belochitski, A. 2008, "Stretched-grid Model Intercomparison Project: decadal regional climate simulations with enhanced variable and uniform-resolution GCMs", *Meteorology and atmospheric physics,* vol. 100, no. 1-4, pp. 159-178.

Francis, P., Gadgil, S. & Vinayachandran, P. 2007, "Triggering of the positive Indian Ocean dipole events by severe cyclones over the Bay of Bengal", *Tellus A,* vol. 59, no. 4, pp. 461-475.

Frank, W.M. & Roundy, P.E. 2006, "The role of tropical waves in tropical cyclogenesis", *Monthly Weather Review,* vol. 134, no. 9, pp. 2397-2417.

Fritsch, J.M. & Kain, J.S. 1993, "Convective parameterization for mesoscale models: the Fritsch-Chappell scheme" in *The representation of cumulus convection in numerical models* Springer, pp. 159-164.

Giorgi, F. & Mearns, L.O. 1999, "Introduction to special section: Regional climate modeling revisited", *Journal of Geophysical Research: Atmospheres (1984–2012),* vol. 104, no. D6, pp. 6335-6352.

Girishkumar, M. & Ravichandran, M. 2012, "The influences of ENSO on tropical cyclone activity in the Bay of Bengal during October–December", *Journal of Geophysical Research: Oceans (1978–2012),* vol. 117, no. C2.

Gray, W.M. 1979, "Hurricanes: Their formation, structure, and likely role in the tropical circulation." in *Meteorology over the Tropical Oceans*, ed. D.B. Shaw, Royal meteorological Society, pp. 155-218.

Gray, W.M. 1968, "Global view of the origin of tropical disturbances and storms", *Monthly Weather Review,* vol. 96, no. 10, pp. 669-700.

Gray, W.M., Landsea, C.W., Mielke Jr, P.W. & Berry, K.J. 1993, "Predicting Atlantic basin seasonal tropical cyclone activity by 1 August", *Weather and Forecasting,* vol. 8, no. 1, pp. 73-86.

Gray, W.M. 1998, "The formation of tropical cyclones", *Meteorology and atmospheric physics,* vol. 67, no. 1-4, pp. 37-69.

Haarsma, R.J., Mitchell, J.F. & Senior, C. 1993, "Tropical disturbances in a GCM", *Climate Dynamics,* vol. 8, no. 5, pp. 247-257.

Henderson-Sellers, A., Zhang, H., Berz, G., Emanuel, K., Gray, W., Landsea, C., Holland, G., Lighthill, J., Shieh, S. & Webster, P. 1998, "Tropical cyclones and global climate change: A post-IPCC assessment", *Bulletin of the American Meteorological Society,* vol. 79, no. 1, pp. 19-38.

Hermes, J. & Reason, C. 2005, "Ocean model diagnosis of interannual coevolving SST variability in the South Indian and South Atlantic Oceans", *Journal of Climate,* vol. 18, no. 15, pp. 2864-2882.

Ho, C., Kim, J., Jeong, J., Kim, H. & Chen, D. 2006, "Variation of tropical cyclone activity in the South Indian Ocean: El Niño–Southern Oscillation and Madden-Julian Oscillation effects", *Journal of Geophysical Research: Atmospheres (1984–2012),* vol. 111, no. D22.

Hoffrage, U., Lindsey, S., Hertwig, R. and Gigerenzer, G. (2000). Communicating statistical information. *Science*, 290, 2261-2262

Holland, G. 1993, "Ready reckoner", *Global guide to tropical cyclone forecasting,* pp. 9.1-9.32.

Houze Jr, R.A. 2010, "Clouds in tropical cyclones", *Monthly Weather Review,* vol. 138, no. 2, pp. 293-344.

IRIN, AFRICA: Coastal populations at risk as climate changes. 2015a, [Homepage of IRINNews], [Online]. Available: http://www.irinnews.org/report.aspx?reportid=84464&&session-id=e3013e597733e3049f60d8a8fe335deb [2015, June].

IRIN, Tropical Cyclone Haruna hits southwestern Madagascar. 2015b, [Homepage of IRINNews], [Online]. Available: http://www.irinnews.org/report/97542/tropical-cyclone-haruna-hits-southwestern-madagascar [2015, April].

JAMSTEC, Indian Ocean Dipole (IOD). 2010, [Homepage of Japan Agency for Marine-Earth Science and Technology], [Online]. Available: http://www.jamstec.go.jp/frcgc/research/d1/iod/iod_home_s.html.en [2015].

Jolliffe, I. & Stephenson, D. 2003, *Forecast Verification: A Practitioner's Guide in Atmospheric Science*, NJ: John Wiley & Sons Ltd.

Jury, M.R. 1993, "A preliminary study of climatological associations and characteristics of tropical cyclones in the SW Indian Ocean", *Meteorology and Atmospheric Physics,* vol. 51, no. 1-2, pp. 101-115.

Kleppek, S., Muccione, V., Raible, C., Bresch, D., Koellner Heck, P. & Stocker, T. 2008, "Tropical cyclones in ERA 40: A detection and tracking method", *Geophysical Research Letters,* vol. 35, no. 10.

Klinman, M. & Reason, C. 2008, "On the peculiar storm track of TC Favio during the 2006–2007 Southwest Indian Ocean tropical cyclone season and relationships to ENSO", *Meteorology and Atmospheric Physics,* vol. 100, no. 1-4, pp. 233-242.

Knaff, J.A. 1997, "Implications of summertime sea level pressure anomalies in the tropical Atlantic region", *Journal of Climate,* vol. 10, no. 4, pp. 789-804.

Knowles, T.N. 2009, *Category 5: The 1935 Labor Day Hurricane,* University Press of Florida.

Knutson, T.R., Sirutis, J.J., Garner, S.T., Held, I.M. & Tuleya, R.E. 2007, "Simulation of the recent multidecadal increase of Atlantic hurricane activity using an 18-km-grid regional model", *Bulletin of the American Meteorological Society,* vol. 88, no. 10, pp. 1549-1565.

Kossin, J.P. & Sitkowski, M. 2009, "An objective model for identifying secondary eyewall formation in hurricanes", *Monthly Weather Review,* vol. 137, no. 3, pp. 876-892.

Kuleshov, Y. & de Hoedt, G. 2003, "Tropical cyclone activity in the Southern Hemisphere", *Bull.Aust.Met.Oceanogr.Soc,* vol. 16, pp. 135-137.

Lambin, E. & Geist, H. 2007*, Causes of land-use and land-cover change*. Available: http://www.eoearth.org/view/article/51cbed2f7896bb431f6905af/ [2015, July].

Landman, W.A., Seth, A. & Camargo, S.J. 2005, "The effect of regional climate model domain choice on the simulation of tropical cyclone-like vortices in the southwestern Indian Ocean", *Journal of Climate,* vol. 18, no. 8, pp. 1263-1274.

Landsea, C. & Dorst, N. 2014, How and why are tropical cyclones named? [Homepage of NOAA - National Oceanic and Atmospheric Administration], [Online]. Available: http://sunburn.aoml.noaa.gov/hrd/tcfaq/B1.html [2015, 13 June 2015].

Liu, Y., Zhang, D. & Yau, M. 1997, "A multiscale numerical study of Hurricane Andrew (1992). Part I: Explicit simulation and verification", *Monthly Weather Review,* vol. 125, no. 12, pp. 3073-3093.

Malherbe, J., Engelbrecht, F.A., Landman, W.A. & Engelbrecht, C. 2012, "Tropical systems from the southwest Indian Ocean making landfall over the Limpopo River Basin, southern Africa: a historical perspective", *International Journal of Climatology,* vol. 32, no. 7, pp. 1018-1032.

Manabe, S., Holloway Jr, J.L. & Stone, H.M. 1970, "Tropical circulation in a time-integration of a global model of the atmosphere", *Journal of the Atmospheric Sciences,* vol. 27, no. 4, pp. 580-613.

Manganello, J.V., Hodges, K.I., Kinter III, J.L., Cash, B.A., Marx, L., Jung, T., Achuthavarier, D., Adams, J.M., Altshuler, E.L. & Huang, B. 2012, "Tropical cyclone climatology in a 10-km global atmospheric GCM: Toward weather-resolving climate modeling", *Journal of Climate,* vol. 25, no. 11, pp. 3867-3893.

Mavume, F.A. 2008, *Tropical cyclones in the South-West Indian Ocean: Intensity changes, oceanic interaction and impacts*, University of Cape Town.

Mavume, F.A., Rydberg, L., Rouault, M. & Lutjeharms, R.E.J. 2009, "Climatology and Landfall of Tropical Cyclones in the South West Indian Ocean", *Western Indian Ocean Journal of Marine Science,* vol. Vol. 8, no. No. 1, pp. 15-36.

Mbedzi, M.P. 2010, *Simulation of tropical cyclone-like vortices over the southwestern Indian Ocean*, University of Pretoria.

Misra, J. 1991, "Phase synchronization", *Information Processing Letters,* vol. 38, no. 2, pp. 101-105.

Morioka, Y., Tozuka, T., Masson, S., Terray, P., Luo, J. & Yamagata, T. 2012, "Subtropical dipole modes simulated in a coupled general circulation model", *Journal of Climate,* vol. 25, no. 12, pp. 4029-4047.

Morioka, Y., Tozuka, T. & Yamagata, T. 2011, "On the growth and decay of the subtropical dipole mode in the South Atlantic", *Journal of Climate,* vol. 24, no. 21, pp. 5538-5554.

Murakami, H. & Wang, B. 2010, "Future Change of North Atlantic Tropical Cyclone Tracks: Projection by a 20-km-Mesh Global Atmospheric Model*", *Journal of Climate,* vol. 23, no. 10, pp. 2699-2721.

Murphy, A.H. (1997), Forecast verification. In: The Economic Value of Weather and Climate Forecasts (eds. R.W. Katz and A.H. Murphy). Cambridge University Press, 19-74.

NASA earth observatory. 2005, Satellite image of Tropical Cyclone Adeline Juliet on 9 April 2005.[image] Retrieved from http://earthobservatory.nasa.gov/NaturalHazards/view.php?id=14820

National Hurricane Center. 2013, Saffir-Simpson Hurricane Wind Scale. [image] Retrieved from http://www.nhc.noaa.gov/aboutsshws.php

NOAA, Remembering the November 1913 “White Hurricane”. 2013, [Homepage of NOAA], [Online]. Available: http://www.nws.noaa.gov/com/weatherreadynation/news/131107_white.html#.VeLMZcuY5pg [2015, August].

National Weather Service, Tropical Cyclone Structure. 2010, [Homepage of National Weather Service], [Online]. Available: http://www.srh.noaa.gov/jetstream/tropics/tc_structure.htm?&session-id=e2221f2646ce61f563e3a28f11ec4d98 [2015, July].

National Weather Service. 2013, Saffir-Simpson Hurricane Wind Scale [Homepage of National Oceanic and Atmospheric Administration], [Online]. Available: http://www.nhc.noaa.gov/aboutsshws.php [2013].

News.com.au. 2014, The Category 5 cyclones that devastated Australia. [image] Retrieved from http://www.news.com.au/national/the-category-5-cyclones-that-devastated-australia/story-fncynjr2-1226880854853

Nguyen, K. & Walsh, K. 2001, "Interannual, decadal, and transient greenhouse simulation of tropical cyclone-like vortices in a regional climate model of the South Pacific", *Journal of Climate,* vol. 14, no. 13, pp. 3043-3054.

Ogier, D. 2013, *Characteristics of Inertial Gravity Waves over Southern Africa as simulated with CAM-EULAG*, University of Cape Town.

Oouchi, K., Yoshimura, J., Yoshimura, H., Mizuta, R., Kusunoki, S. & Noda, A. 2006, "Tropical cyclone climatology in a global-warming climate as simulated in a 20 km-mesh global atmospheric model: Frequency and wind intensity analyses", *Journal of the Meteorological Society of Japan,* vol. 84, no. 2, pp. 259-276.

Palmén, E. 1948, "On the formation and structure of tropical hurricanes", *Geophysica,* [Online], vol. Vol. 3, no. 1, pp. 14 August 2013-26-38. Available from: http://www.geophysica.fi/pdf/geophysica_1948_3_1_026_palmen.pdf.

PhysicalGeography.net. 2014, Tropical Weather and Hurricanes. [image] Retrieved from http://www.physicalgeography.net/fundamentals/7u.html

Reed, K.A., Jablonowski, C. & Taylor, M.A. 2012, "Tropical cyclones in the spectral element configuration of the Community Atmosphere Model", *Atmospheric Science Letters,* vol. 13, no. 4, pp. 303-310.

Rodrigues, R.R., Campos, E.J. & Haarsma, R. 2015, "The Impact of ENSO on the South Atlantic Subtropical Dipole Mode", *Journal of Climate,* vol. 28, no. 7, pp. 2691-2705.

Rowlett, R. 2001, "*Beaufort Scales (Wind Speed)*.", [Online], vol. 2013, . Available from: http://www.unc.edu/~rowlett/units/scales/beaufort.html.

Saha, K.K. & Wasimi, S.A. 2013, "Interrelationship between Indian Ocean Dipole (IOD) and Australian Tropical Cyclones", *International Journal of Environmental Science and Development,* vol. 4, no. 6, pp. 647.

Saji, N., Goswami, B.N., Vinayachandran, P. & Yamagata, T. 1999, "A dipole mode in the tropical Indian Ocean", *Nature,* vol. 401, no. 6751, pp. 360-363.

Schmidt, F. 1977, "Variable fine mesh in the spectral global models", *Beitr. Phys. Atmos.,* vol. 50, pp. 211-217.

Shen, W., Ginis, I. & Tuleya, R.E. 2002, "A numerical investigation of land surface water on landfalling hurricanes", *Journal of the Atmospheric Sciences,* vol. 59, no. 4, pp. 789-802.

Singh, O., Gupta, M., Santha, K., Saikia, D. & Khanuja, S. 2008, "Indian Ocean dipole mode and tropical cyclone frequency", *CURRENT SCIENCE-BANGALORE-,* vol. 94, no. 1, pp. 29.

Smith, D.M., Eade, R., Dunstone, N.J., Fereday, D., Murphy, J.M., Pohlmann, H. & Scaife, A.A. 2010, "Skilful multi-year predictions of Atlantic hurricane frequency", *Nature Geoscience,* [Online], vol. 3, pp. 14 November 2014-846-849. Available from: http://www.nature.com/ngeo/journal/v3/n12/pdf/ngeo1004.pdf.

Smith, T.M., Reynolds, R.W., Peterson, T.C. & Lawrimore, J. 2008, "Improvements to NOAA's historical merged land-ocean surface temperature analysis (1880-2006)", *Journal of Climate,* vol. 21, no. 10, pp. 2283-2296.

Staniforth, A.N. & Mitchell, H.L. 1978, "A variable-resolution finite-element technique for regional forecasting with the primitive equations", *Monthly Weather Review,* vol. 106, no. 4, pp. 439-447.

Sterl, A. & Hazeleger, W. 2003, "Coupled variability and air-sea interaction in the South Atlantic Ocean", *Climate Dynamics,* vol. 21, no. 7-8, pp. 559-571.

Stowasser, M., Wang, Y. & Hamilton, K. 2007, "Tropical cyclone changes in the western North Pacific in a global warming scenario", *Journal of Climate,* vol. 20, no. 11, pp. 2378-2396.

Strachan, J., Vidale, P.L., Hodges, K., Roberts, M. & Demory, M. 2013, "Investigating Global Tropical Cyclone Activity with a Hierarchy of AGCMs: The Role of Model Resolution", *Journal of Climate,* [Online], vol. Vol. 26, no. 1, pp. 5 November-133-152. Available from: http://journals.ametsoc.org/doi/pdf/10.1175/JCLI-D-12-00012.1.

Sugi, M., Noda, A. & Sato, N. 2002, "Influence of the global warming on tropical cyclone climatology: An experiment with the JMA global model.", *Journal of the Meteorological Society of Japan,* vol. 80, no. 2, pp. 249-272.

Suzuki-Parker, A. 2011, *An assessment of uncertainties and limitations in simulating tropical cyclone climatology and future changes*, Georgia Institute of Technology.

Tozuka, T., Abiodun, B.J. & Engelbrecht, F.A. 2014, "Impacts of convection schemes on simulating tropical-temperate troughs over southern Africa", *Climate Dynamics,* vol. 42, no. 1-2, pp. 433-451.

Venegas, S., Mysak, L. & Straub, D. 1997, "Atmosphere-ocean coupled variability in the South Atlantic", *Journal of Climate,* vol. 10, no. 11, pp. 2904-2920.

Vitart, F., Anderson, J., Sirutis, J. & Tuleya, R. 2001, "Sensitivity of tropical storms simulated by a general circulation model to changes in cumulus parametrization", *Quarterly Journal of the Royal Meteorological Society,* vol. 127, no. 571, pp. 25-51.

Vitart, F., Anderson, J. & Stern, W. 1997, "Simulation of interannual variability of tropical storm frequency in an ensemble of GCM integrations", *Journal of Climate,* vol. 10, no. 4, pp. 745-760.

Vitart, F., Anderson, D. & Stockdale, T. 2003, "Seasonal forecasting of tropical cyclone landfall over Mozambique", *Journal of Climate,* vol. 16, no. 23, pp. 3932-3945.

Wakimoto, R.M. & Black, P.G. 1994, "Damage survey of Hurricane Andrew and its relationship to the eyewall", *Bulletin of the American Meteorological Society,* vol. 75, no. 2, pp. 189-200.

Waliser, D., Lau, K., Stern, W. & Jones, C. 2003, "Potential predictability of the Madden-Julian oscillation", *Bulletin of the American Meteorological Society,* vol. 84, no. 1, pp. 33-50.

Walsh, K. & Watterson, I.G. 1997, "Tropical cyclone-like vortices in a limited area model: comparison with observed climatology", *Journal of Climate,* vol. 10, no. 9, pp. 2240-2259.

Walsh, K., Fiorino, M., Landsea, C. & McInnes, K. 2007, "Objectively determined resolution-dependent threshold criteria for the detection of tropical cyclones in climate models and reanalyses", *Journal of Climate,* vol. 20, no. 10, pp. 2307-2314.

Walsh, K., Nguyen, K. & McGregor, J. 2004, "Fine-resolution regional climate model simulations of the impact of climate change on tropical cyclones near Australia", *Climate Dynamics,* vol. 22, no. 1, pp. 47-56.

Wang, B. & Chan, J.C. 2002, "How strong ENSO events affect tropical storm activity over the western North Pacific", *Journal of Climate,* vol. 15, no. 13, pp. 1643-1658.

Wheeler, M.C. & Hendon, H.H. 2004, "An all-season real-time multivariate MJO index: Development of an index for monitoring and prediction", *Monthly Weather Review,* vol. 132, no. 8, pp. 1917-1932.

Wheeler, M. & Weickmann, K.M. 2001, "Real-time monitoring and prediction of modes of coherent synoptic to intraseasonal tropical variability", *Monthly Weather Review,* vol. 129, no. 11, pp. 2677-2694.

Wong, M.L. & Chan, J.C. 2006, "Tropical cyclone motion in response to land surface friction", *Journal of the Atmospheric Sciences,* vol. 63, no. 4, pp. 1324-1337.

World Meteorological Organization, Tropical Cyclone Naming. 2015, [Homepage of World Meteorological Organization], [Online]. Available: https://www.wmo.int/pages/prog/www/tcp/index_en.html [2015, April].

Wu, R., Kinter III, J. & Kirtman, B.P. 2005, "Discrepancy of interdecadal changes in the Asian region among the NCEP-NCAR reanalysis, objective analyses, and observations", *Journal of Climate,* vol. 18, no. 15, pp. 3048-3067.

Yoshimura, J., Sugi, M. & Noda, A. 2006, "Influence of greenhouse warming on tropical cyclone frequency", *Journal of the Meteorological Society of Japan,* vol. 84, no. 2, pp. 405-428.

Zarzycki, C.M. & Jablonowski, C. 2014, "A multidecadal simulation of Atlantic tropical cyclones using a variable resolution global atmospheric general circulation model", *Journal of Advances in Modeling Earth Systems,* vol. 6, no. 3, pp. 805-828.

Zarzycki, C.M., Jablonowski, C. & Taylor, M.A. 2014, "Using variable-resolution meshes to model tropical cyclones in the Community Atmosphere Model", *Monthly Weather Review,* vol. 142, no. 3, pp. 1221-1239.

Zhao, M. & Held, I.M. 2012, "TC-Permitting GCM Simulations of Hurricane Frequency Response to Sea Surface Temperature Anomalies Projected for the Late-Twenty-First Century", *Journal of Climate,* [Online], vol. Vol. 24, no. 8, pp. 15 November 2014-2995-3009. Available from: http://journals.ametsoc.org/doi/pdf/10.1175/JCLI-D-11-00313.1.

Zhu, P. 2008, "Impact of land-surface roughness on surface winds during hurricane landfall", *Quarterly Journal Of The Royal Meteorological Society,* [Online], vol. Vol. 134, no. 633, pp. 12 March 2013-1051-1057. Available from: http://onlinelibrary.wiley.com/doi/10.1002/qj.265/pdf.

APPENDIX A

Table A.1: Tropical Cyclone tracking criteria and threshold used by past global/regional climate modeling studies. T'xxx refers to horizontal temperature anomaly at xxxhPa, and Vxxx refers to maximum Wind speed criteria at xxxhPa.

	Model Resolution	Wind Speed	Vorticity at 850 hPa	Structure	Temperature Anomaly (K)	Duration (days)
Bengtsson *et al.* (1982)	200 km	>25 m/s at 850hPa	$>7.00 \times 10^{-5} s^{-1}$	-	-	-
Haarsma *et al.* (1993)	2.5° × 3.75°	-	$>3.50 \times 10^{-5} s^{-1}$	-	T'700+T'500+T'300 > 3	3
Bengtsson *et al.* (1995)	T42	>15 m/s at surface	$>3.50 \times 10^{-5} s^{-1}$	T'300>T'850; V850>V300	T'700+T'500+T'300 > 3	1.5
Walsh and Watterson (1997)	125 km	>6-10 m/s at 10 m	$>2.00 \times 10^{-5} s^{-1}$	T'300>T'850; V850>V300	-	2
Nguyen and Walsh (2001)	125 km	>5m/s at 10 m	$>1.00 \times 10^{-5} s^{-1}$	T'300>T'850; V850>V300	T'700+T'500+T'300> 0	1
Sugi *et al*. (2002)	125 km	>15 m/s at 850 hPa	$>3.50 \times 10^{-5} s^{-1}$	V850>V300	T'850+T'700+T'500+T'300 > 3	2
Oouchi *et al*. (2006)	20 km	>17 m/s at 850 hPa	$>3.50 \times 10^{-5} s^{-1}$	V300<V850 or <35° latitude	T'300+T'500+T'700>2	1.5
Chauvin *et al.* , 2006	~50 km	>15 m/s at 850 hPa	$>14.00 \times 10^{-5} s^{-1}$	T'300>T'850; V850>V300	T'300+T'500+T'700>0	1.5
Knutson *et al* ., 2007	18 km	>17 m/s at lowest model level	$>1.60 \times 10^{-5} s^{-1}$	-	mean(T'300~T'500)>0.8	2
Stowasser *et al* .,2007	~50 km	>17 m/s at lowest model level	$>2.50 \times 10^{-5} s^{-1}$	V850>V300	mean(T'300~T'850)>0	2
Murukami and Wang, 2010	20 km	>14 m/s at 850 hPa	$>3.00 \times 10^{-5} s^{-1}$	V850-V300>2.5 and <45° latitude	T'300+T'500+T'700>1.2	1.5